WAVE INDUCED MIXING IN THE OCEAN

by

Affonso da Silveira Mascarenhas, Jr.

B.S. Universidade de Sao Paulo (Brasil)
(1967)

M.Sc. Institute de Pesquisas Espacias (Brasil)
(1975)

S.M. Massachusetts Institute of Technology
(1979)

Submitted to the Department of
Meteorology and Physical Oceanography
in Partial Fulfillment
of the Requirements of the
Degree of

DOCTORATE IN PHILOSOPHY

at the
Massachusetts Institute of Technology

January, 1983

c Massachusetts Institute of Technology 1983

Signature of Author _____
Department of Meteorology
and Physical Oceanography

Certified by _____
Thesis Supervisor

Accepted by _____
Chairman, Dept. Committee
on Graduate Students

WITHDRAWN FROM MIT LIBRARIES
Lindgren
MASSACHUSETTS INSTITUTE OF TECHNOLOGY
APR 14 1983
LIBRARIES

Table of Contents

		Page
Abstract		3
Acknowledgements		3a
	Chapter 1 - Introduction	4
1.1.	The mixing in the ocean	6
1.2.	Oceanic fronts, their dynamics and importance	8
1.3.	Some aspects of remote sensing in oceanography	11
	Chapter II - Wave Induced Mixing in Horizontal Stratification	
2.1.	Introduction	13
2.2.	Basic equations and assumptions	14
2.3.	Computation of the fluxes	17
2.4.	Application to a simple model	23
2.5.	Applications to observations	39
2.6.	Further comments	42
	Chapter III - Wave Induced Layering in Fronts	
3.1.	Introduction	45
3.2.	The mean field, perturbation equations and scaling	46
3.3.	Planar wave solutions	55
3.4.	The computation of the fluxes	68
3.5.	Discussion and results	86
	Chapter IV - Applications to estimates of fluxes induced by forced internal waves.	
4.1.	Introduction	112
4.2.	Massachusetts Bay observations	115
4.3.	Knight Inlet observations	123
	Chapter V - Remote Sensing of Frontal Structures	
5.1.	Introduction	127
5.2.	LANDSAT-2 images	129
5.3.	Synthetic-aperture radar images	130
5.3.1.	Orbital level	130
5.3.2.	Aircraft level	145
5.4.	Infrared radiometer	145
5.4.1.	Satellite level	145
5.4.2.	Aircraft level	145
5.5.	Possible correlation between results of previous chapters and remote sensed frontal features	148
	Chapter VI - Conclusions and Suggestions for Future Work	152
	References	154

WAVE INDUCED MIXING IN THE OCEAN

by

AFFONSO DA SILVEIRA MASCARENHAS, JR.

Submitted to the Department of Meteorology
and Physical Oceanography
in partial fulfillment of the requirements for the degree of
Doctorate in Philosophy

ABSTRACT

The passage of a wave of small amplitude through a nearly inviscid fluid will result in net particle displacements that are small compared to the particle amplitude of oscillation. As a result the distortion of a mean temperature field or a mean salinity field will be relatively unaffected by the net particle displacement caused by the passage of a wave packet. On the other hand, the passage of a wave distorts the temperature field and will induce unsteady changes in diffusion of heat and salt, so there will be oscillations in diffusion that will not, in general, have a zero net value. Furthermore, the oscillation in temperature and velocity may be correlated on the average, so as to result in a resultant average convective transport.

A simple theory of wave induced mixing is presented and then applied to a simple case of linear stratification. The results indicate that freely propagating internal waves on a thermocline or on a front have a relatively small effect. On the other hand forced internal waves, like waves forced by flow over topography, will induce large fluxes and large Nusselt numbers. The depth average divergence of heat flux is zero, indicating that there is no vertical exchange of heat but only a tendency to form layers in the stratification. Layered structures found in temperature and salinity in the vicinity of topographic features could well be a manifestation of the wave induced mixing. Examples of wave induced mixing by topographic waves are shown, and observations of frontal striations are visible in sea surface remote sensing images.

Thesis Supervisor: Dr. Erik L. Mollo-Christensen
Professor of Oceanography

ACKNOWLEDGEMENTS

I would especially like to thank my advisor, Erik Mollo-Christensen, for introducing me to the intriguing world of internal waves, for his confidence in my abilities, for his unlimited patience, and most of all for his inspiration and encouragement during all these years.

I thank all the members of my thesis committee for their discussions and suggestions; Ed Harrison, Mark Cane, and especially Glenn Flierl, who assisted me tirelessly in the final phase of this work.

I am grateful to Ken Morey, who introduced me to the PDP-11 and assisted me througout my tortuous way as a programmer.

My gratitude for my educational experience extends to Woods Hole in the person of Hank Stommel with whom I had enlightening lessons about large scale meridional heat transport in the oceans.

During my studenthood I have enjoyed the company of remarkable collegues both in Meteorology and Oceanography. As an oceanography student my closest contact have been with future oceanographers. I should cite John Lillibridge, Peter Shaw, Eric D'Asaro, Al Campbell, Xin Huang, and especially Teri Chereskin and Bill Dewar. Teri and Bill were the best classmates I could have had, and we shared moments of frustration and joy. It was my pleasure to have them and Ken as cruise mates during the Great Massachusetts Bay Adventure.

A special thanks to Jane McNabb and Virginia Mills, who, as administrators, helped with the necessary logistics, and more than that, offered me their warm friendship, so needed in the loneliness of this last phase. My memories of "Jack and Jill's" dinners and Jane's banquets will long endure.

Virginia Mills did an excellent job of typing the manuscript and editing the Brazilian English. Sam Ricci offered me his experience in my drafting experiments and Diana Spiegel advised in programming. I will always have fond memories of the lyrical poetry of Joel Sloman and the faultless forecasting of Ed Nelson.

My thanks are extended to Prof. Dr. Plinio Soares Moreira, Prof. Dr. Yoshimine Ikeda, and the staff of Oceanographic Institute of U.S.P. for their encouragement and support. I would also like to express my gratitude to Captain Emmanuel Gama de Almeida, whose dedication to the development of oceanography in Brasil has been appreciated.

A warm thanks to my wife Terumi, my daughter Teozinha, and my son, Jorge, to whom I dedicate this work. They were the final inspiration that drove me during all these years. Thanks to Terumi for her patience and for taking all the responsibilities of the home during my absence.

Most of the financial support was provided by the Conselho Nacional de Desenvolvimento Cientifico e Tecnologico (CNPq), Brasil, and also by the Organization of American States (OAS).

This work was supported by the Office of Naval Research, under contract No. N00014-80-C-0273.

Chapter I.

Introduction

Mixing processes in the interior of the ocean may well be responsible for the creation of layered structures in density, salinity and temperature. Such layering often takes the form of superimposed layers of nearly uniform density and other properties. One can see these layers in vertical profiles as well as in the form of striations in the sea surface temperature at ocean current edges and oceanic fronts, as seen in Synthetic Aperture Radar images and other remote sensing imagery.

This thesis deals with the effect of shear-diffusion-advection as flux process capable of creating some of the layering that has been observed in fronts and pycnoclines. The purpose of the work is to assess the possible importance of internal waves and other disturbances as causes of induced fluxes across layers that changes the gradient field in temperature and salinity from relatively smooth to stepwise. This work is inspired by observations of examples of multi-layered structure such as found at the inshore edge of the Gulf Stream front, as well as examples of stepwise stratification in temperature and salinity found elsewhere in the open ocean. Since fronts on occasion can serve as wave guides for internal waves, and because waves distort the gradient field in salinity and temperature, and thus change the molecular flux, it is possible that the effect due to the passage of a wave has a non-zero net consequence for the stratification.

Chapter I discusses the general subject of mixing processes in the ocean, and possible applications of remote sensing observations for elucidation of such phenomena. In Chapter II, a general , simple theory of wave induced mixing is presented, and then applied to a simple case of linear stratification. Then the results are discussed as applied to wave induced mixing in horizontal layering. Chapter III deals with the problem of wave induced mixing in an inclined frontal zone, and the results are discussed in terms of applications to the ocean in Chapter IV. Chapter V shows examples of layering in different fronts as seen from remote sensing images and data.

We find that freely propagating waves do not induce significant fluxes in front and layer as compared to forced waves originating from flow over topography or surface forcing. We also find that tidal frequency waves induced by tidal flow over topography can cause significant fluxes , and that current flowing over or along topographic features also is capable of inducing significant fluxes that can cause layering and other changes in stratification.

The main result is that topographic waves and waves due to tidal forcing can cause significant flux and may be the cause of mixing and layer formation in some localities and contribute significantly to mixing processes.

1.1 The Mixing in the Ocean

The mixing processes in the interior of the ocean are generally classified as either mechanically driven or convectively driven. As stated by Turner (1981), the overall Richardson number, $Rio = g \Delta \rho d / \rho u^2$, where u and d are velocity and length scales based on the velocity and density differences over the whole depth of the ocean, is typically very large, implying that the associated flow is dynamically very stable. On the other hand, the profiles of density, temperature and salinity are known to be very nonuniform, and take the form of superimposed nearly homogeneous layers.

Several processes have been proposed as possible causes of cross gradient mixing in the ocean. They can be divided into three main processes:

i) shear instabilities of internal waves,

ii) boundary mixing, and

iii) double diffusion.

In some cases the fluxes are associated with baroclinic instabilities, but there is still a need to find some other processes that are directly linked to mixing at molecular scales.

Using energy considerations, Turner (1981) showed that in a transition region of linear gradients of velocity and density and between well mixed layers, there is not enough kinetic energy in the local mean motion to produce the observed, nonuniform profiles, even when dissipation is neglected. In the absence of convective energy

additional extra energy must be propagated into the region from the boundaries if mixing is to be sustained; this energy is likely to be in the form of inertial or internal gravity waves. Turner also showed that the transport of momentum by turbulent processes is much less efficient in the interfaces where du/dz is larger, and it is impossible to have constant turbulent fluxes of buoyancy and momentum through the whole depth. But the existence of interfacial waves provides a complementary mechanism to transport momentum across the steep gradient regions without a corresponding increase in the buoyancy flux. Even in a frontal region where the shear is large there is not enough kinetic energy to produce the observed layered profiles. If an extra amount of kinetic energy is furnished by internal waves, how are the layers formed?

Garrett (1979) wrote: "Fluctuations in ocean temperature produced by surface heating and cooling, and in salinity due to evaporation, precipitation, run-off and freezing, are stirred into the ocean by permanent current systems and large scale eddies, and finally dissipated by molecular action on small scale irregularities produced by a variety of processes". This statement emphasizes the role of the fine and micro structure as defined by Munk (1981) in the ocean dynamics. On the other hand, ocean fine structure is usually the result of internal wave straining but in some regions the fine structure is dominated by intrusive processes.

Voorhis et al. (1976) for instance, suggest that the layering shown in their observations arise from alternate cross-frontal intrusions of

shelf and slope water, which are swept downstream and are distorted and thinned by the horizontal and vertical current shear. They also observed that the layer thickness varied from a maximum of 20-30m to less that 1m, with an average of about 10m. They further observed a heat and salt exchange during the period of their experiment and the time scale of this exchange was of the order 1-3 days, which was considered too rapid for pure molecular diffusion. They computed the cross-frontal vertical temperature and salinity fluxes and found 2.5x1013cal/km/day and 1.5x1010g of salt/km/day respectively, being the diffusion of fluxes accounted for by convection cells or fingers, or turbulence generated by internal waves.

1.2 Oceanic Fronts: Their Dynamics and Importance

An extensive discussion of fronts is found in Bowman and Esaias (1978). Some of their ideas are repeated here.

Frontal zones, defined roughly as the boundary between horizontally juxtaposed water masses of dissimilar properties, are an important feature of geophysical turbulence and play important roles in ocean dynamics. They are regions of convergence and relatively strong vertical motions. Frontal circulation can represent a mechanism for cascading energy from large to small scales.

Fronts form where there are horizontal variations in energy exchange such as kinetic and potential, and in dissipation processes.

Important physical driving forces are air-sea transfers, leading to upwelling and concomitant frontal formation. Other processes that can lead to front formation are input of fresh water from runoff, confluence in the velocity field, velocity shear, and turbulent stirring due to bottom topography.

Fronts are found in the surface layers, at mid depths, and near the ocean bottom. Coastal fronts can be classified as follows:

i) shelf break fronts, formed at the boundary of shelf and slope waters such as the one found in the Middle Atlantic Bight;

ii) upwelling fronts, formed as surface manifestations of an inclined pynocline, commonly formed during a coastal upwelling process;

iii) plume fronts, as by discharge of rivers into coastal waters;

iv) shallow seas fronts, formed in continental seas and estuaries, around islands, banks, capes and shoals. These are commonly located in boundary regions between shallow wind and tidally mixed nearshore waters and stratified deeper offshore waters.

v) fronts representing the edge of major western boundary currents. These fronts are associated with the the intrusion of warm, salt water of tropical origin into higher latitudes.

All of these frontal systems share the common properties of persistence, ranging from hours to months in spite of diffusion of properties across strong horizontal gradients, and surface convergence.

Fronts are important dynamically, biologically and chemically, as well as operationally from a meteorological forecasting viewpoint. The dynamic importance is that they are regions where vertical advection and

exchange of momentum and other properties are locally intensive. Depending on their length scale they are important in air-sea interaction effects on the weather and climate. Formation of sea fog at coastal fronts is a well-known occurence.

The biological importance of fronts is illustrated by the fact that they are areas of high biological productivity for the whole food chain, from phytoplankton through fish and marine mammals.

The environmental importance of fronts is that one or two-sided surface convergences are very effective in collecting and concentrating floating detritus and other particulate matter. Consequently the knowledge of the persistence of local fronts is important to the project and positioning of industries dumping contaminants in the ocean.

The economic importance of fronts relies mainly in the establishment of fishing strategies of maximum yields. Finally, strategically speaking, fronts are important for the underwater acousticians, interested in anomalous propagation of sound in the upper ocean.

The cross front mixing is not important from the point of view of annihilation of the front, since the annihilation is much more related to the forcing than to the mixing. But there is no doubt that cross mixing is very important in the exchange of properties between the water masses on each side, and their effect in the circulation.

Horne et al. (1978) ennumerated the following as dynamic processes affecting cross-frontal mixing:

i) Ekman transport within internal boundary layers across geostrophically balanced fronts;

ii) cross frontal interleaving and mixing across fronts where the horizontal density gradient may approach zero;

iii) cabbeling, defined as the sinking of mixed water of different temperature and salinity, but same density resulting in a slightly dense water, has been suggested as a mechanism for surface convergence, and the removal of mixed water from the frontal interface in density balanced fronts;

iv) turbulent entrainment and downwelling induced by interfacial shear.

1.3 Some Aspects of Remote Sensing in Oceanography

Since the advent of the era of satellites, there has been an enormous effort by governmental agencies of many countries to introduce remote sensing as an established technique in the oceanographic community. As the name indicates, remote sensing means obtaining information about a target taken from a distance, usually restricted to sensing of electromagnetic radiation.

Since remote sensing only reveals information about the surface and in some cases information about near-surface properties of the target area, the basic philosophy of this technique is inference. The only problem is that inference is based on what is seen in the surface. This may be enough for certain disciplines like geology, geography, and agriculture. Once one knows the spectral and directional reflectance or

emission of a target, one knows its "signature", from which inference starts. Anything measured remotely that resembles that signature will be classified like the target. Sensing in different wavelength bands increases the possibility of a better identification of the target through the use of pattern recognition techniques. Unfortunately this approach, when applied to oceanography, does not yield any information about the dynamics of the phenomenom, but only beautiful and impressive pictures. Transported sediments and radiometric temperatures used as tracers were and are presently taken as representation of the surface velocity field, but we still do not know what is going on in the third dimension, i.e., in the sub-surface.

As pointed out by Mollo-Christensen (1981) another approach is parallel numerical modeling of localized phenomena, and once one has constructed a numerical model and verified it against in situ observations, one can start the model so that the initial conditions match surface remote sensing imagery. Then, if the model surface patterns move and develop in agreement with further observations, one is in a position to claim that the model represents the interior motions.

Another important point is the need to access data in retrievable computer-compatible form and with adequate navigational labelling. The need to know with a reasonable accuracy the position of a given oceanographic phenomena is a necessity for an oceanographer.

Because remote sensing shows a continuous horizontal view of an oceanographic phenomenon, it can be used to obtain synoptic pictures where we can see scales of the phenomenon not sampled by traditionally

oceanographic means. Striation and layering in frontal structures can be observed in satellite and aircraft images, while they can remain completely unnoticed by usual oceanographic techniques. A proof of this is the set of synthetic-aperture radar images shown in Fu and Holt (1981).

Chapter II

Wave Induced Mixing in Horizontal Stratification

2.1 Introduction

Following the idea of wave induced transports of heat and other constituents, we will study in this chapter the mixing across horizontal stratification induced by internal waves.

The passage of a wave of small amplitude through a nearly inviscid fluid will result in net particle displacements that are small compared to the particle amplitude of oscillation . As a result the distortion of a mean temperature field or a mean salinity field will be relatively unaffected by the net particle displacement caused by the passage of a wave packet. On the other hand, the passage of a wave distorts the temperature field and will induce unsteady changes in diffusion of heat and salt, so there will be oscillations in diffusion that will not, in general, have a zero net value. Furthermore, the oscillations in temperature and velocity may be correlated on the average, so as to result in a resultant average advective transport. If no diffusion were present, the time derivative of the temperature fluctuation induced by the waves would be approximately proportional to the velocity parallel to the temperature gradient, and the mean advective flux, proportional to the product of temperature and velocity, would be zero. But the effect of diffusion will change the correlation between velocity and temperature fluctuations, and this can result in large net heat transport caused by passing waves.

Before studying wave-induced heat and salt transport, and consequently mixing across a frontal zone, we will start from a horizontally stratified ocean, in an attempt to establish a general theory for further applications in a tractable and relatively simple context.

2.2 Basic Equations and Assumptions.

In this section we will establish the basic assumptions and write down the model equations. The ocean is assumed to be an incompressible stably stratified fluid obeying the Boussinesq approximation. A constant depth of the ocean and the f-plane approximation are assumed. Under these conditions, the equations of conservation of momentum, density and continuity are:

$$u_t + \mathbf{u}\cdot\nabla u - fv = -\frac{1}{\rho_0} P_x \tag{2.2.1}$$

$$v_t + \mathbf{u}\cdot\nabla v + fu = -\frac{1}{\rho_0} P_y \tag{2.2.2}$$

$$w_t + \mathbf{u}\cdot\nabla w = -\frac{1}{\rho_0} P_z - \frac{\rho'}{\rho_0} g \tag{2.2.3}$$

$$\rho_t + \mathbf{u}\cdot\nabla\rho + w\bar{\rho}_z = 0 \tag{2.2.4}$$

$$u_x + v_y + w_z = 0 \tag{2.2.5}$$

where $\rho = \rho(z) + \rho'(x,y,z)$ is the density, u,v and w are the velocities along the coordinate axes x, y and z ; P is the pressure less the hydrostatic part and $g\rho'/\rho_0$ is the buoyancy.

After the elimination of pressure, density and horizontal velocity we get the equation for w , Philips (1977):

$$(\nabla^2 w)_t + f^2 w_{zz} + N^2 \nabla_H^2 w = N \qquad (2.2.6)$$

Where N stands for the nonlinear terms and ∇_H^2 is the horizontal Laplacian. For infinitesimal disturbances in the absence of mean shear, equation (2.2.6) is linear. If we assume a modal structure like

$$w = Re\left\{ W(z) \exp\left[i(kx + ly - \sigma t) \right] \right\} \qquad (2.2.7)$$

We have the equation for the amplitude of the vertical velocity

$$W_{zz} + \frac{(\sigma^2 - N^2)}{(f^2 - \sigma^2)} \alpha^2 W = 0 \qquad (2.2.8)$$

where, for the two-dimensional case, considered from now on

$$k = 0 \quad \text{and} \quad \alpha^2 = l^2 \qquad (2.2.9)$$

The boundary conditions at the surface and at the bottom are, respectively,

$$W = 0 \quad \text{at} \quad z = 0, -H \tag{2.2.10}$$

We need two more equations to compute the fluxes, that is, the temperature and the salinity diffusion equations,

$$T_t + \vec{u} \cdot \nabla T = k_T \nabla^2 T \tag{2.2.11}$$

and

$$S_t + \vec{u} \cdot \nabla S = k_S \nabla^2 S \tag{2.2.12}$$

where K_T and K_S are the molecular diffusivities of temperature and salt. Their values are $K_T = 1.5 \times 10^{-3} cm^2/s$ and $K_S = 1.3 \times 10^{-5} cm^2/s$. Perturbations in S and T are related to the density by the linearized equation of state

$$\rho = \rho_0 (1 - \alpha_T \Delta T + \beta \Delta S) \tag{2.2.13}$$

where α_T is the thermal expansion coefficient, here having the constant value $\alpha_T = 2.0 \times 10^{-4} {}^{\circ}c^{-1}$ and β is the salinity contraction coefficient also assumed constant and equal to $\beta = 7.3 \times 10^{-4}$ $‰^{-1}$.

From (2.2.13) we can see that we can have gradients in temperature and salt, without a density gradient, provided that $\alpha_T \Delta T$ balances $\beta \Delta S$. This argument can be used to justify the omission of density density diffusion terms in (2.2.4) but retention of diffusion of temperature and salinity terms in (2.2.11) and (2.2.12).

2.3 Computation of the Fluxes

Here we are going to develop a method to compute wave induced fluxes of temperature. The salt fluxes are similar, one just has to replace the heat diffusivity K_T by the salt diffusivity K_S and the temperature gradient $\bar{T}_z$ by the salt gradient $\bar{S}_z$.

In the previous section we assumed a vertical velocity field like (2.2.7) whose amplitude $W(z)$ satisfied equation (2.2.8).

We assume a temperature field like

$$T(y,z,t) = \bar{T}(z) + T'(y,z,t) \tag{2.3.1}$$

where $\bar{T}(z)$ is assumed to be linear. The same could be done for the salinity field. By the substitution of (2.3.1) in (2.2.11) where the velocity field can be replaced by its perturbation part only after neglecting the second order terms we get

$$T'_t - K_T (T'_{yy} + T'_{zz}) = - w \bar{T}_z \tag{2.3.2}$$

where $\bar{T}_z$ is constant. We assume that the solution of (2.3.2) will have the form

$$T' = Re [T(z) \exp i(ly - \sigma t)] \tag{2.3.3}$$

which substituted in (2.3.2) yields

$$T'_{zz} + \frac{i\sigma}{K_T} T' = w \frac{\bar{T}_z}{K_T} \tag{2.3.4}$$

Here we have neglected the horizontal diffusion term compared to the vertical one, since $\ell^2 << \sigma / k_T$.

The Green's function G(z,a) appropriate to the differential equation (2.3.4) is

$$G(z,a) = \begin{cases} \dfrac{\exp(i-1)(\sigma/2k_T)^{1/2}(z-a)}{2(i-1)(\sigma/2k_T)^{1/2}} , & z < a \\ \\ \dfrac{-\exp(i-1)(\sigma/2k_T)^{1/2}(z-a)}{2(i-1)(\sigma/2k_T)^{1/2}} \end{cases} \tag{2.3.5}$$

where the boundary conditions used were

$$G(\pm\infty) = 0 \tag{2.3.6}$$

The solution of the equation (2.3.4) will then be

$$T' = -\frac{\overline{T}_z}{K_T} \int_{-\infty}^{+\infty} G(z,a)\, w(a)\, da \tag{2.3.7}$$

Here we will try to maintain the discussion as general as possible to arrive at an expression for the fluxes, which will depend only on w and N(z) . The vertical scale of variations of w is given by $(w/w_{zz})^{1/2}$ and if we assume $(|w|/|w_{zz}|)^{1/2} >> (K_T/\sigma)^{1/2}$, that is the scale of diffusion, we can write

$$w(a) = w + (z-a)\frac{w_z}{1!} + (z-a)^2\frac{w_{zz}}{2!} + \ldots$$

Then substitute in (2.3.8) and perform the integration term by term. The first real, nonzero term arises from the third integral

$$\int_{-\infty}^{+\infty} G(z,a)(z-a)^2 \frac{w_{zz}}{2!}\, da \qquad (2.3.8)$$

resulting for T'

$$T' = \frac{w \bar{T}_z}{i\sigma} + \frac{K_T \bar{T}_z}{\sigma^2} w_{zz} + \cdots \qquad (2.3.9)$$

The vertical temperature flux will be

$$\langle w'T' \rangle = K_T \bar{T}_z \frac{\overline{w\, w_{zz}}}{\sigma^2} \qquad (2.3.10)$$

where the overbar means a phase average over a period. Once the average is performed we can rewrite (2.3.10) as

$$\langle w'T' \rangle = K_T \bar{T}_z \frac{W W_{zz}}{2\sigma^2} \qquad (2.3.11)$$

where $W(z)$ is now the amplitude of the vertical velocity and solution of equation (2.3.2). Here we must have in mind that when averaging over a period

$$\overline{w\, w_{zz}} = \frac{W W_{zz}}{2} \qquad (2.3.12)$$

An interesting parameter to analyse is the Nusselt number Nu , a non-dimensional heat flux, defined as the ratio of the actual heat transport to the purely diffusive flux which would occur through a linear temperature gradient. The Nusselt number can be computed from (2.3.11), being

$$N_u = -\frac{\langle w'T' \rangle}{k_T \bar{T}_z} = -\frac{\overline{w\, w_{zz}}}{\sigma^2} \tag{2.3.13}$$

Now if we multiply equation (2.2.8) by W^* we get

$$W^* W_{zz} = -\frac{(N^2 - \sigma^2) l^2 W^2}{(\sigma^2 - f^2)} \tag{2.3.14}$$

that when substituted in the expression for the temperature flux (2.3.12) yields

$$\langle w'T' \rangle = -\frac{k_T \bar{T}_z}{\sigma^2} \frac{(N^2 - \sigma^2) l^2}{(\sigma^2 - f^2)} \frac{W^2}{2} \tag{2.3.15}$$

Similar expressions for salinity flux can be obtained by exchanging the diffusivity coefficient by K_S and the gradient by the salinity one, $\bar{S}_z$.

At this point if we know the Brunt-Vaisala frequency distribution, the dispersion relation and W2 we will be able to compute the vertical temperature flux. Here we can see more clearly the dependence of the temperature flux on the frequency and wave number.

A quick look at equation (2.3.15) would suggest that the fluxes will be large near $\sigma = f$ and negligible near $\sigma = N$, but on the other hand the vertical velocity spectrum near f will be negligible since at this frequency we only expect to have horizontal motions.

In equation (2.3.10) and (2.2.13) $w w_{zz}$ is a measure of the deformation of the field. We would then expect that more deformation will be achieved by short wavelength (large wave numbers) waves. So the ℓ^2 dependence in (2.3.15) will make the flux smaller for waves of small wave numbers.

Equation (2.3.15) is an important result in the sense that once we know the spectrum of the vertical velocity we will be able to know the contribution in temperature flux for a given frequency band or wave number band, as well as the contribution for all the internal wave spectrum. In order to obtain this information just integrate (2.3.15) over the frequency or the wavenumber. Better results will be attained with a numerical integration. A more rapid answer can be obtained by fitting a straight line to the desired frequency (wave number) band of the spectra to obtain the local slope, and then integrating (2.3.15) analytically, but at a cost of accuracy.

Another interesting result to note is that the Nusselt numbers for temperature and salinity will be the same, and equal to

$$Nu = \frac{(N^2 - \sigma^2)}{(\sigma^2 - f^2)} \frac{\ell^2}{\sigma^2} \frac{w^2}{2} \qquad (2.3.16)$$

Again we see that larger Nusselt numbers will be attained at low frequencies.

In order to estimate the importance of this process we can estimate an effective heat diffusivity coefficient from (2.3.10) as

$$A_T = K_T \frac{\overline{w w_{zz}}}{\sigma^2} \qquad (2.3.17)$$

If we assume a vertical displacement of the thermocline of 10m due to an internal tidal wave $w \sim 0(2.2\text{x}10^{-2}\text{cm/s})$, and also assuming $\overline{w w_{zz}} \sim 0(2.2\text{x}10^{-6}\text{cm}^{-1}\text{sec}^{-1})$ and $\sigma \sim 0(10^{-4}\text{sec}^{-1})$ an estimate of the effective coefficient will be given by

$$A = 3.7\text{x}10\text{-}3 \text{ cm}2/\text{s}$$

and an estimate for the Nusselt number will be of 2.5. These figures are neither big enough to confirm the importance of the process, nor small enough to dismiss it.

2.4 Applications to a Simple Model

In order to apply the results of the previous section, we shall use the simplest possible stratification, a constant N. Let the constant frequency of Brunt-Vaisala be N_o, and assume a flat bottom of a depth $-H$. Assuming a vertical velocity as in (2.2.7), the governing equation will be

$$W_{zz} + \frac{(N_o^2 - \sigma^2)}{(\sigma^2 - f^2)} l^2 W = 0 \tag{2.4.1}$$

The Brunt-Vaisala frequency is given by

$$N_o^2 = g \alpha_T \bar{T}_z \tag{2.4.1a}$$

The boundary conditions are:

$$W = 0 \quad \text{at} \quad z = 0, -H \tag{2.4.3}$$

Then if

$$\gamma^2 = l^2 \frac{(N_o^2 - \sigma^2)}{(\sigma^2 - f^2)} \tag{2.4.3}$$

The solution of (2.4.1) and (2.4.2) is

$$W = RB \sin \gamma z \tag{2.4.4}$$

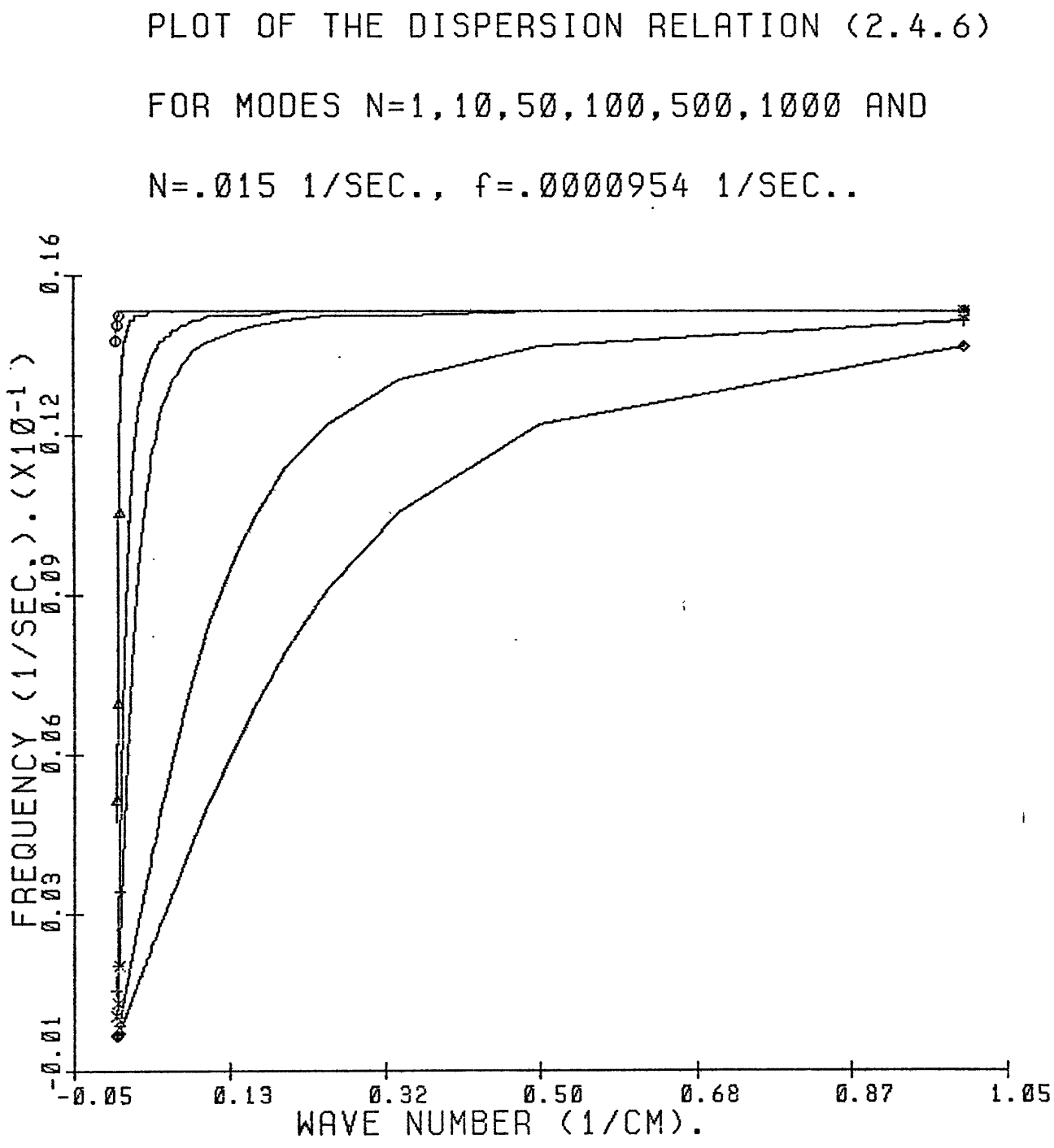


Figure 2.4.1. The dispersion relation (2.4.6) for modes n= 1,10,50,100, 500 and 1000. For f=.0000954 sec^{-1}, N=.01958 sec^{-1} and H= 100 m.

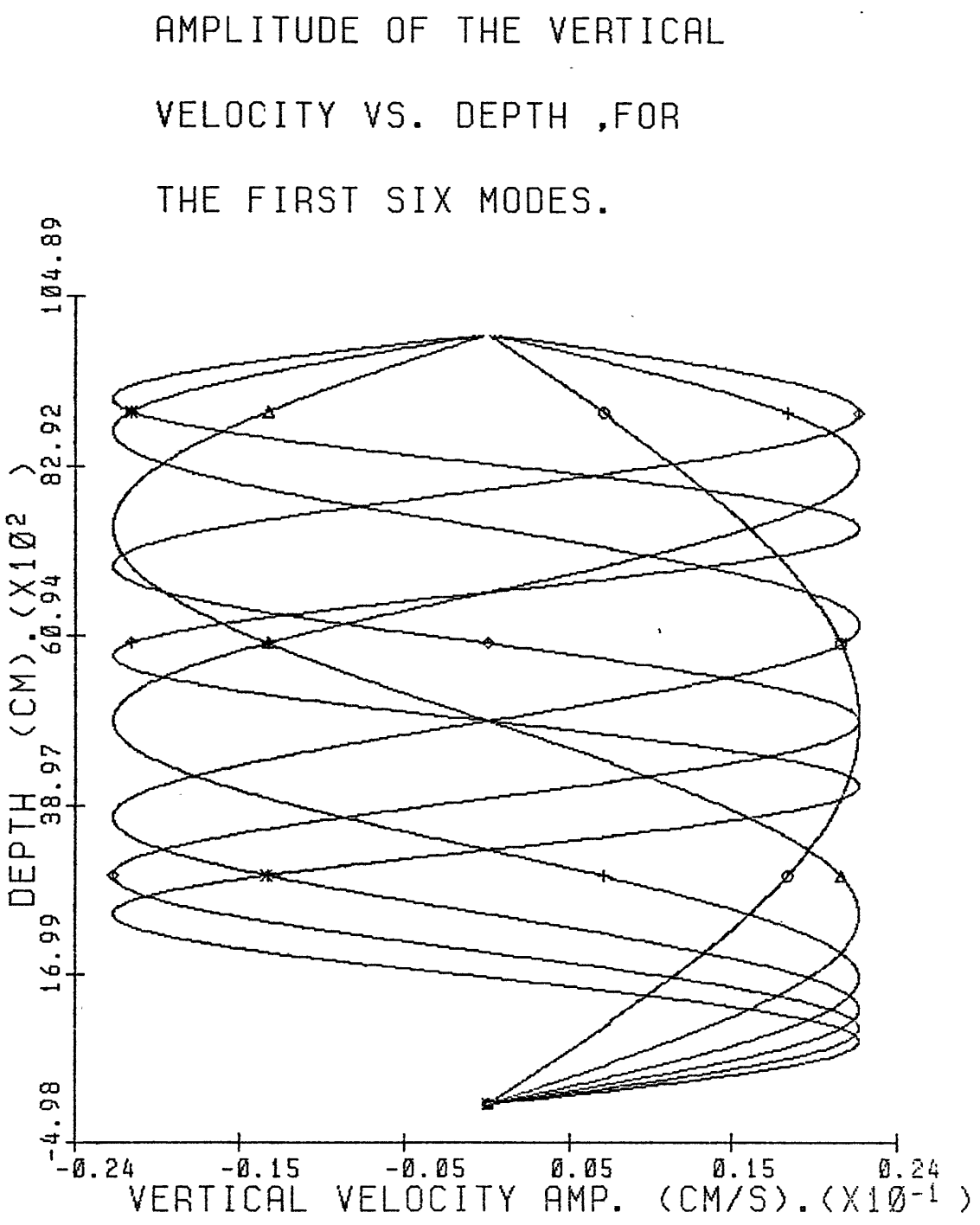


Figure 2.4.1a. The six first modes of the vertical velocity amplitude for the constant N case, f=.0000954 sec^{-1} ,N=.01958 sec^{-1} and H=100m.

where R is a specified amplitude and B is a constant. Here we are going to specify the value of R as .02 cm/s. The application of the second boundary condition gives us the eigenvalues

$$\gamma_H = n\pi \qquad (n = 1,2,3,\ldots) \qquad (2.4.5)$$

so the dispersion relation is

$$\ell = \frac{n\pi}{H}\left(\frac{\sigma^2 - f^2}{N_o^2 - \sigma^2}\right)^{1/2} \qquad (2.4.6)$$

In order to determine the constant B we apply the normalization condition

$$\int_{-H}^{0} w\, w^* \, dz = H$$

ending up with $B = \sqrt{2}$.

Then the solution is

$$w(y,z,t) = R\sqrt{2}\, \sin \frac{n\pi z}{H} \cos(\ell y - \sigma t) \qquad (2.4.7)$$

A plot of the dispersion relation (2.4.6) for mode numbers n=1,10,50,200,500 and 1000 and of the first six modes of the vertical velocity amplitude is shown in figures 2.4.1,2.4.2 with R=.02 cm/sec.

At this point the next step would be solve the thermal diffusion equation (2.3.3). But in view of the results of the previous section, to compute the temperature flux and the Nusselt number we need only (2.4.7) and its second derivative with respect to z . Following this procedure the vertical temperature flux will be

$$\langle w'T' \rangle = -k_T \bar{T}_z \frac{R^2 \ell^2}{\sigma^2} \left(\frac{N_0^2 - \sigma^2}{\sigma^2 - f^2} \right) \sin^2 \frac{n\pi z}{H} \tag{2.4.8a}$$

or using (2.4.6) for

$$\langle w'T' \rangle = -k_T \bar{T}_z \frac{R^2 n^2 \pi^2}{\sigma^2 H^2} \sin^2 \frac{n\pi z}{H} \tag{2.4.8b}$$

and the corresponding Nusselt number,

$$N_u = \frac{R^2 n^2 \pi^2}{\sigma^2 H^2} \sin^2 \frac{n\pi z}{H} \tag{2.4.9}$$

The vertical divergence of the temperature flux will be

$$(\langle w'T' \rangle)_z = -\frac{n\pi}{H} k_T \bar{T}_z \frac{R^2 \ell^2}{\sigma^2} \frac{(N_0^2 - \sigma^2)}{(\sigma^2 - f^2)} \sin \frac{2n\pi z}{H} \tag{2.4.10}$$

From (2.4.10) we can see the tendency to form layers where $(\langle w'T' \rangle)_z > 0$. This would suggest as scale of the layers, $H/2n\pi$ or for $H = 100m$ the layers will form at approximately 16m, 8m , 5m and 4m for waves mode 1, 2, 3 and 4.

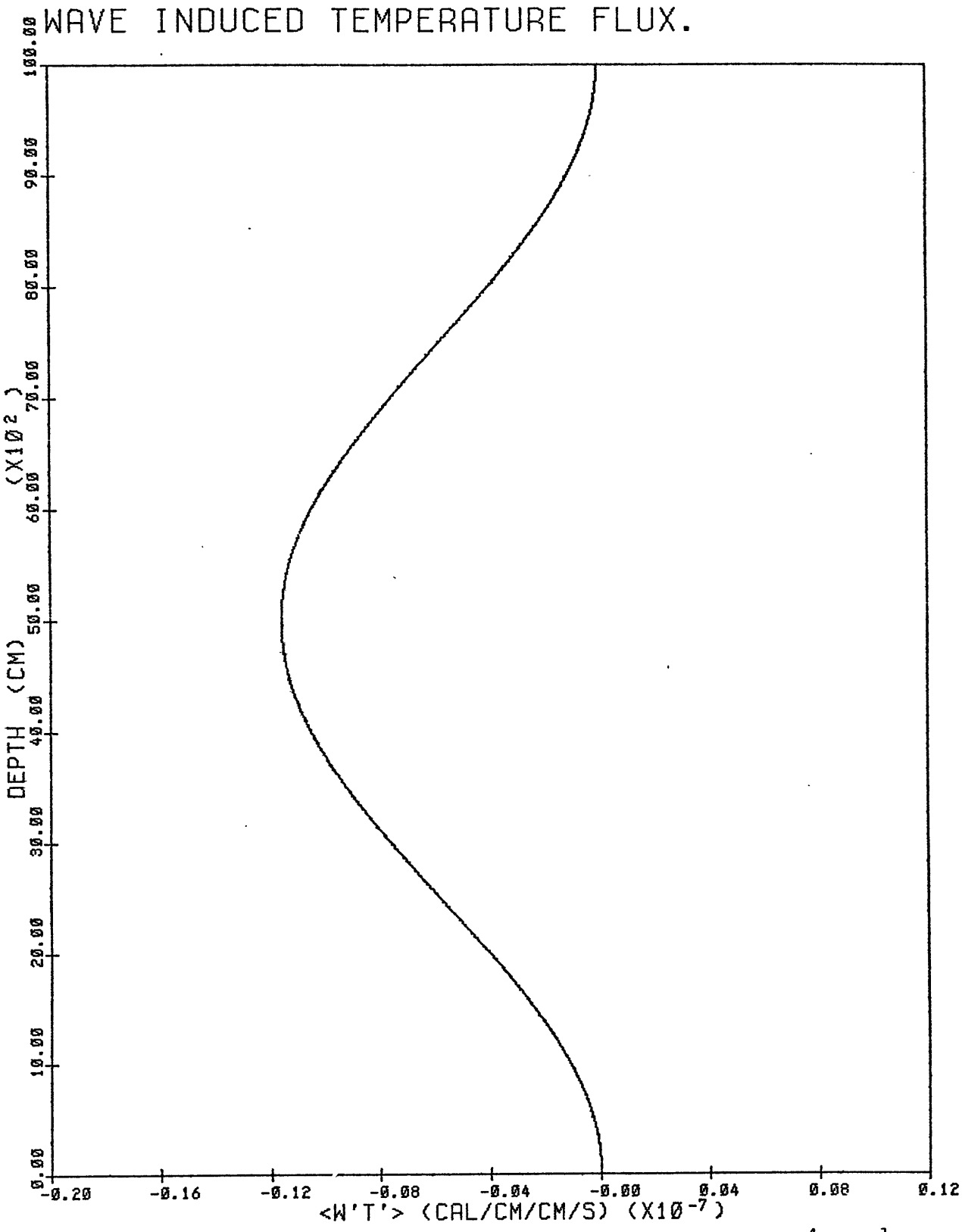


Figure 2.4.2. Wave induced heat flux due to wave n=1, $\sigma = 10^{-4}$ sec.$^{-1}$, $\ell = 4.8 \times 10^{-7}$ cm^{-1} and R=.02 cm/sec. in a constant N ocean 100m deep.

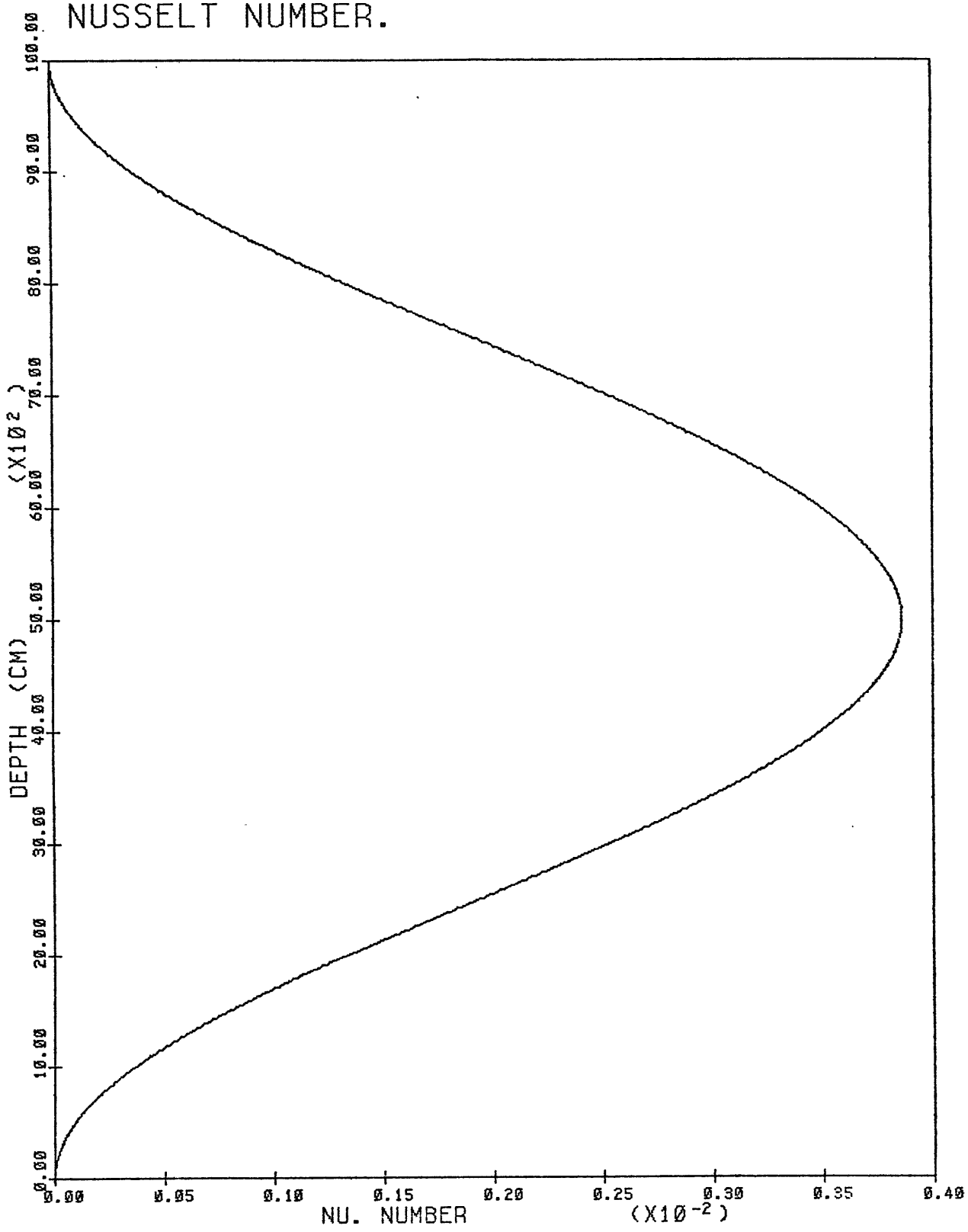


Figure 2.4.3. Nusselt number corresponding the wave induced flux of figure 2.4.2.

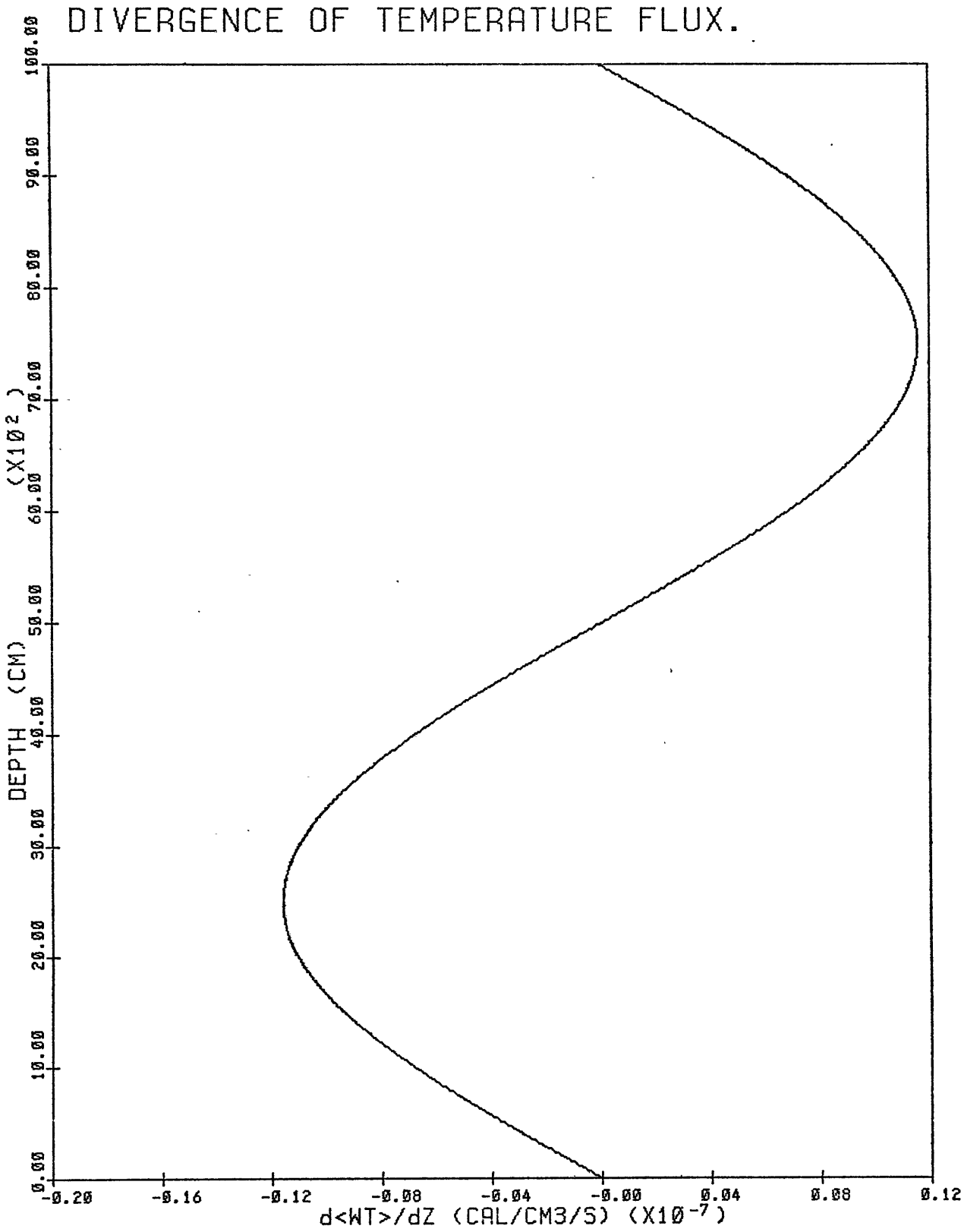


Figure 2.4.4. Vertical divergence of heat flux corresponding the wave induced flux of figure 2.4.2.

The waves in this simple case obey a dispersion relation such that at low frequencies $0(10^{-4}sec^{-1})$ the corresponding wave numbers are very small $0(10^{-6}cm^{-1})$. Wave numbers of $0(10^{-4}cm^{-1})$ are found for frequencies of $0(4.5x10^{-3}sec^{-1})$. All these results are for the first mode wave, n=1 . As one increases the mode the wave number increases for the same frequency. For the mode 10 wave (n=10) the typical M2 tide frequency $\sigma \backsim 1.48x10^{-4}sec^{-1}$ will correspond to a wavenumber of $0(2.4x10^{-5}cm^{-1})$.

The reason for this speculation about the M_2 tidal frequency and the corresponding wavenumber, is the surmise that the internal waves generated by tidal flow over topography could be responsible for a reasonable amount of mixing since most of the vertical signal comes from the tide. Surface manifestation of internal waves show groups or packets of width 3km to 5km separated by distances ranging from 4 to 40km. The wavelengths fall between 400m and 2200m (Mascarenhas, 1979).

In the present case the wavelengths derived from the dispersion relation are larger than what should be expected for the low mode waves, likely due to the density model that was used. Of course in the observed packets case, the Brunt-Vaisala frequency was approximately a sech 2 Az type, typical for summer thermocline. Meanwhile, N here is constant, making analogies difficult.

Figures 2.4.2 to 2.4.4 show the temperature flux, Nusselt number and the divergence of the flux, for an ocean 100m deep, for the first mode waves with $\sigma = 10^{-4}sec^{-1}$ and with the wave number computed from dispersion relation (2.4.6); $\ell = 4.8x10^{-7}cm^{-1}$. The flux Nu and

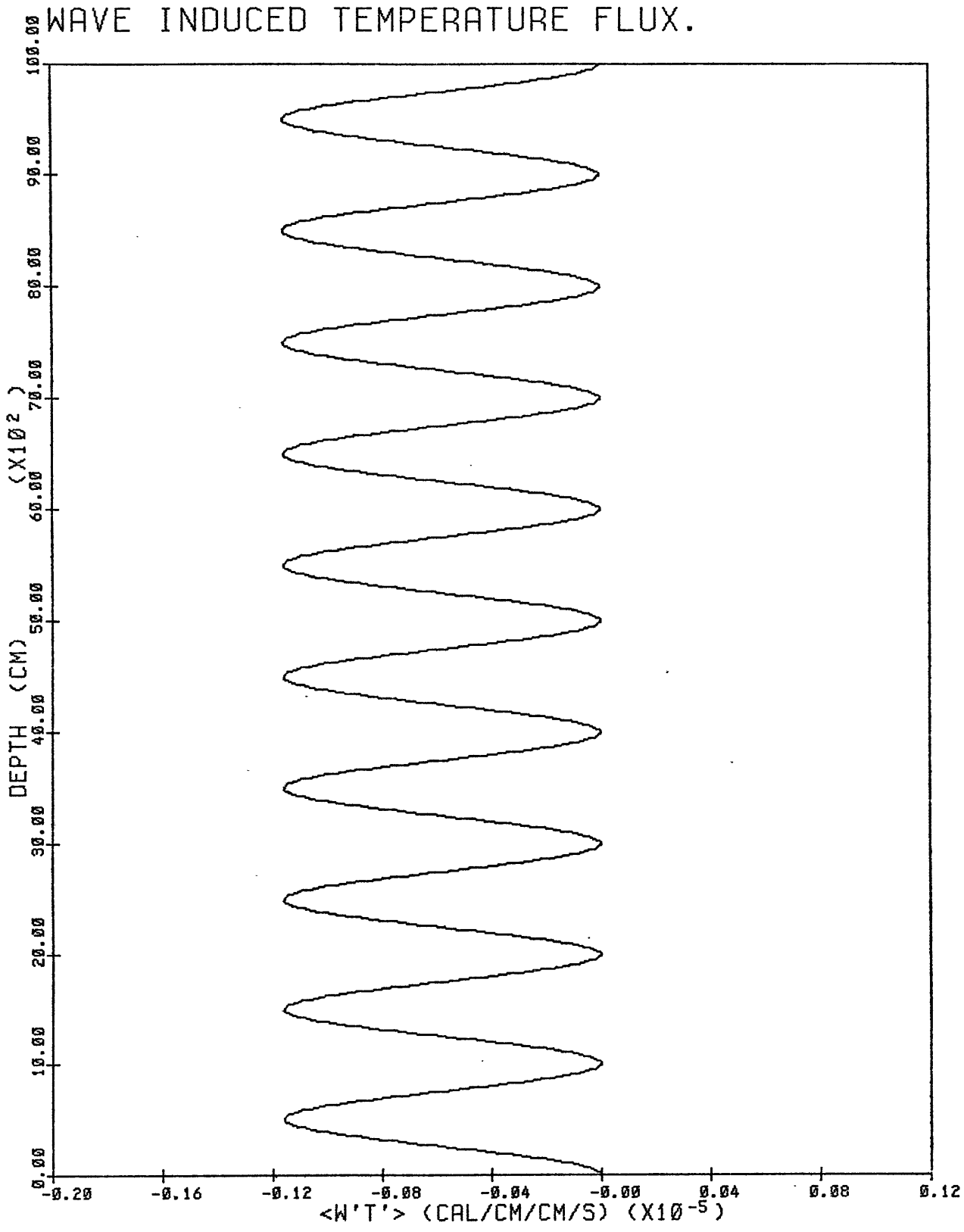


Figure 2.4.5. Wave induced heat flux due to wave n=10, $\sigma = 10^{-4}$ sec.$^{-1}$ $\ell = 4.8 \times 10^{-7}$ cm and R=.02 cm/sec. in a constant N ocean 100m deep.

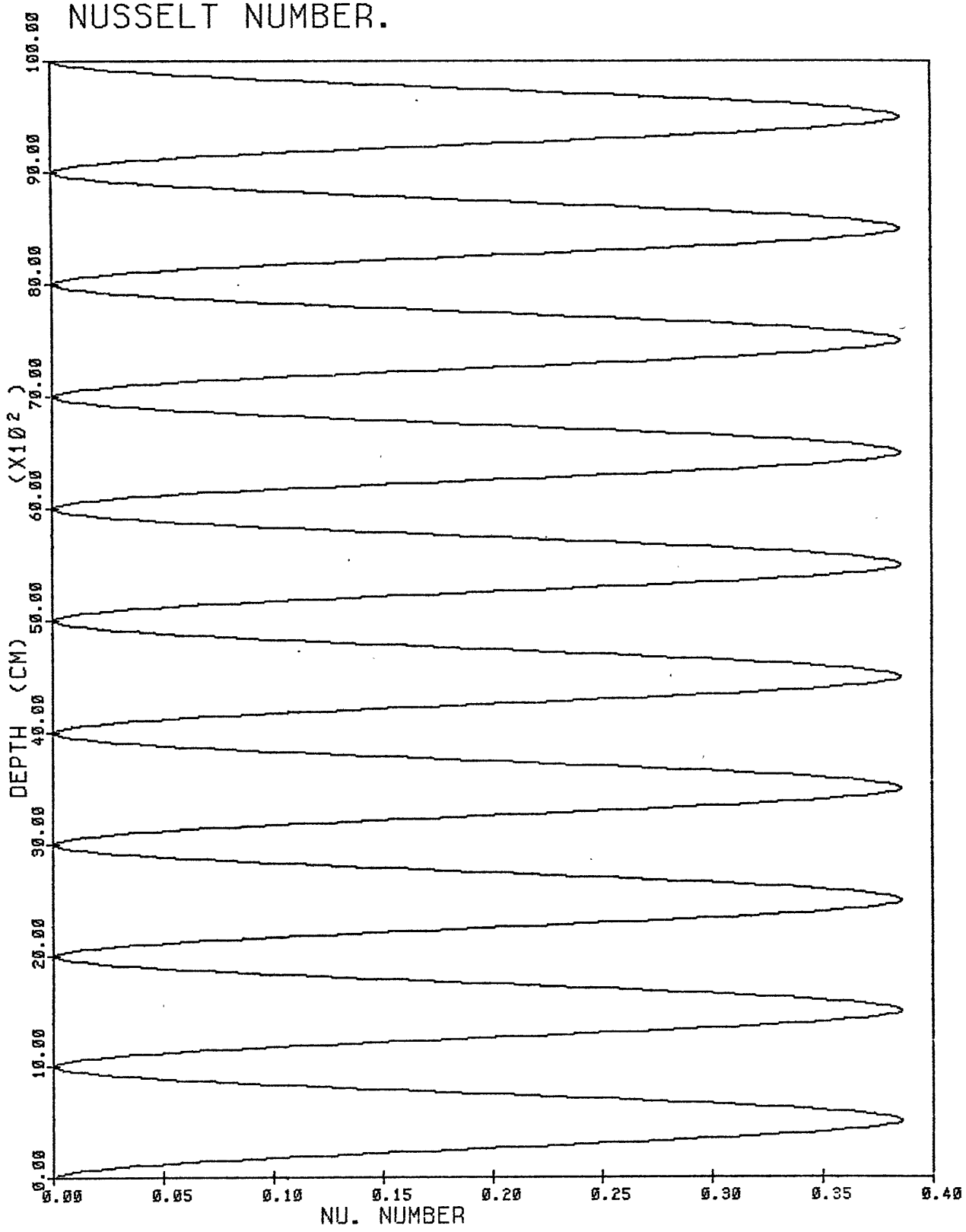


Figure 2.4.6. Nusselt number corresponding the wave induced flux of figure 2.4.5.

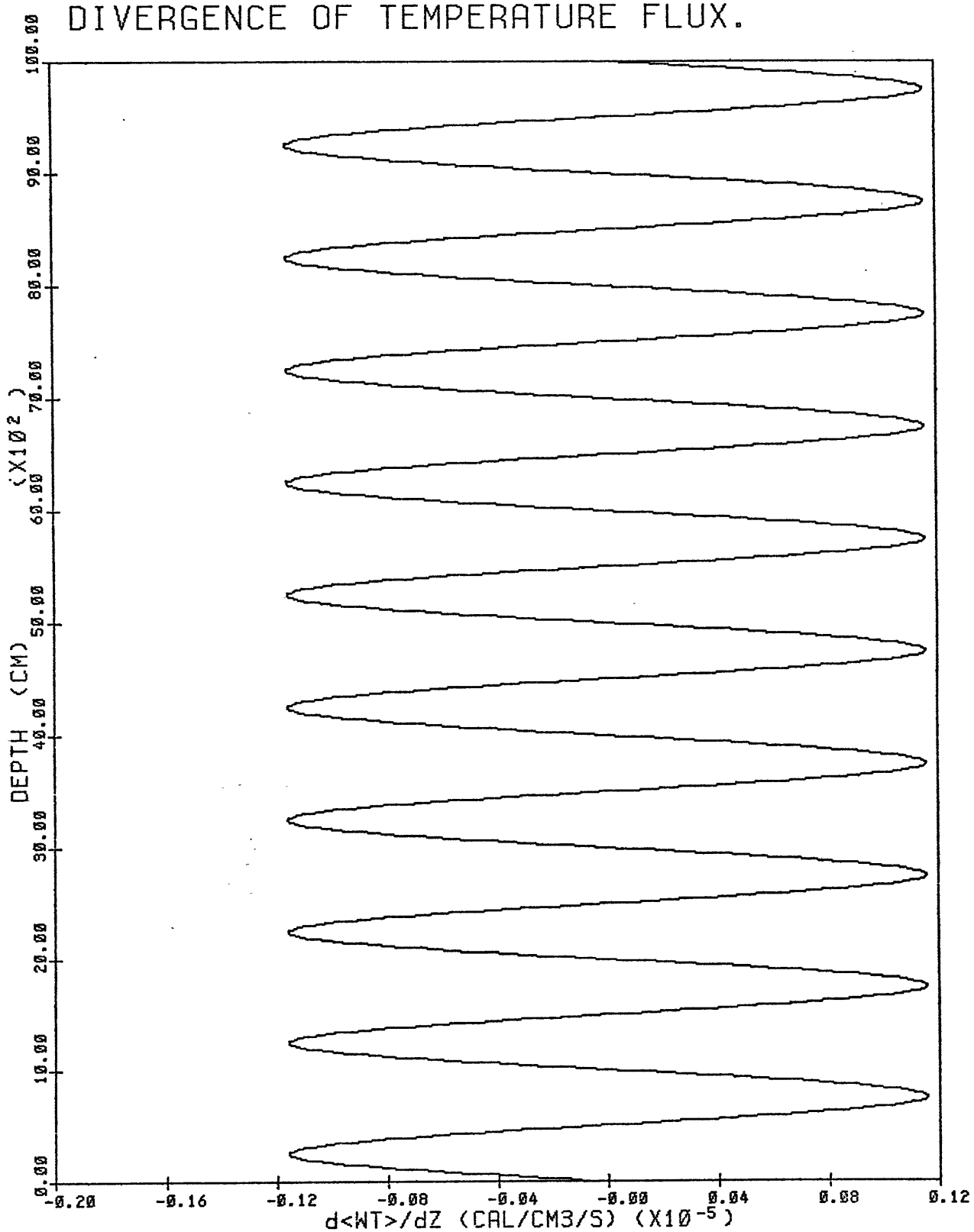


Figure 2.4.7. Vertical divergence of heat flux corresponding the wave induced flux of figure 2.4.5.

the divergence are negligible because even though the wave is low frequency the wave number is awfully small. The wave-induced fluxes are always negative, meaning that the fluxes are in the same direction as the molecular fluxes. Also, the mean divergence of heat flux is zero indicating that there is no vertical exchange of heat but only a tendency to layer the smooth stratification.

The next figures, 2.4.5 to 2.4.7, show plots of the same quantities for the same conditions but for a 10th mode wave, showing that the flux, Nu and the divergence increasing by two orders of magnitude, with Nu = .5. The same quantities computed for a wave with mode number n=100, but not shown here, yield fluxes of $0(10^{-4}cal/cm^2/s)$ and Nu=0(50). Computation of the above quantities for frequency of one order of magnitude less also yields negligible values for Nu . On the other hand, taking mode number n=1 , and choosing the pair of frequency $\sigma = 10^{-4}sec^{-1}$ and wavenumber $\ell = 10^{-4}cm^{-1}$ we find values of temperature flux of $0(10^{-4}cal/cm^2/sec)$, Nusselt numbers of 0(200) and a divergence of the flux $0(10^{-4}cal/cm^3/sec)$. These results are shown in figures 2.4.8 to 2.4.10.

As already mentioned before, the reason why high frequency wave exhibit negligible values of wave-induced fluxes is because there is not enough time for diffusion of temperature in each cycle. A last calculation was made for $\sigma = 10^{-3}sec^{-1}$ and n=10 yielding a $\ell = 1.6x10^{-4}cm^{-1}$ for wave number and fluxes, Nu and divergences of the same order of magnitude as for the case $\sigma = 10^{-4}sec^{-1}$ and n=1.

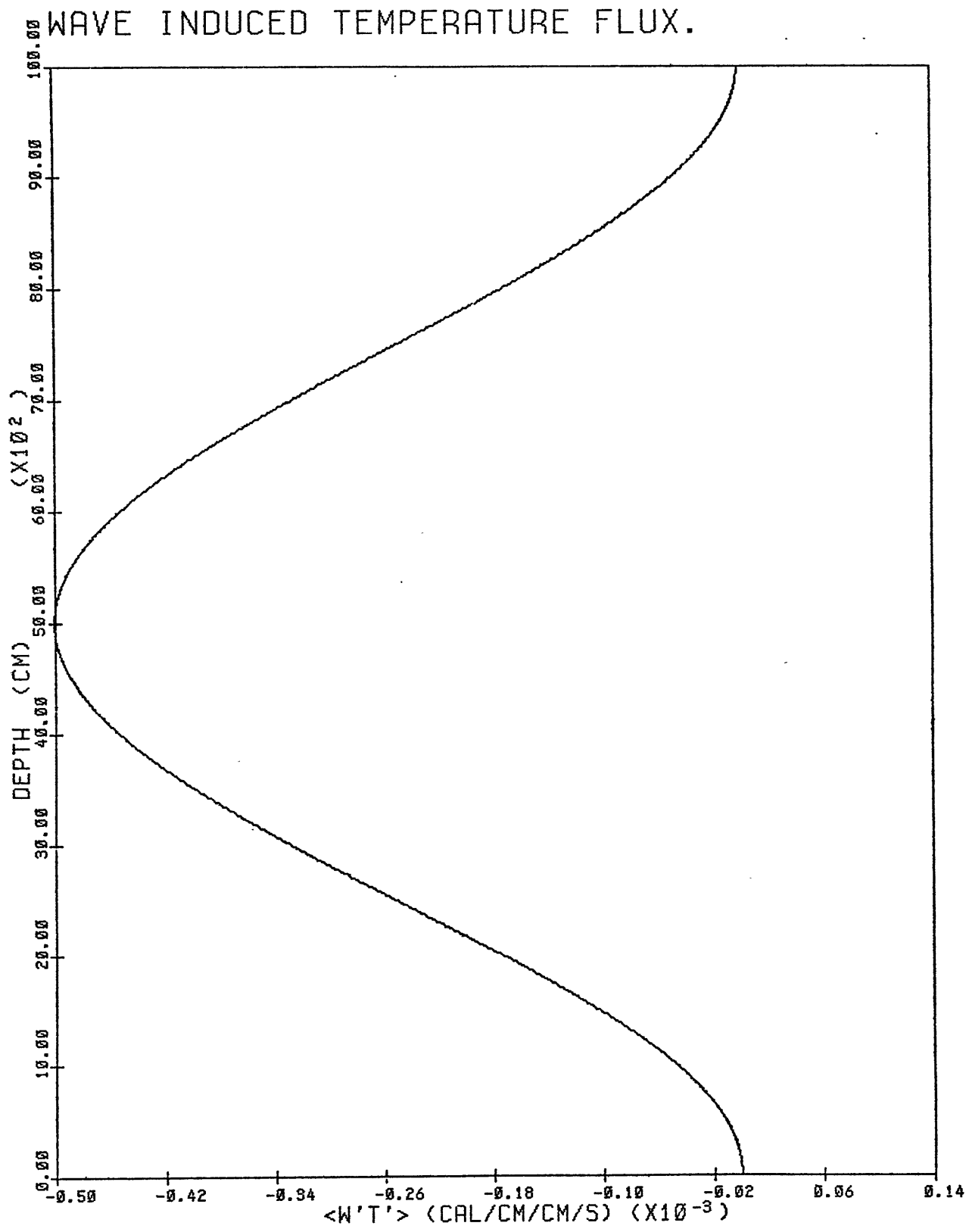


Figure 2.4.8. Wave induced heat flux due to a wave n=1, $\sigma = 10^{-4}\,\mathrm{sec}^{-1}$ $\ell = 10^{-4}\,\mathrm{cm}^{-1}$ and R=.02 cm/sec. in a constant N ocean 100m deep.

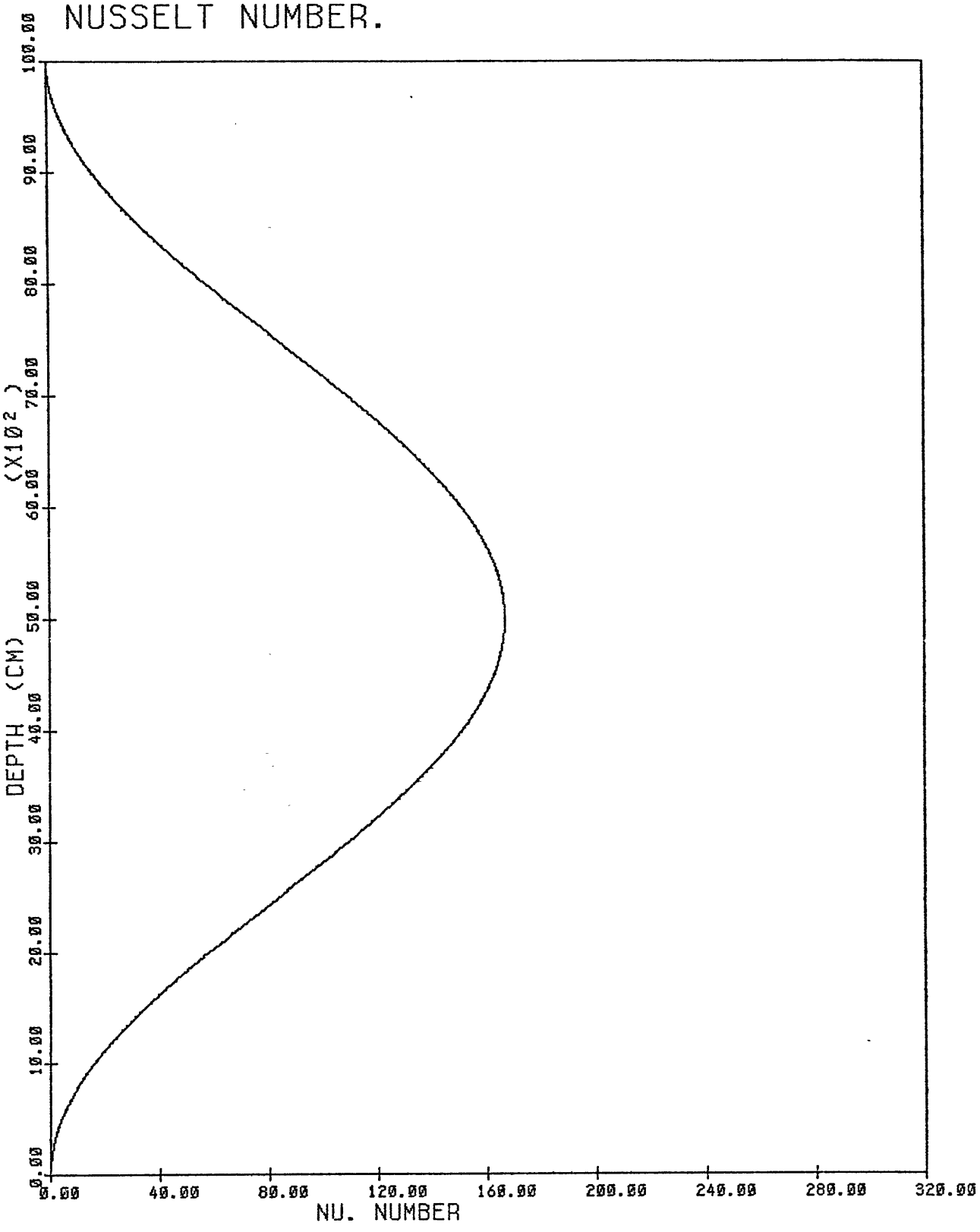


Figure 2.4.9. Nusselt number corresponding the wave induced flux of figure 2.4.8.

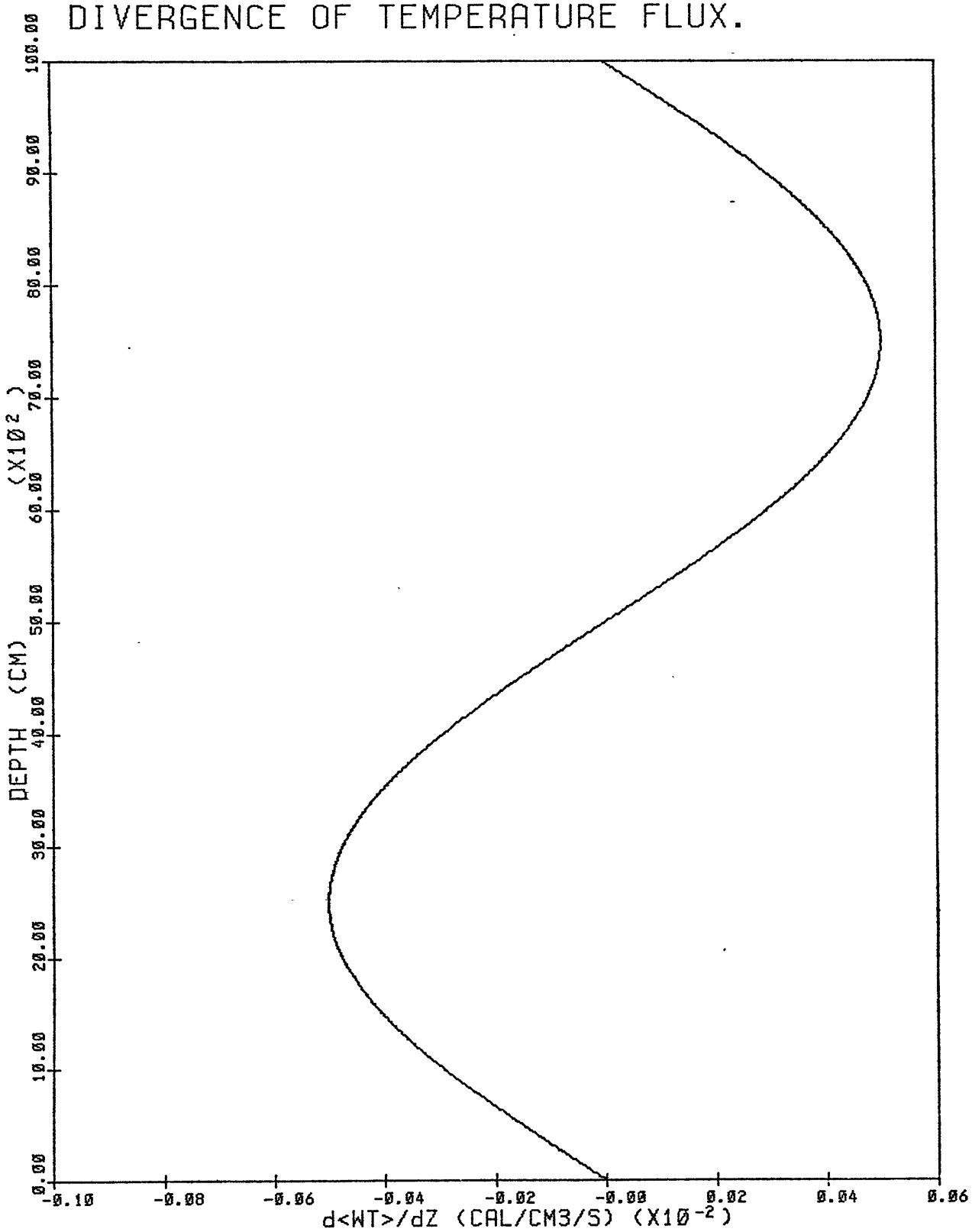


Figure 2.4.10. Vertical divergence of heat flux corresponding the wave induced flux of figure 2.4.8.

Since low frequency free internal waves tend to have low wave number, what we can conclude from the results is that we cannot expect the wave induced process be effective for free internal waves. On the other hand, forced internal waves will probably make the process effective.

2.5 Relationship to observations

It is more difficult to measure velocity fluctuations in internal waves than it is to measure temperature. In addition to fine strucutre contamination, problems of instrumental inertia and positioning are critical. In spite of these difficulties, long records of horizontal velocity variations have been obtained by Fofonoff and Webster (1971), Gould, Schmitz and Wunsch (1974). Even more problematic are measurements of the vertical velocity. The primary reason for the difficulty is the instrument alingnment problem, to avoid serious contamination from the much stronger horizontal motion. The first attempts in doing such measurements were done by Webb and Worthington (1968) and Voorhis (1968) using a neutrally buoyant rotating float. Voorhis' measurements indicate the potential energy of vertical displacements is approximately equal to the kinetic energy of the

horizontal velocity components. These results stimulated investigations of the relationship between horizontal and vertical components of velocity in the ocean, as in the simple model by Fofonoff (1969).

There are at least two approaches by which the vertical velocity w can be computed from mooring measurements. Here we are going to apply the one used by Ruddick and Joyce (1979).

If we assume that the temperature variations are primarily due to vertical advection, we can write

$$w = - T_t / \bar{T}_z \tag{2.5.1}$$

Now if we take the Fourier transform of (2.5.1), and its conjugate, defined as

$$\hat{w} = \frac{1}{n\Delta t} \int_{-n\Delta t/2}^{n\Delta t/2} w(y,z,t)\, e^{-i\sigma t}\, dt \tag{2.5.2}$$

where $n\Delta t$ is the duration of the record, we have

$$\hat{w} = - i\sigma \hat{T} / \bar{T}_z \tag{2.5.3a}$$

$$\hat{w}^* = i\sigma \hat{T}^* / \bar{T}_z \tag{2.5.3b}$$

Then the auto spectra will be

$$\hat{w}\hat{w}^* = \frac{\sigma \hat{T}\hat{T}^*}{\overline{T}_z^2} \tag{2.5.4}$$

The important question in this section is: What do we need to measure in the field, in order to estimate the wave-induced fluxes? If we take the Fourier transform of equation (2.3.2), under the assumption $\ell^2 << \sigma/k_T$, and multiply by the Fourier transform of the conjugate of T , we get

$$-i\sigma \hat{T}\hat{T}^* + \hat{w}\hat{T}^*\overline{T}_z = k_T \hat{T}_{zz}\hat{T}^* \tag{2.5.5}$$

Now take the FT of the conjugate equation (2.3.2) and multiply by the FT of T , obtaining

$$i\sigma \hat{T}^*\hat{T} + \hat{w}^*\hat{T}\overline{T}_z = k_T \hat{T}^*_{zz}\hat{T} \tag{2.5.6}$$

If we add (2.5.5) and (2.5.6)

$$(\hat{w}\hat{T}^* + \hat{w}^*\hat{T}) = \frac{k_T}{\overline{T}_z}(\hat{T}^*\hat{T}_{zz} + \hat{T}^*_{zz}\hat{T}) \tag{2.5.7}$$

or

$$\langle \hat{w}\hat{T} \rangle = -\frac{g\alpha_T k_T}{N^2} \langle \hat{T}\hat{T}_{zz} \rangle \tag{2.5.8}$$

The expression (2.5.8) tells us that in order to have an estimate of the wave-induced temperature flux, we need one mooring with at least two temperature recorders sufficiently spaced to give enough vertical resolution. It is clear that a linear model cannot yield the slope of the spectrum as a function of frequency because the fluctuations at each frequency are independent of all other frequencies and the slope of the spectrum must depend upon nonlinear interactions as discussed by Garrett and Munk (1972,1975). The ideal here would be to relate $\omega^2 \omega_{zz}$ to the temperature spectra or to the vertical velocity spectra through equation 2.5.4.

2.6 Further comments

In spite of our being much more concerned here with the cause of the irregular layering in the vertical structure of temperature and salinity in the ocean than with consequent mixing, we are tempted to trace a parallel to other processes of vertical mixing. The main problem with this is that the other processes that are known to be the most important source of energy for the generation of micro-structure in the ocean have different lengths and time scales. According to Munk's terminology the process studied here is classified as fine structure. Meanwhile the model of Osborn and Cox (1972) which proposes to explain vertical diffusion by turbulent mixing is classified as microstructure process. We personally think that they overlap in the upper end of microscale and lower end of fine scale. Our present study has the time

scale of $2\pi/f \sim 12$ hours. Osborn and Cox suggest time scales ranging from seconds to days, depending upon the thickness of the layers. In spite of everything, we still think a comparison of orders of magnitude is valid.

In an earlier work, Osborn and Cox (1972) presented some of the first detailed vertical temperature profiles obtained from a free-fall instrument. In the same paper, they proposed a model for estimating, under certain restrictions, the local vertical diffusion based on knowledge of the average variance of the temperature micro-structure and the value of the mean vertical temperature gradient. The assumptions of the Osborn-Cox model are that the only heat flux is vertical and arises from internally generated turbulence that can be observed as microstructure in a vertical profile. According to their data, estimates of the turbulent heat flux and effective coefficient were respectively,

$$\langle w'\theta' \rangle \simeq .55\text{x}10^{-5} \text{ cal/cm}^2\text{/s}$$

$$A_T \simeq 6.0\text{x}10^{-2} \text{ cm}^2\text{/s}$$

for a measured $\partial\theta/\partial z \sim 10\text{-}4$ c/cm.

A month-long series of vertical temperature gradient profiles performed in the C-scale region by Elliott and Oakey (1979) during the GATE using a microstructure measuring instrument named "Octuprobe" was used to estimate vertical diffusion. They used the Osborn-Cox model and

their results yield a mean value of A_T of about $5.3 \times 10^{-3} cm^2/s$ to $1.6 \times 10^{-2} cm^2/s$.

The effective diffusivity coefficient (2.3.17) for the linear stratification case is

$$A_T = \frac{K_T R^2 n^2 \pi^2}{\sigma^2 H^2} = 5.9 \times 10^2 \frac{n^2}{H^2} \qquad (2.7.1)$$

where we used the values $K_T = 1.5 \times 10^{-3} cm^2/s$, R=.02 cm/s and $\sigma = 10^{-4} s^{-1}$. So for H= 100m, n=1, $A_T = 5.9 \times 10^{-6} cm^2/s$, meanwhile for n=10 , $A_T = 5.9 \times 10^{-4} cm^2/s$. For H=40m and n=10 , $A_T = 3.7 \times 10^{-3} cm^2/s$. Also for comparison estimates of heat flux can be taken from figure 2.4.2, even for the most non propitious case examined the wave-induced fluxes are $O(.2 \times 10^{-8} cal/cm^2/s)$, yielding larger values for highest modes, as already seen.

The other process that could be accounted for by mixing is the double-diffusive instabilities. It is important to realise that the net mass flux in these processes is downwards. The calculation of Schmitt and Evans (1978) for the central water of the North Atlantic implies an eddy diffusivity for heat of $3.10^{-2} cm^2/s$ and about $10^{-1} cm^2/s$ for salt. As we can see the findings are not encouraging if we imagine the process as due to free internal wave. But if instead we think in forced internal waves, as for instance topographic internal waves due to tide, we will expect larger amplitudes and larger wave numbers, yielding consequently large fluxes and Nusselt numbers.

Chapter III

Wave Induced Layering in Fronts

3.1 Introduction

Remote sensing images of oceanic fronts, especially the ones taken by synthetic-aperture radar (SAR), show some oceanographic features never observed before. They appear like small-scale linear striations trapped between the two current boundaries and approximately parallel to the current boundaries. It is a well-known fact that mixing processes can be generated by instabilities generated by double diffusion processes (Turner, 1973). The importance of these mechanisms in the mixing process is discussed by Worthem et al. (1983), who showed that shear and rotation in combination can induce thermohaline instability and cause mixing under conditions that would otherwise be stable. A recent review of the phenomenon is that of Huppert and Turner (1981). They cited that the strongest layering, in general, is found near boundaries between water masses of different origin. Layers are most prominent when there is large horizontal contrast in temperature and salinity, but a small net density difference. We should therefore expect to find layers in frontal zones, not only constricted to zones where the gradient of temperature and salinity are the strongest.

In this chapter, using some results of Chapter II, we will show that a wave perturbation propagating along a front will induce fluxes of temperature and salinity due to the deformations of the mean field. From these fluxes we see the tendency to form layers, and we suggest

that the striations are a result of the advection of those layers by shear in combination with diffusion.

3.2 The mean field, perturbation equations, and scaling.

Let us consider a typical front parallel to the xy plane, tilted with respect to the horizontal by an angle α , as shown in figure 3.2.1. The densities on both sides of the front are considered uniform. The front itself is a layer of thickness h , in which the density varies only in the direction perpendicular to the front. The velocity field is considered to vary in the cross front direction with a constant value U above the front and negligible below it.

The momentum equations in the x,y,z directions, assuming no variations along x axis and using the Boussinesq approximation are

$$u_t + \vec{u}.\nabla_2 u - fv = \nu \nabla_2^2 u \qquad (3.2.1)$$

$$v_t + \vec{u}.\nabla_2 v + fu = -\frac{1}{\rho_o} p_y + \nu \nabla_2^2 v \qquad (3.2.2)$$

$$w_t + \vec{u}.\nabla_2 w = -\frac{1}{\rho_o} p_z - \frac{g\rho'}{\rho_o} + \nu \nabla_2^2 w \qquad (3.2.3)$$

Here $\vec{u}$ =(u,v,w) is the velocity in terms of its components, f = 2Ω sin φ is the Coriolis parameter, p is the pressure less the hydrostatic part, ρ' denotes the density perturbation and ∇_2 denotes the operator in the y and z directions only. the equation of continuity under the same conditions reads,

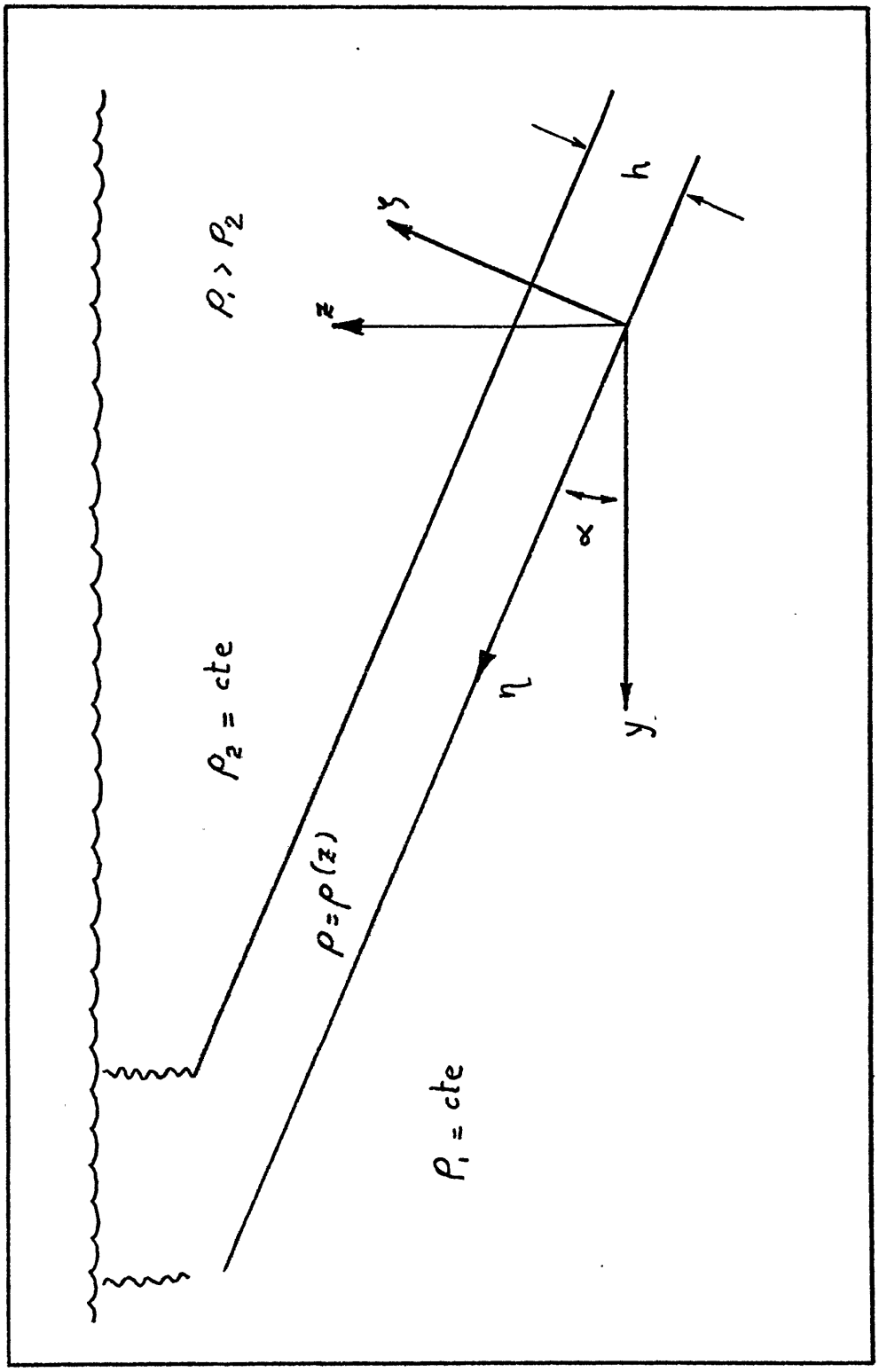


Figure 3.2.1. Sketch of the front and the system of coordinate.

$$v_y + w_z = 0 \tag{3.2.4}$$

and finally the density equation,

$$\rho'_t + \underline{u} \cdot \nabla_2 \rho' + w \bar{\rho}_z = 0 \tag{3.2.5}$$

Now choose a coordinate system η , ζ tilted by an angle α with respect to y , such that the axis $O\eta$ is parallel to the front layer. The new system is related to the old one by

$$\eta = y \cos\alpha + z \sin\alpha \tag{3.2.6a}$$

$$\zeta = -y \sin\alpha + z \cos\alpha \tag{3.2.6b}$$

so the deviations in the new system will be

$$\frac{\partial}{\partial z} = \sin\alpha \frac{\partial}{\partial \eta} + \cos\alpha \frac{\partial}{\partial \zeta} \tag{3.2.7a}$$

$$\frac{\partial}{\partial y} = \cos\alpha \frac{\partial}{\partial \eta} - \sin\alpha \frac{\partial}{\partial \zeta} \tag{3.2.7b}$$

Expressions for the velocity and higher derivatives are found, for instance, in Pedlosky (1979). Before going further we can make some simplifications concerning the trigonometric terms. For a typical frontal slope like the New England shelf break we have $\tan\alpha$ = 100m/52000m, or a slope of 1.9×10^{-3}, Flagg (1977) so we can approximate:

$$\sin\alpha \simeq \alpha$$

$$\cos\alpha \simeq 1$$

The equations, after dropping terms of higher order in α are:

$$\hat{u}_t + \hat{v}\hat{u}_\eta + \hat{w}\hat{u}_\zeta - f\hat{v} = \nu(\hat{u}_{\eta\eta} + \hat{u}_{\zeta\zeta}) \tag{3.2.8a}$$

$$\hat{v}_t + \hat{v}\hat{v}_\eta + \hat{w}\hat{v}_\zeta + f\hat{u} = -\frac{1}{\rho_0}P_\eta - g\frac{\rho'}{\rho_0} + \nu(\hat{v}_{\eta\eta} + \hat{v}_{\zeta\zeta}) \tag{3.2.8b}$$

$$\hat{w}_t + \hat{v}\hat{w}_\eta + \hat{w}\hat{w}_\zeta - \alpha f\hat{u} = -\frac{1}{\rho_0}P_\zeta - g\frac{\rho'}{\rho_0} + \nu(\hat{w}_{\eta\eta} + \hat{w}_{\zeta\zeta}) \tag{3.2.8c}$$

$$\hat{v}_\eta + \hat{w}_\zeta = 0 \tag{3.2.8d}$$

$$\rho_t + \hat{v}\rho_\eta + \hat{w}\rho_\zeta + \hat{w}\bar{\rho}_\zeta + \alpha(\hat{v}\bar{\rho}_\zeta + \hat{w}\bar{\rho}_\eta) = 0 \tag{3.2.8e}$$

where the over-hat symbol means velocities in the new system of coordinates.

Now we define a velocity field decomposed into a field U along x , being the only function of ζ and a fluctuating field (u', v', w')

$$\vec{u} = [U(\zeta), 0, 0] + (u', v', w') \tag{3.2.9}$$

When the Boussinesq approximation was assumed the density field was already split up, but if we further make the assumption that in the frontal zone the mean density $\bar{\rho}$ depends only upon ζ , we have

$$\rho = \bar{\rho}(\zeta) + \rho'(\eta, \zeta, t) \tag{3.2.10}$$

The effect of this in the equations (3.2.8) is the drop of one term of order α in the equation (3.2.8e). Substituting the new values in the equations and after dropping the second order terms and dropping primes and hat symbols;

$$u_t + w U_\zeta - fv = \nu(u_{\eta\eta} + u_{\zeta\zeta}) \tag{3.2.11a}$$

$$v_t + f(U+u) = -\frac{1}{\rho_0} P_\eta - g\alpha \frac{\rho'}{\rho_0} + \nu(v_{\eta\eta} + v_{\zeta\zeta}) \tag{3.2.11b}$$

$$w_t - \alpha f(U+u) = -\frac{1}{\rho_0} P_\zeta - g\frac{\rho'}{\rho_0} + \nu(w_{\eta\eta} + w_{\zeta\zeta}) \tag{3.2.11c}$$

$$v_\eta + w_\zeta = 0 \tag{3.2.11d}$$

$$\rho_t + \alpha v \bar{\rho}_\zeta + w\bar{\rho}_\zeta = 0 \tag{3.2.11e}$$

In the absence of the perturbation field the above equations reduce to

$$0 = \nu U_{\zeta\zeta} \tag{3.2.12a}$$

$$fU = -\frac{1}{\rho_0}\bar{P}_\eta - g\alpha\frac{\bar{\rho}}{\rho_0} \tag{3.2.12b}$$

$$-\alpha f U = -\frac{1}{\rho_0}\bar{P}_\zeta - g\frac{\bar{\rho}}{\rho_0} \tag{3.2.12c}$$

from which the thermal wind equation for the front is obtained;

$$\rho_0 f U_s = -\alpha g \bar{\rho}_s \tag{3.2.13}$$

the integration of (3.2.13) from $s<0$ to s yields

$$\rho_0 f U(s) = -\alpha g [\rho(s) - \rho_1] \tag{3.2.14}$$

After subtracting the mean field equation (3.2.12) from equation (3.2.11), our next step is to scale the resulting equations in order to see if we can get rid of difficult terms. Since we are going to perturb the system with an internal wave of wavenumber ℓ and frequency σ, we already have two scales for the problem; the along front scale ℓ^{-1} and the time scale σ^{-1}. The cross front scale will be scaled by the front thickness H, the along front velocity will be scaled by a typical velocity U and the cross front velocity derived using the continuity equation. The pressure will be scaled by the geostrophic balance in the η direction, the density will be scaled by the density equation, and the cross front shear by the frontal thermal wind equation. The non-dimensional variables are defined as follows:

$$\eta = \ell^{-1}\eta^* \quad , \quad s = Hs^* \quad , \quad t = \sigma^{-1}t^*$$

$$u = Uu^* \quad , \quad v = Uv^* \quad , \quad w = U\ell H w^*$$

$$p = \frac{\rho f U}{\ell} p^* \quad , \quad \rho = \frac{U\ell H \rho_0 N^2}{g\sigma} \rho^* \quad , \quad U_s = \frac{\alpha g \Delta\rho}{H} U_s^*$$

After the substitution, the non-dimensional equations are

$$\frac{\partial u^*}{\partial t^*} + \left(\frac{g\alpha l \Delta\rho}{\sigma}\right) w^* U_\zeta^* - \left(\frac{f}{\sigma}\right) v^* = \left(\frac{\nu l^2}{\sigma}\right) \frac{\partial^2 u^*}{\partial \eta^{*2}} + \left(\frac{\nu}{\sigma H^2}\right) \frac{\partial^2 u^*}{\partial \zeta^{*2}} \qquad (3.2.15a)$$

$$\frac{\partial v^*}{\partial t^*} + \left(\frac{f}{\sigma}\right) u^* = \left(\frac{f}{\sigma}\right) \frac{\partial P^*}{\partial \eta^*} - \alpha l H \left(\frac{N^2}{\sigma^2}\right) \rho^* + \left(\frac{\nu l^2}{\sigma}\right) \frac{\partial^2 v^*}{\partial \eta^{*2}} + \left(\frac{\nu}{\sigma H^2}\right) \frac{\partial^2 v^*}{\partial \zeta^{*2}} \qquad (3.2.15b)$$

$$\frac{\partial w^*}{\partial t^*} - \frac{\alpha}{lH}\left(\frac{f}{\sigma}\right) u^* = -\left(\frac{1}{lH}\right)^2 \left(\frac{f}{\sigma}\right) \frac{\partial P^*}{\partial \zeta^*} - \left(\frac{N^2}{\sigma^2}\right) \rho^* + \left(\frac{\nu l^2}{\sigma}\right) \frac{\partial^2 w^*}{\partial \eta^{*2}} + \left(\frac{\nu}{\sigma H^2}\right) \frac{\partial^2 w^*}{\partial \zeta^{*2}} \qquad (3.2.15c)$$

$$\frac{\partial v^*}{\partial \eta^*} + \frac{\partial w^*}{\partial \zeta^*} \qquad (3.2.15d)$$

$$\frac{\partial \rho^*}{\partial t^*} + \left(\frac{\alpha g'}{lHN^2}\right) v^* \bar{\rho}_\zeta + \left(\frac{g'}{HN^2}\right) w^* \bar{\rho}_\zeta = 0 \qquad (3.2.15e)$$

where g' is the reduced gravity. The scaling parameters are shown in Table 3.2.1 (shown on the following page).

TABLE 3.2.1

Scaling parameters independent of forcing

H	Thickness of the front	10^4cm
U	Along front velocity	1 cm/s
f	Coriolis parameter (φ=45°)	1.03x10-4s-1
N	Brunt-Vaisala frequency	$10^{-2}s^{-1}$
ν	Kinematic molecular viscosity	10^{-2}cm/s
$\Delta\rho$	Density difference	$10^{-3}g/cm^3$
g	Acceleration of gravity	$10^3cm/s^2$
α	Slope of the front	10^{-3}

For either low or high frequency and small or large wave number the diffusion of momentum, the shear term and and the term neglected in the density equation are small. On the other hand, depending of the values of the forcing parameters σ and ℓ, consequently the values of f/σ, N/σ and $H\ell$, the set of equations (3.12.15) can be used for either end of the internal wave spectrum. So to solve the most general case, where the specific case of low frequency as well as high

frequencies waves is included, the following set of equations will be used in the unscaled form

$$u_t - fv = 0 \tag{3.2.16a}$$

$$v_t + fu = -\frac{1}{\rho_0} P_\eta - g\alpha \frac{\rho'}{\rho_0} \tag{3.2.16b}$$

$$w_t - \alpha f u = -\frac{1}{\rho_0} P_\varsigma - g\frac{\rho'}{\rho_0} \tag{3.2.16c}$$

$$v_\eta + w_\varsigma = 0 \tag{3.2.16d}$$

$$\rho_t + w\bar{\rho}_\varsigma = 0 \tag{3.2.16e}$$

The elimination of the pressure, density, and horizontal velocity using the standard procedures yields a partial differential equation for

$$(w_{\eta\eta} + w_{\varsigma\varsigma})_{tt} + f^2(\alpha w_{\varsigma\eta} + w_{\varsigma\varsigma}) \tag{3.2.17}$$

$$- N^2(\varsigma)(\alpha w_{\varsigma\eta} - w_{\eta\eta}) = 0$$

3.3 Planar wave solutions

The partial differential equation (3.2.17) is linear. We assume as solutions planar waves propagating along the front of the form

$$w(\eta, \zeta, t) = Q(\zeta)\, e^{i(l\eta - \sigma t)} \tag{3.3.1}$$

Here l is the wave number in the η direction and σ the frequency. After substitution of (3.3.1) in (3.2.17) we have for $Q(\zeta)$ the following equation:

$$Q''(\zeta) - il\alpha \frac{(f^2 - N^2)}{(f^2 - \sigma^2)} Q'(\zeta) + l^2 \frac{(\sigma^2 - N^2)}{(f^2 - \sigma^2)} Q(\zeta) = 0 \tag{3.3.2}$$

which is an ordinary differential equation with a variable coefficient $N = N(\zeta)$ and resembles equation (2.2.8).

Now for the sake of simplicity we can assume a step like Brunt-Vaisala frequency shown in figure 3.3.1 and defined as,

$$N(\zeta) = 0 \quad , \quad \zeta > h$$

$$N(\zeta) = N \quad , \quad 0 < \zeta < h$$

$$N(\zeta) = 0 \quad , \quad \zeta < 0$$

Assuming solutions like $Q(\zeta) = \exp \gamma\zeta$, the characteristic equation will be

$$\gamma^2 - il\alpha \frac{(f^2 - N_0^2)}{(f^2 - \sigma^2)} \gamma + l^2 \frac{(\sigma^2 - N_0^2)}{(f^2 - \sigma^2)} = 0 \tag{3.3.4}$$

with the roots,

$$\gamma = i\ell\alpha \frac{(f^2-N_0^2)}{2(f^2-\sigma^2)} \pm \frac{1}{2}\left[\frac{-\ell^2\alpha^2(f^2-N_0^2)^2 - 4\ell^2(\sigma^2-N_0^2)(f^2-\sigma^2)}{(f^2-\sigma^2)^2}\right]^{1/2} \qquad (3.3.5)$$

the discriminant

$$\Delta = \frac{-\ell^2\alpha^2(f^2-N_0^2)^2 - 4\ell^2(\sigma^2-N_0^2)(f^2-\sigma^2)}{(f^2-\sigma^2)^2} \qquad (3.3.6)$$

will always be negative in the range of the internal gravity waves, $f < \sigma < N_0$. Since we are interested here in semi-diurnal frequencies M2 , there will be two different imaginary roots and an oscilatory solution is expected.

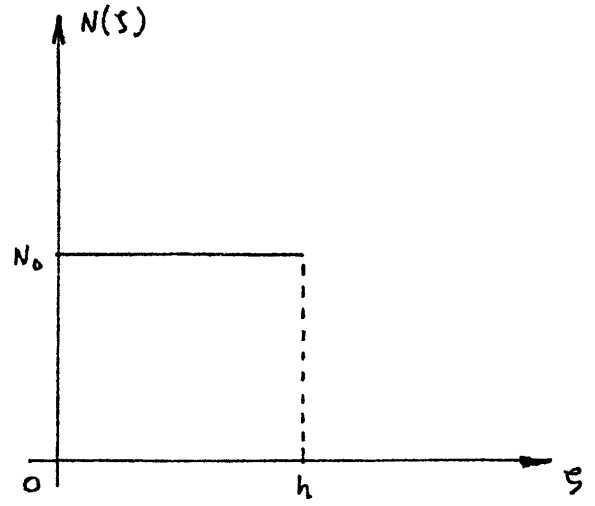


Figure 3.3.1 Brunt-Vaisala frequency distribution

If we call

$$H = |\Delta|^{1/2} \tag{3.3.7}$$

and

$$\Theta = \frac{f^2 - N_0^2}{f^2 - \sigma^2} \tag{3.3.8}$$

The solutions of the characteristic equation become

$$\gamma_{1,2} = \left(\frac{i\alpha\Theta}{2} \pm \frac{H}{2} \right) = \frac{1}{2}\left(i\alpha\Theta \pm H \right) \tag{3.3.9}$$

and the general solution for the equation (3.3.3) is

$$Q_2(\zeta) = A\, e^{i\gamma_1 \zeta} + B\, e^{i\gamma_2 \zeta} \tag{3.3.10}$$

where the constants A and B are complex, $\gamma_1 = \beta + H$, $\gamma_2 = \beta - H$, and

$$\beta = \frac{i\alpha\Theta}{2} \tag{3.3.11}$$

The subscript 2 on Q is to indicate that this solution holds inside the frontal layer, where $0 < \zeta < h$, different from the solutions

outside this layer which will have subscripts $1\ (y<0)$ and $3\ (y>h)$.

The solution outside the layer will be found by just making $N^2(y)=0$ in the discriminant (3.3.7), then

$$\Delta' = \left[-l^2\alpha^2 f^4 - 4l^2\sigma^2(f^2-\sigma^2)\right] / (f^2-\sigma^2)^2 \qquad (3.3.12)$$

since $\sigma > f$, $f^2-\sigma^2<0$ or rewriting as $-(\sigma^2-f^2)$, then in order to have exponentially decaying solutions, we must have

$$4\sigma^2(\sigma^2-f^2) > \alpha^2 f^4 \qquad (3.3.13)$$

So the frequency obeys the biquadratic inequality (3.3.13). The solutions being

$$\sigma^2 > \frac{f^2}{2}\left[1 \pm (1+\alpha^2)^{1/2}\right]$$

or since $\alpha \sim O(10^{-3})$ picking up the positive root,

$$\sigma > f\left(1+\frac{\alpha^2}{4}\right)^{1/2} \qquad (3.3.14)$$

This relation is obviously true when we deal with proper internal waves. Having the discriminant greater than zero means two different complex roots with real parts yielding exponentially decaying and growing solutions in $\mathcal{Y}$. The solution of the characteristic equation in this case will be

$$\gamma_{3,4} = i\beta_0 \pm H_0 \tag{3.3.15}$$

where

$$\beta_0 = \frac{\ell \alpha \theta_0}{2} \qquad \text{and} \qquad H_0 = \frac{H(N^2=0)}{2} \tag{3.3.15a}$$

and the correspondent solution for eq. (3.3.3)

$$Q(\zeta) = C\, e^{(H_0 + i\beta_0)\zeta} + D\, e^{(-H_0 + i\beta_0)\zeta} \tag{3.3.16}$$

Since we are interested in solutions decaying outside the frontal layer, the boundary conditions imposed are:

$$Q_1(\zeta) = 0 \qquad \text{as} \quad \zeta \to -\infty \quad , \quad \zeta < 0 \tag{3.3.17a}$$

$$Q_3(\zeta) = 0 \qquad \text{as} \quad \zeta \to +\infty \quad , \quad \zeta > h \tag{3.3.17b}$$

and the solution in each region is,

$$Q_1(\zeta) = C\, e^{H_0 \zeta} e^{i\beta_0 \zeta} \quad , \quad \zeta > 0 \tag{3.3.18}$$

$$Q_3(\zeta) = D\, e^{-H_0 \zeta} e^{i\beta_0 \zeta} \quad , \quad \zeta > h \tag{3.3.19}$$

These solutions must be continuous across the frontal layer, so we have to match them at $\zeta = 0$ and $\zeta = h$. The two matching conditions are kinematical and dynamic boundary conditions. They are

$$\left[Q(\zeta)\right] = 0 \quad \text{at} \quad \zeta = 0 \quad \text{and} \quad \zeta = h \tag{3.3.20}$$

and

$$\left[Q'(\zeta)\right] = 0 \quad \text{at} \quad \zeta = 0 \quad \text{and} \quad \zeta = h \tag{3.3.21}$$

The application of these conditions to the solutions (3.3.11), (3.3.18) and (3.3.19) leads us to an algebraic set of equations in the unknowns, A,B,C and D. The set of equations can be written as

$$\begin{aligned}
&A + B - C + 0 = 0 \\
&i(\beta+H)A + i(\beta-H)B - (H_0+i\beta_0)C + 0 = 0 \\
&e^{i(\beta+H)h}A + e^{i(\beta-H)}B + 0 - e^{(-H_0+i\beta_0)h}D = 0 \\
&i(\beta+H)e^{i(\beta+H)h}A + i(\beta-H)e^{i(\beta-H)h}B + 0 - (-H_0+i\beta_0)e^{i(-H_0+i\beta_0)h}D = 0
\end{aligned} \tag{3.3.22}$$

For this set to have non-trivial solution the determinant of the coefficients must vanish,

$$\begin{vmatrix}
1 & 1 & -1 & 0 \\
i(\beta+H) & i(\beta-H) & -(H_0+i\beta_0) & 0 \\
e^{i(\beta+H)h} & e^{i(\beta-H)h} & 0 & -e^{(-H_0+i\beta_0)h} \\
i(\beta+H)e^{i(\beta+H)h} & i(\beta-H)e^{i(\beta-H)h} & 0 & -(H_0+i\beta_0)e^{(-H_0+i\beta_0)h}
\end{vmatrix} = 0 \tag{3.3.23}$$

Equation (3.3.23) then yields the dispersion relation when we equate both the real and imaginary parts to zero.

$$\varphi(\cos\omega_1 - \cos\omega_2) + \psi(\sin\omega_1 + \sin\omega_2) = 0 \qquad (3.3.24a)$$

$$\varphi(\sin\omega_1 - \sin\omega_2) - \psi(\cos\omega_1 + \cos\omega_2) = 0 \qquad (3.3.24b)$$

where

$$\varphi = \beta^2 - H^2 + \beta_0^2 + H_0^2 - 2\beta_0\beta$$

$$\psi = 2H_0H$$

$$\omega_1 = (\beta - H)h$$

$$\omega_2 = (\beta + H)h$$

The dispersion relation (3.3.24a) is essentially the same as (3.3.24b) as will be shown. Using the formulas of sums and differences of trigonometric functions we have

$$\cos\omega_1 - \cos\omega_2 = 2\sin A \sin B$$

$$\sin\omega_1 + \sin\omega_2 = 2\sin A\cos B$$

$$\sin\omega_1 - \sin\omega_2 = -2\sin B\cos A$$

$$\cos\omega_1 + \cos\omega_2 = 2\cos A\cos B$$

where

$$A - B = \Phi_1$$

$$A + B = \Phi_2$$

and

$$A = \beta h \quad , \quad B = Hh$$

Then the real part of the dispersion relation will turn out to be

$$\varphi \sin Hh + \psi \cos Hh = 0$$

or

$$\tan Hh = -\psi / \varphi \qquad (3.3.24c)$$

which is exactly the relation for the imaginary part also. So the pair of values of frequency and wave numbers satisfies the real and imaginary part of the dispersion relation.

A plot of the dispersion relation (3.3.24c) is shown in figure 3.3.2 and 3.3.3. In the first plot, H=100m and in the second, H=40m. In both we can notice many wave numbers for the same frequency showing the wavenumbers as eignevalues. Also we notice that for the same domain of wavenumbers there are less eigenvalues for a thinner front. This can be seen if we rewrite the dispersion relation (3.3.24c) as

$$\sigma = \left[f^2 + \frac{2\varphi \tan Hh}{\delta} \right]^{1/2}$$

where

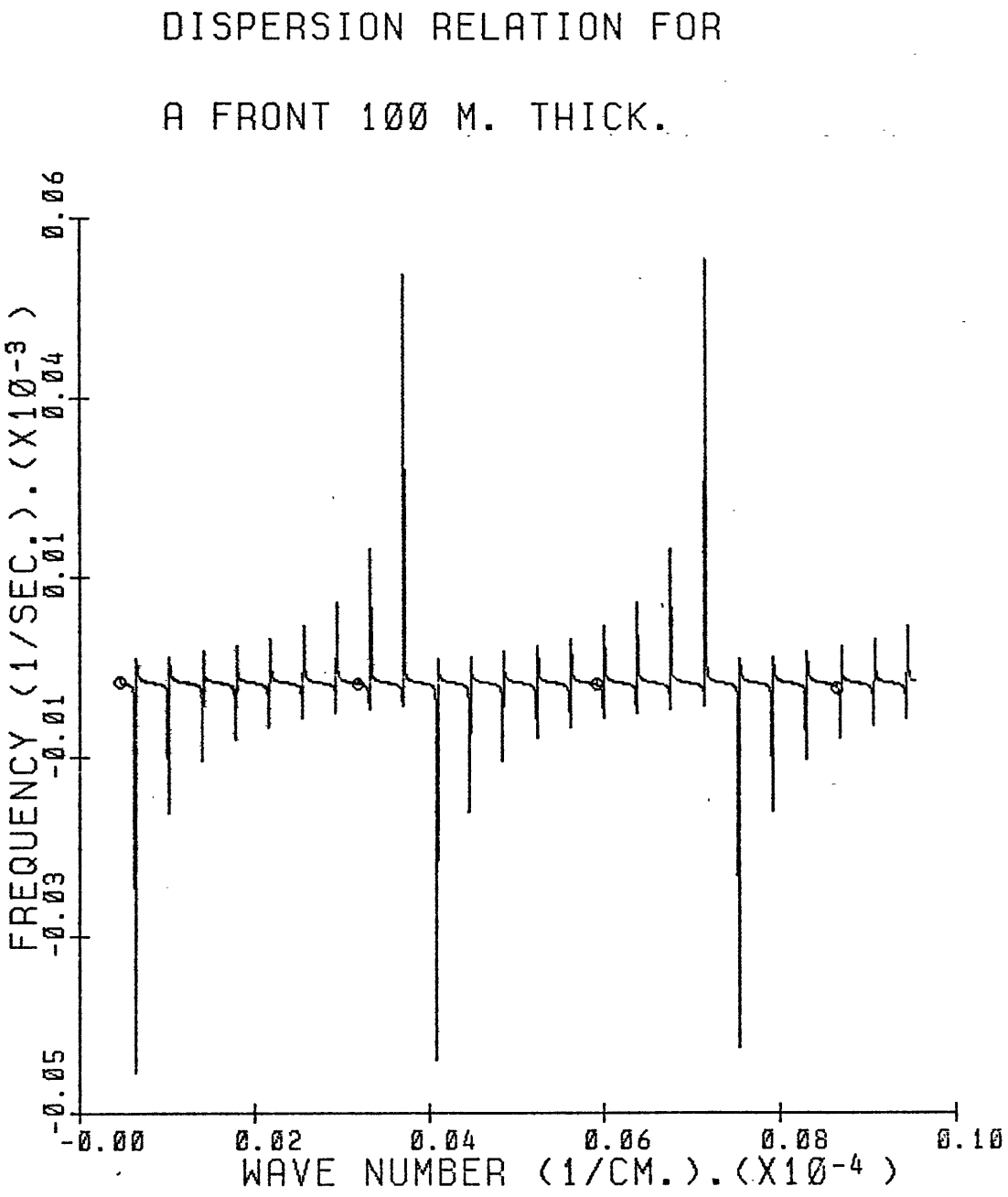


Figure 3.3.1. Dispersion relation (3.3.24c) with f=.0000954 sec^{-1}, N=.011 sec^{-1} in a 100m thick front.

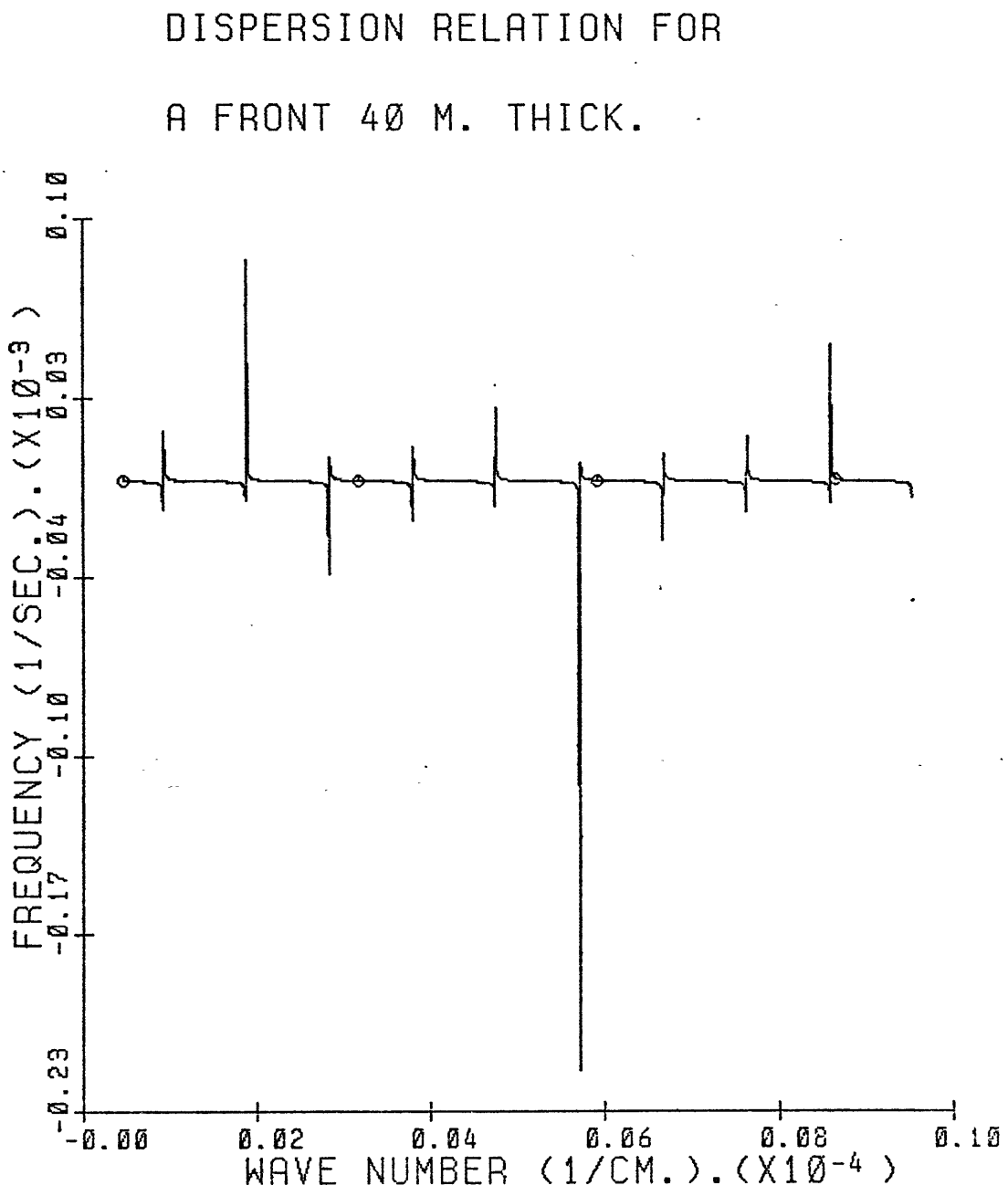


Figure 3.3.2. Dispersion relation (3.3.24c) with f=.0000954 sec^{-1}, N=.011 sec^{-1} in a 40m thick front.

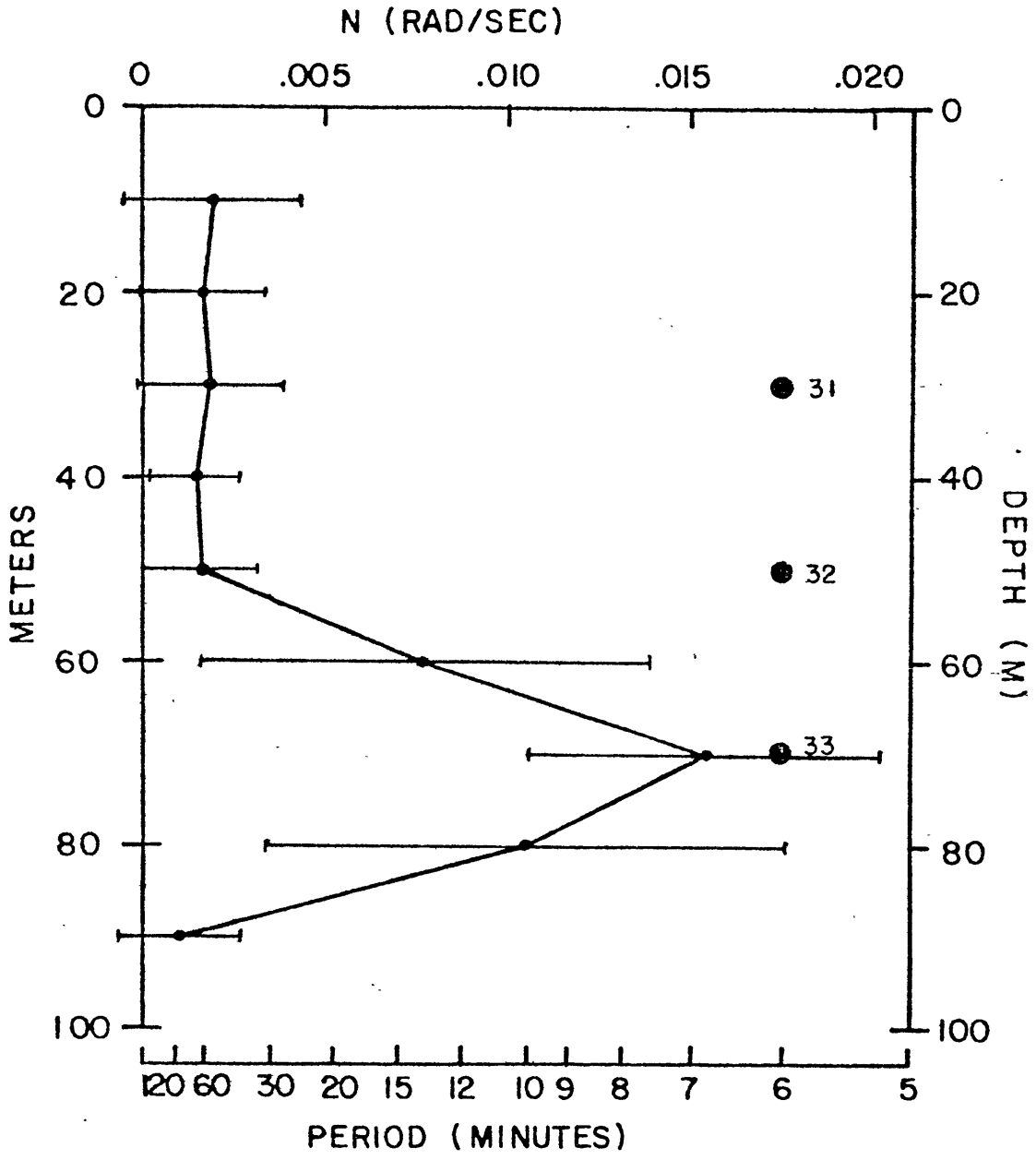


Figure 3.3.3 Vertical frofile of the average Brunt-Vaisala frequency estimated from four hyhrographic cruises during March 1974 at the New England front. (From Flagg,1977).

$$\delta = \left\{ \left[\frac{-\alpha^2 f^4}{(f^2-\sigma^2)} - 4\sigma^2 \right] \left[\frac{\alpha^2 (f^2-N^2)^2}{(f^2-\sigma^2)} + 4(\sigma^2-N^2) \right] \right\}^{1/2}$$

If we decrease the value of the argument of the tangent, there is going to be less crossings on the zero line per unit length. In both plots the Brunt-Vaisala frequency was taken as .011 1/sec, being the value based in an average Brunt-Vaisala frequency profile from Flagg (1977), shown in figure 3.3.4.

The set of algebraic linear equations (3.3.23) is homogeneous, and since we impose the condition (3.3.23) for the existence of a solution, the rank of the coefficient matrix is at most 3, less than the number of unknowns 4. In this condition the set of equations admits infinitely many solutions depending upon the value we assign to the number of arbitrary constants, which here is 4-3=1 . If we choose

$$C = (1+i)R$$

where R is another arbitrary constant, we then have

$$\begin{aligned} A \quad &+ \quad B \quad = \quad C \\ i(\beta+H)A \; &+ \; i(\beta-H)B \; = \; (H_0 + i\beta_0)C \\ e^{i(\beta+H)h} A \; &+ \; e^{i(\beta-H)h} B \; = \; e^{(-H_0+i\beta_0)h} D \end{aligned} \qquad (3.3.25)$$

Solving the set for the real and imaginary part we set the values

$$A = A_R + iA_I = \frac{R(H_o+\beta_o-\beta+H)}{2H} - i\,\frac{R(H_o-\beta_o+\beta-H)}{2H} \tag{3.3.26a}$$

$$B = B_R + iB_I = \frac{-R(H_o+\beta_o-\beta-H)}{2H} - i\,\frac{R(H_o-\beta_o+\beta+H)}{2H} \tag{3.3.26b}$$

$$D = D_R + iD_I = e^{H_o h} G_{R2} + i\, e^{H_o h} G_{I2} \tag{3.3.26c}$$

where

$$G_{R2} = A_R \cos\zeta_1 - A_I \sin\zeta_1 + B_R \cos\zeta_2 - B_I \sin\zeta_2 \tag{3.3.27a}$$

$$G_{I2} = A_I \cos\zeta_1 + A_R \sin\zeta_1 + B_I \cos\zeta_2 + B_R \sin\zeta_1 \tag{3.3.27b}$$

Here, for the sake of simplicity, we are going to continue to write A,B and D despite knowing their values.

Then the solution for w of (3.3.11), (3.3.18) and (3.3.19) can be written as a complex amplitude. The real part of w is

$$w_1(\eta,\zeta,t) = R\, e^{H_o\zeta}(\cos\beta_o\zeta - \sin\beta_o\zeta)\cos(l\eta-\sigma t) \quad , \zeta \le 0 \tag{3.3.28}$$

$$w_2(\eta,\zeta,t) = F_\zeta \cos(l\eta-\sigma t) \quad , 0 \le \zeta \le h \tag{3.3.29}$$

$$w_3(\eta,\zeta,t) = (D_R\cos\beta_o\zeta - D_I\sin\beta_o\zeta)\, e^{H_o(h-\zeta)} \cos(l\eta-\sigma t) \quad , \zeta \ge h \tag{3.3.30}$$

where

$$F_s = A_R \cos(\beta+H)s - A_I \sin(\beta+H)s + B_R \cos((\beta-H)s - B_I \sin(\beta-H)s \quad (3.3.31)$$

3.4 Computation of the fluxes.

The computation of temperature and salinity fluxes are important since it will give us a hint about the way the velocities, determined in the previous section, will tend to modify the mean distribution of salt and heat. We will also anticipate that the net flux is not zero. Now we write the heat diffusion equation as

$$T_t + u \cdot \nabla T = K_T \nabla^2 T \quad (3.4.1)$$

and expressing the temperature field as

$$T = \bar{T}(s) + T'(\eta, s, t) \quad (3.4.2)$$

After changing the coordinates, substituting the fields and neglecting the second order terms and terms of order α we have

$$T'_t - k_T \nabla^2 T' = -w' \bar{T}_s \quad (3.4.3)$$

where we assume $\overline{T_S}$ constant. First we are going to solve equation (3.4.3) as it is and compute the fluxes. Afterwards we will scale it and solve it by perturbation comparing the results. In the first case we expect the solutions of (3.4.3) to have the form

$$T' = F_S \left[M_T \cos(\ell\eta - \sigma t) + N_T \sin(\ell\eta - \sigma t) \right] \tag{3.4.4}$$

Here we have used for w the solution (3.3.28) inside the frontal layer, substituting this in equation (3.4.3) and equating the terms $\cos(\ell\eta - \sigma t)$ and $\sin(\ell\eta - \sigma t)$, we end up with a set of two equations and two unknowns M_T and N_T, that solved yield the result

$$M_T = \frac{-\bar{T}_S F_S K_T (\ell^2 F_S - F_S'')}{\sigma^2 F_S^2 + k_T^2 (\ell^2 F_S - F_S'')^2} \tag{3.4.5}$$

$$N_T = \frac{\sigma \bar{T}_S F_S^2}{\sigma^2 F_S^2 + k_T^2 (\ell^2 F_S - F_S'')^2} \tag{3.4.6}$$

Here the F_S'' means the second derivative of F_S. The same procedure can be done with the salinity equation

$$S_t' - k_S \nabla^2 S' = -w' \bar{S}_S \tag{3.4.7}$$

ending up with a solution

$$S' = F_S \left[M_S \cos(\ell\eta - \sigma t) + N_S \sin(\ell\eta - \sigma t) \right] \tag{3.4.8}$$

where the constants are

$$M_S = \frac{-\bar{S}_S F_S K_S (l^2 F_S - F_S'')}{\sigma^2 F_S^2 + K_S^2 (l^2 F_S - F_S'')^2} \tag{3.4.9a}$$

and

$$N_S = \frac{\sigma \bar{S}_S F_S'}{\sigma^2 F_S^2 + K_S^2 (l^2 F_S - F_S'')^2} \tag{3.4.9b}$$

Basically the difference between the two solutions are in the constants, since while the molecular diffusivity of temperature is two orders of magnitude larger than that one of the salt.

The next step is to compute the fluxes of heat $\langle w'T' \rangle$ and of salt $\langle w'S' \rangle$ averaged over the phase angle $\nu = l\eta - \sigma t$. In order to compute the velocity v we use the continuity equation (3.2.8d), since $u_x = 0$,

$$v' = -\int \frac{\partial w'}{\partial S} d\eta \tag{3.4.10}$$

$$v' = -\frac{F_S'}{l} \sin(l\eta - \sigma t) \tag{3.4.11}$$

where F_S' is the first derivative of F_S with respect to S . The temperature flux in the η direction averaged over the phase will be

$$\langle v'T' \rangle = -\frac{F_S' F_S}{2l} N_T \tag{3.4.12}$$

similarly the flux in the S direction will be

$$\langle w'T' \rangle = \frac{F_s^2 M_T}{2} \tag{3.4.13a}$$

We can see that in (3.4.12) and (3.4.13) we have powers and products of F_γ and F'_γ giving rise to terms like $\cos^n \gamma s$ and $\sin^n \gamma s$, but these terms through the elementary trigonometric power relations can be written as $\cos n\gamma s$, $\sin n\gamma s$, where n is the exponent. The appearance of those terms show the trend towards formation of a multilayer structure in the frontal zone.

The similar fluxes of salt are:

$$\langle v's' \rangle = - \frac{F_s F'_s N_S}{2\ell} \tag{3.4.14}$$

$$\langle w's' \rangle = \frac{F_s^2 M_s}{2} \tag{3.4.15a}$$

The correspondent Nusselt number for temperature and salinity will be respectively

$$Nu_T = \frac{-F_s^3(\ell^2 F_s - F_s'')}{2\left[\sigma^2 F_s^2 + k_T^2 (\ell^2 F_s - F_s^{4})^2\right]} \tag{3.4.15b}$$

$$Nu_S = \frac{-F_s^3(\ell^2 F_s - F_s'')}{2\left[\sigma^2 F_s^2 + k_S^2 (\ell^2 F_s - F_s'')^2\right]} \tag{3.4.15c}$$

We can see that they will be equal, the conclusion we have reached in chapter II, if we neglect the second term in the denominator of

(3.4.15). This approximation is only valid for very small wave numbers, corresponding to low frequency waves.

It is also interesting to compute the ratios between the fluxes as the ratio between the vertical and the horizontal fluxes of temperature

$$\frac{\langle w'T' \rangle}{\langle v'T' \rangle} = 2 \frac{l}{\sigma} K_T (l^2 F_S - F_S'') \tag{3.4.16}$$

where we see that the longer the wave length the smaller the ratio will be. The ratio between the horizontal fluxes of salinity and temperature is

$$\frac{\langle v'S' \rangle}{\langle v'T' \rangle} = \frac{\bar{S}_S}{\bar{T}_S} \frac{\sigma^2 F_S^2 + K_T^2 (l^2 F_S - F_S'')^2}{\sigma^2 F_S^2 + K_S^2 (l^2 F_S - F_S'')^2} \tag{3.4.17}$$

where we can see that is roughly proportional to the ratio between the gradients of salinity and temperature. We can also compute the fluxes for the solutions outside the frontal layer as for instance (3.3.28). Again using the same procedure as before we find for the vertical temperature flux

$$\langle w'T' \rangle_1 = R^2 e^{2H_0 S} (\cos \beta_0 S - \sin \beta_0 S)^2 \frac{M_T'}{2}, \quad S < 0 \tag{3.4.18}$$

where the subscript 1 means fluxes using solution for region 1 and the new coefficients M'_T and N'_T are respectively

$$M'_T = \frac{\bar{T}_3 \rho k_T (\rho l^2 + G)}{\sigma^2 \rho^2 + k_T^2 (\rho l^2 + G)^2} \tag{3.4.19}$$

and

$$N'_T = \frac{\bar{T}_3 \sigma \rho^2}{\sigma^2 \rho^2 + k_T^2 (\rho l^2 + G)^2} \tag{3.4.20}$$

Being

$$G = Q \cos \beta_0 \zeta - R \sin \beta_0 \zeta$$

$$R = H_0^2 + 2\beta_0 H_0 - \beta_0^2$$

$$Q = H_0^2 - 2\beta_0 H_0 - \beta_0^2$$

$$P = \cos \beta_0 \zeta - \sin \beta_0 \zeta$$

Again the tendency of form layers is evident in (3.4.18).

If we had used the other outside solution (3.3.30), the temperature flux would be

$$\langle w'T' \rangle_3 = \frac{M''_T}{2} (D_R \cos \beta_0 \zeta - D_I \sin \beta_0 \zeta)^2 e^{2H_0(h-\zeta)} \tag{3.4.21}$$

where the new coefficients M''_T and N''_T are

$$M''_T = \frac{\sigma \bar{T}_3 \rho'^2}{\rho'^2 \sigma^2 + k_T^2 (l^2 \rho' - G)^2} \tag{3.4.22a}$$

and

$$N_T'' = \frac{\sigma \bar{T}_y P'^2}{P'^2\sigma^2 + K_T^2 (l^2 P' - G')^2} \tag{3.4.22b}$$

Being

$$Q' = (H_0 D_R + \beta_0 D_I)(H_0 - \beta_0)$$

$$R' = (\beta_0 D_R - H_0 D_I)(H_0 + \beta_0)$$

$$G' = Q' \cos\beta_0 y + R' \sin\beta_0 y$$

$$P' = D_R \cos\beta y - D_I \sin\beta_0 y$$

Going back to the solutions inside the front, if we compute the ratio between the vertical heat and salt fluxes we have

$$\frac{\langle w'T' \rangle}{\langle w'S' \rangle} = \frac{M_T}{M_S} = \left(\frac{\bar{T}_y}{\bar{S}_y}\right)\left(\frac{K_T}{K_S}\right) \frac{\sigma^2 F_S^2 + K_S^2 (l^2 F_S - F_S'')^2}{\sigma^2 F_S^2 + K_T^2 (l^2 F_S - F_S'')^2} \tag{3.4.23}$$

which compared to the ratio of the horizontal fluxes yields

$$\frac{\langle w'T' \rangle}{\langle w'S' \rangle} = \left(\frac{K_T}{K_S}\right) \frac{\langle v'T' \rangle}{\langle v'S' \rangle} \tag{3.4.24}$$

The fluxes were computed from chosen wave numbers and frequencies from the dispersion relation (3.3.24c) for a front 100m and another 40m thick. The results are shown and discussed in the next section.

Going back to equation (3.4.3), we are now going to scale it in the same way we did in the previous section, introducing the new scales

$$T = T_o T^* \qquad \text{and also} \qquad \bar{T}_\zeta \sim \frac{N^2}{\alpha_T g}$$

where α_T is the thermal expansion coefficient, assumed here to be constant and equal to $\alpha_T = .0001955^\circ C^{-1}$. The scaled equation is then

$$\frac{\partial T^*}{\partial t^*} + \left(\frac{U \ell H N^2}{T_o \alpha_T g \sigma}\right) w^* = \left(\frac{K_T \ell^2}{\sigma}\right) \frac{\partial^2 T^*}{\partial \eta^{*2}} + \left(\frac{K_T}{\sigma H^2}\right) \frac{\partial^2 T^*}{\partial \zeta^{*2}} \qquad (3.4.25)$$

For low frequency waves the scaling parameter of $w\,\bar{T}_\zeta$ is of order one, being the along front diffusion term negligible for large wave numbers. What makes sense, since in the physics of the problem the diffusion is important, and at high frequencies there is not enough time for diffusion. Equation (3.4.25) can be rewritten, dropping the stars (*), as

$$T_t + w = \varepsilon\, T_{\zeta\zeta} \qquad (3.4.25a)$$

where the horizontal diffusion term was neglected compared to the vertical diffusion and $\varepsilon = K_T / \sigma H^2 \ll 1$, also the scaling parameter of w is of 0(1).

If we expand T in powers of the small parameter ε, (see, for instance, Bender and Orszag, 1978)

$$T = T^{(0)} + \varepsilon T^{(1)} + \varepsilon^2 T^{(2)} + \cdots \tag{3.4.26}$$

and substitute back in (3.4.25) and equate powers of ε we get the following set of equations:

$$T_t^{(0)} + w = 0 \tag{3.4.27a}$$

$$T_t^{(1)} - T_{yy}^{(0)} = 0 \tag{3.4.27b}$$

$$T_t^{(2)} - T_{yy}^{(1)} = 0 \tag{3.4.27c}$$

Differentiating (3.4.27b) with respect to t and using (3.4.27a),

$$T_{tt}^{(1)} + w_{yy} \tag{3.4.28}$$

In view of the solutions (3.3.29-30) for w, we have for T in the three different regions of the front in the dimensional form,

$$T_1^{(1)} = k_T \bar{T}_s R \frac{\mathcal{F}_1(s)}{\sigma^2} \cos(\ell\eta - \sigma t) \tag{3.4.29a}$$

$$T_2^{(1)} = k_T \bar{T}_s \frac{F_2^0}{\sigma^2} \cos(\ell\eta - \sigma t) \tag{3.4.29b}$$

$$T_3^{(1)} = k_T \bar{T}_s \frac{\mathcal{F}_3(s)}{\sigma^2} \cos(\ell\eta - \sigma t) \tag{3.4.29c}$$

where

$$\mathcal{F}_1(\zeta) = e^{H_0\zeta}\left[(H_0^2-\beta_0^2)(\cos\beta_0\zeta - \sin\beta_0\zeta) - 2H_0\beta_0(\cos\beta_0\zeta + \sin\beta_0\zeta)\right]$$

$$\mathcal{F}_3(\zeta) = e^{H_0(h-\zeta)}\left[(H_0^2-\beta^2)(D_R\cos\beta_0\zeta - D_I\sin\beta_0\zeta) + 2H_0\beta_0(D_I\cos\beta_0\zeta + D_R\sin\beta_0\zeta)\right]$$

the constant of integration was choosen in such a way to eliminate the linear trend in t .

When comparing (3.4.29a,b,c) with 3.4.18,13,21 we can notice a difference in the expressions for the fluxes of heat. Since (3.4.29) is an approximation we will next prove that. Let us take the coefficient M_T , for the solution inside the front which is defined in (3.4.5). The following results are supported by physical reasoning as well as computations for different wave numbers and frequencies. The local vertical length scale of the motion is defined as F_ζ'' / F_ζ , for small ℓ, $F_\zeta'' \ll F_\zeta$, for large ℓ , $F_\zeta'' \gg F_\zeta$, so in any case we can write

$$M_T \simeq \frac{\bar{T}_\zeta k_T F_\zeta F_\zeta''}{\sigma^2 F_\zeta^2 + k_T^2 F_\zeta''^2}$$

again for small ℓ , $\sigma^2 F_\zeta^2 + k_T^2 F_\zeta''^2 \simeq \sigma^2 F_\zeta^2$

Then the coefficient M_T can be in an approximated form written as

$$M_T \simeq \frac{\bar{T}_S k_T F_S''}{\sigma^2 F_S} \tag{3.4.30}$$

The corresponding heat flux will be

$$\langle w'T' \rangle = \bar{T}_S k_T \frac{F_S F_S''}{2\sigma^2} \tag{3.4.31}$$

a result that agreed with the theory developed in chapter II. So the fluxes will yield a good approximation for small wavenumbers, but not for large wavenumbers. We will discuss this further in chapter V.

The velocity inside the front, temperature and salinity flux, the divergence and Nusselt numbers, are plotted in figures 3.4.1 to 3.4.7 for a wave with σ =10^{-4}sec^{-1}, the wavenumber computed from (3.3.24c), ℓ =8x10-9cm-1 and a front thickness of 100m. It can be seen that for this special values of the pair frequency and wave number the wave induced fluxes are negligible.

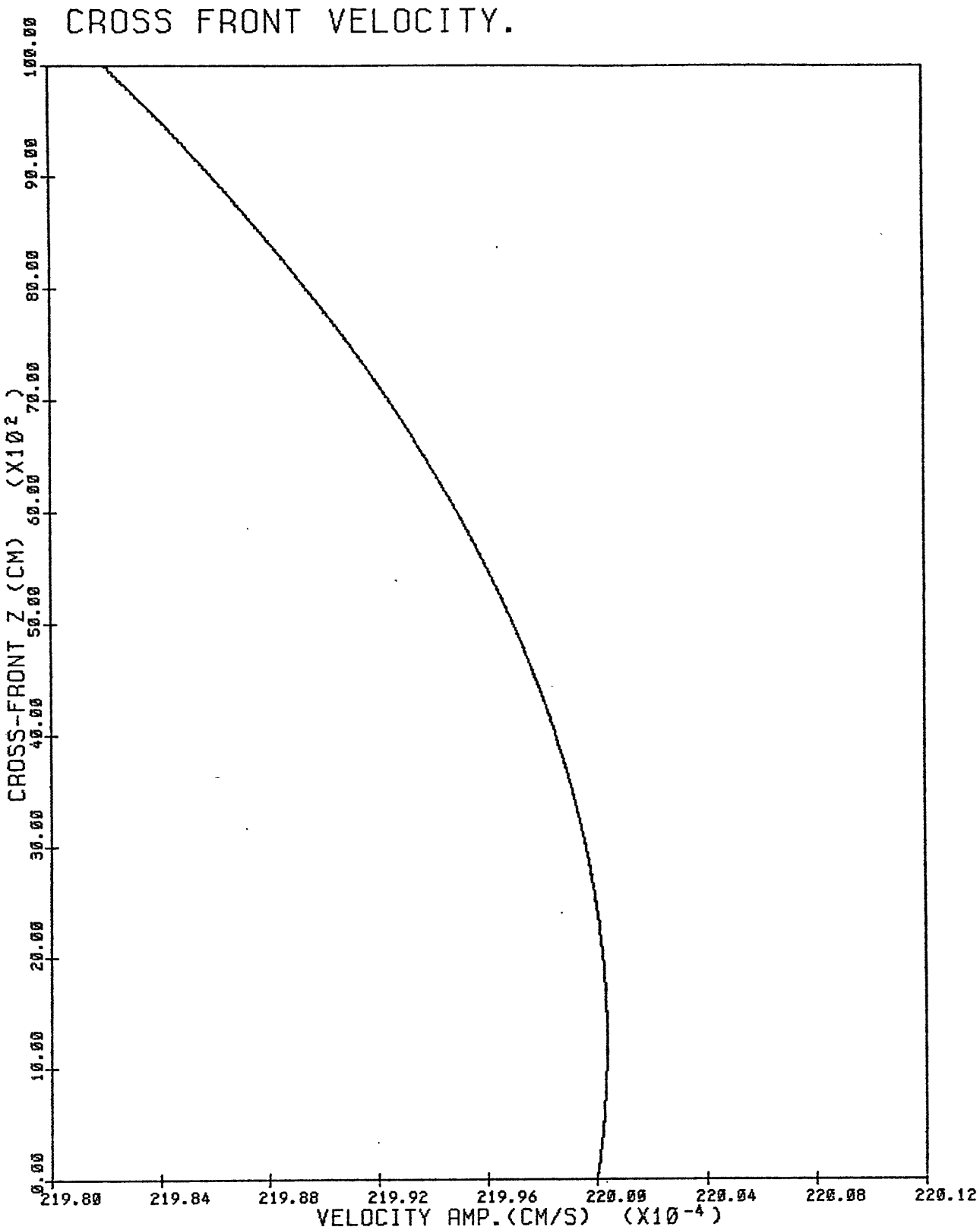


Figure 3.4.1. Cross front velocity amplitude for a wave $\sigma = 10^{-4}\ sec^{-1}$ $\ell = 8 \times 10^{-9}$ cm and R= .02 cm/sec in a front 100m thick. The values of f,N,T and S are the same as for NE front.

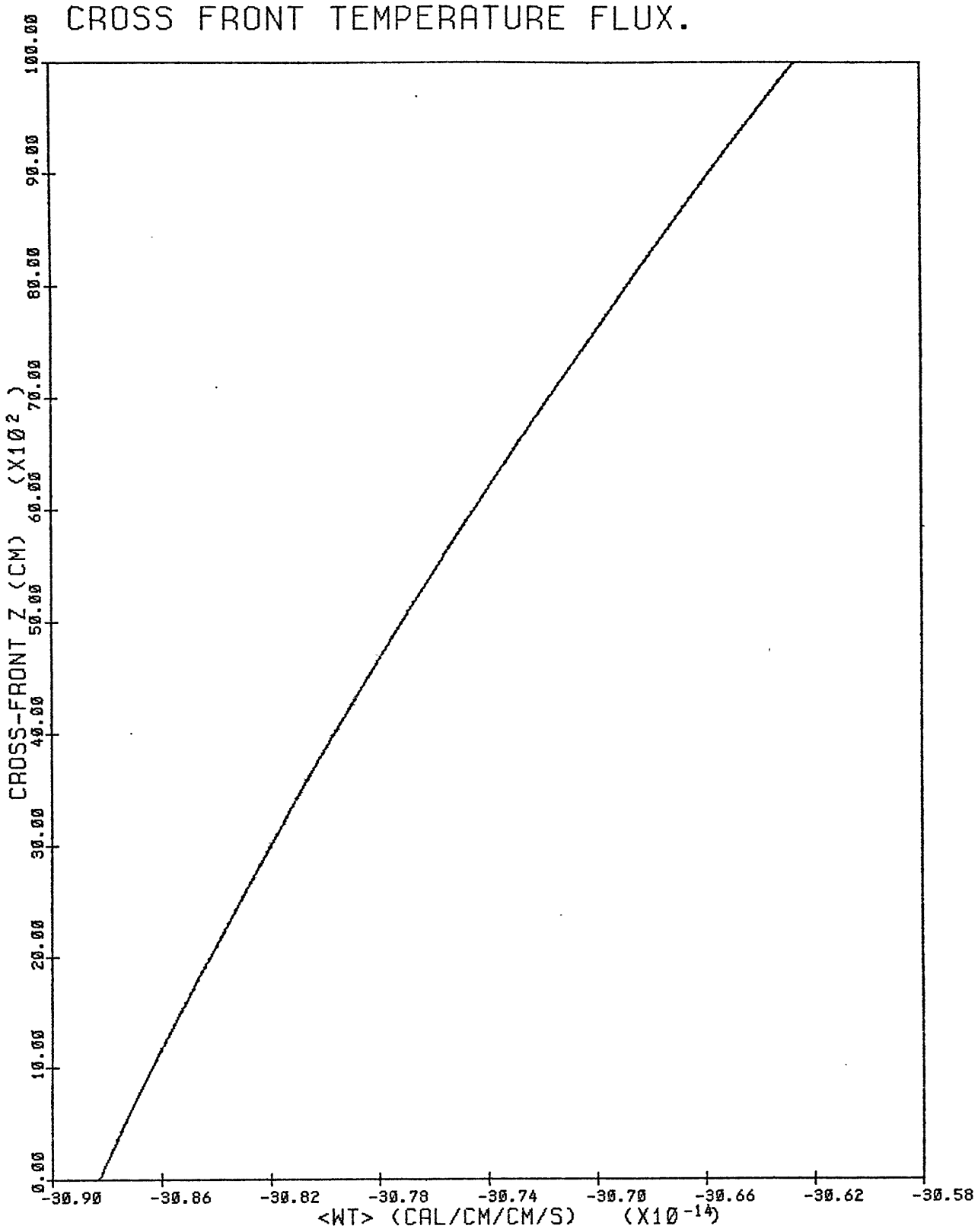


Figure 3.4.2. Cross front wave induced heat flux due to the wave of figure 3.4.1.

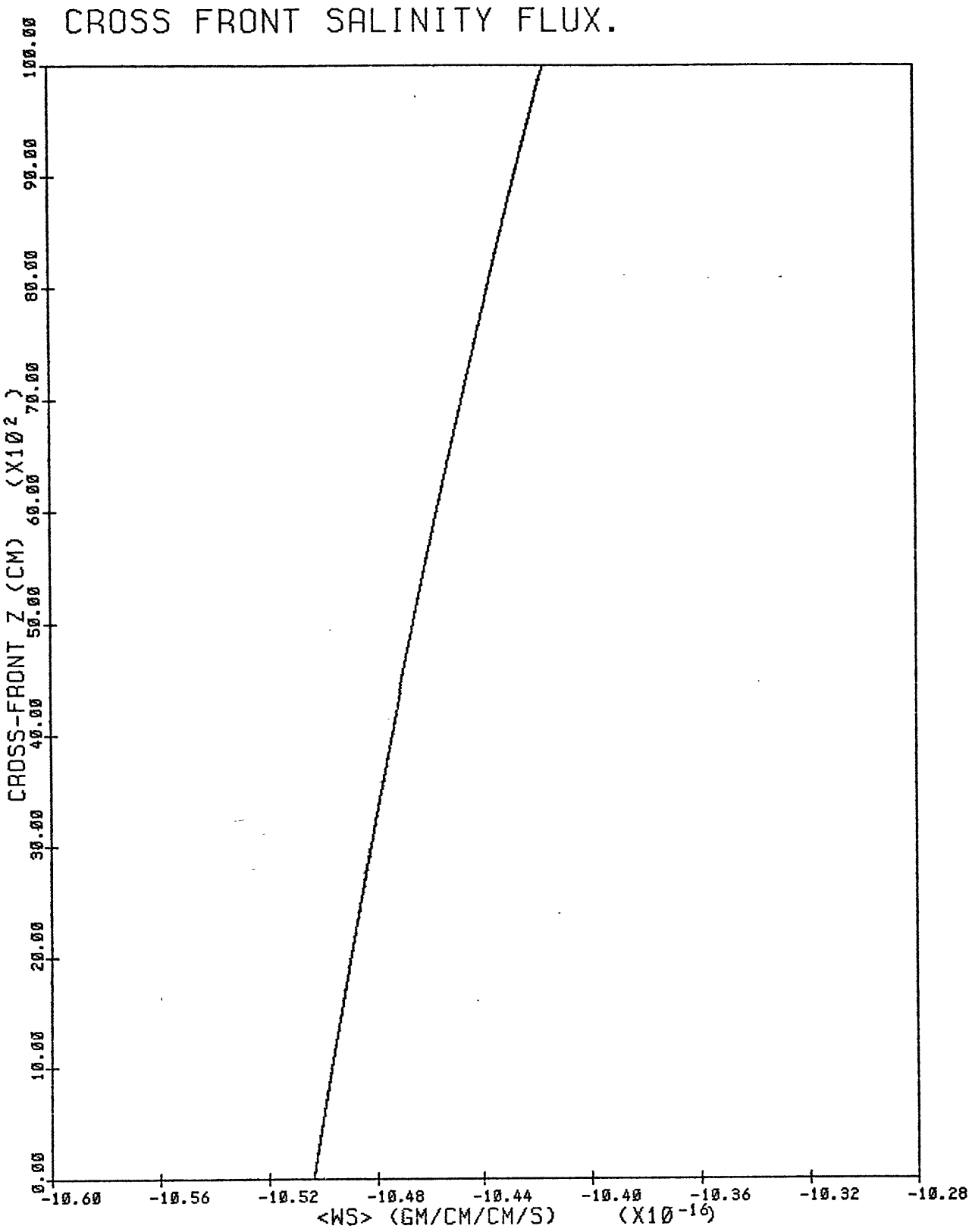


Figure 3.4.3. Cross front wave induced salt flux due to the wave of figure 3.4.1.

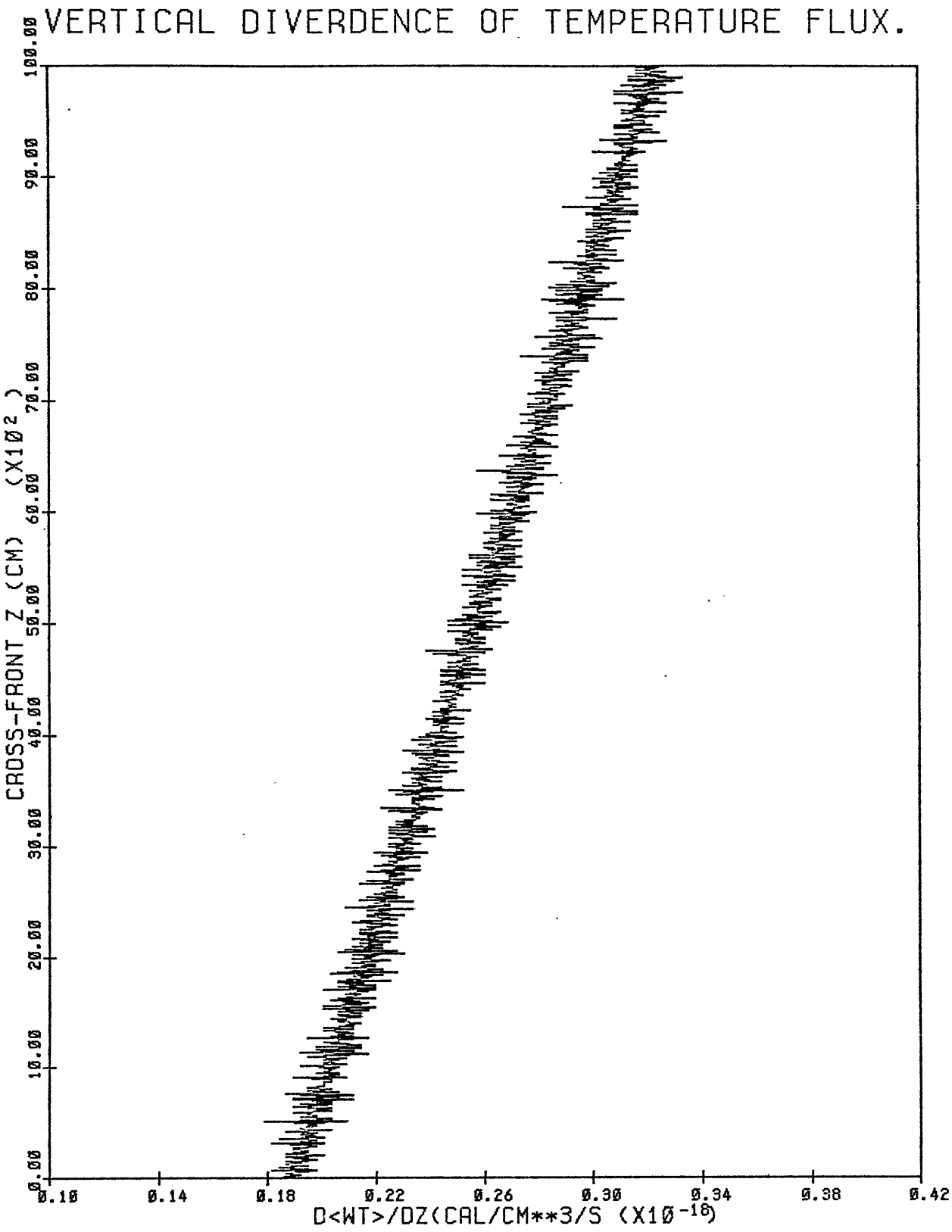


Figure 3.4.4. Vertical divergence of heat flux corresponding to the wave induced flux of figure 3.4.2.

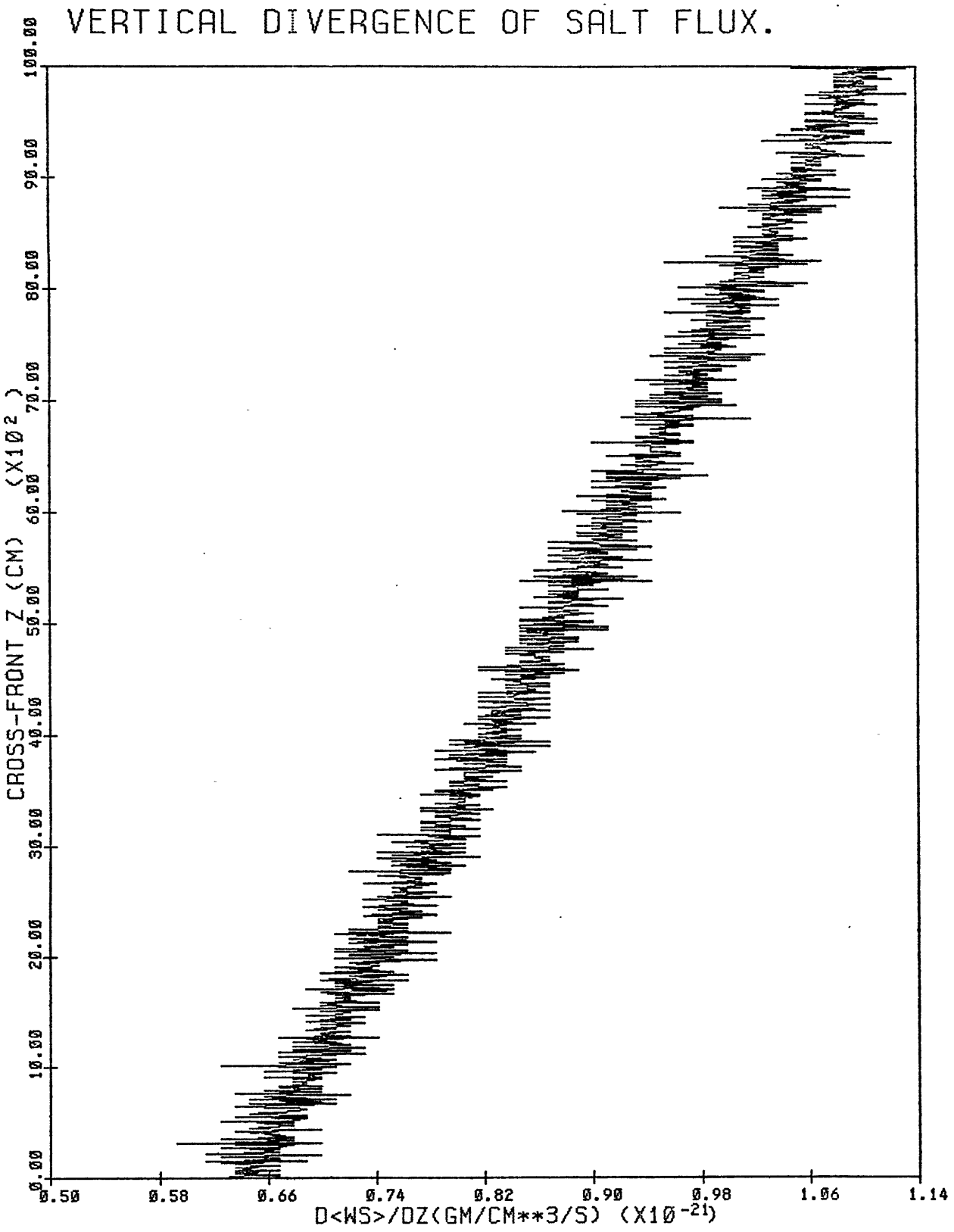


Figure 3.4.5. Vertical divergence of salt flux corresponding to the wave induced flux of figure 3.4.3.

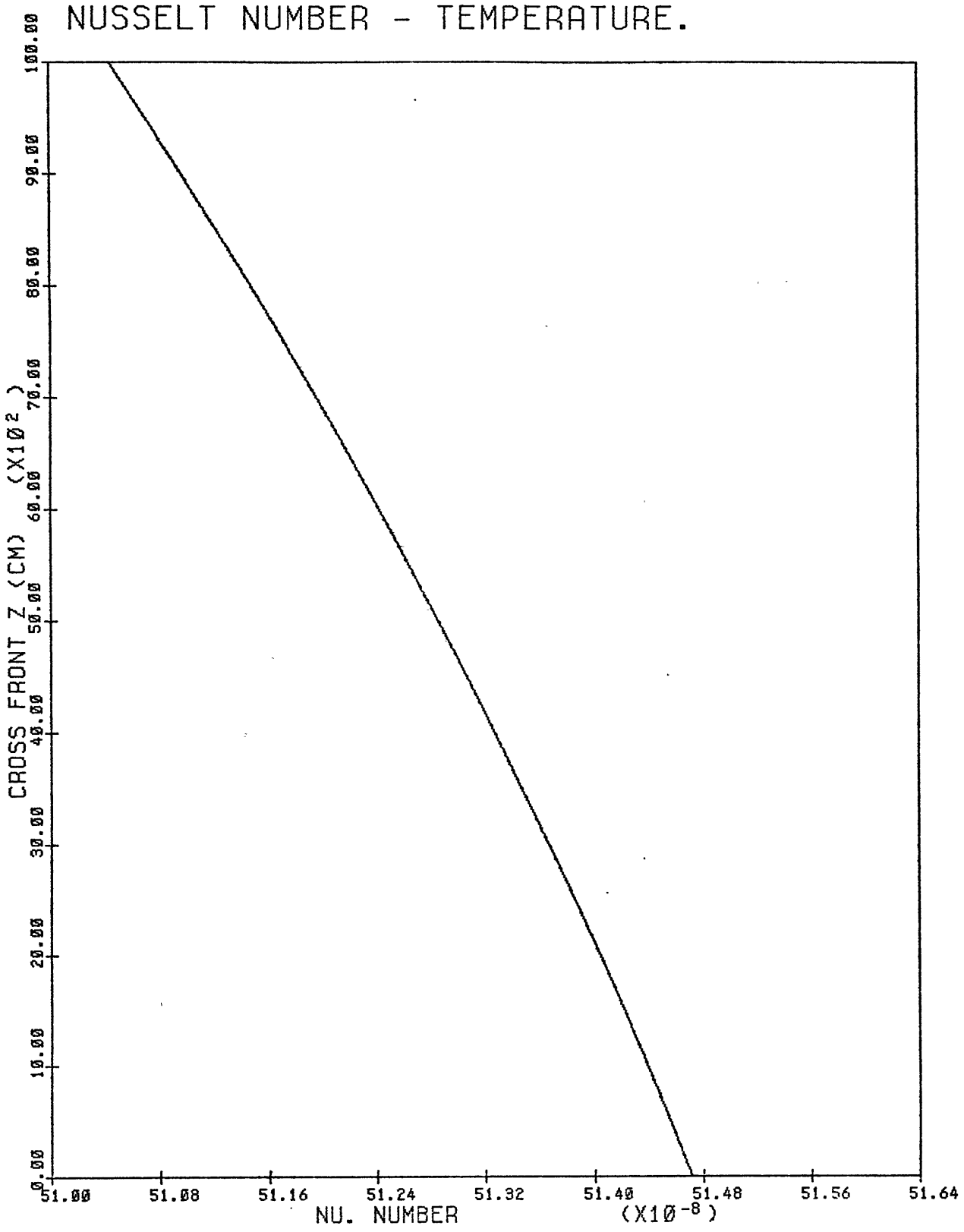


Figure 3.4.6. Nusselt number corresponding to the wave induced heat flux of figure 3.4.2.

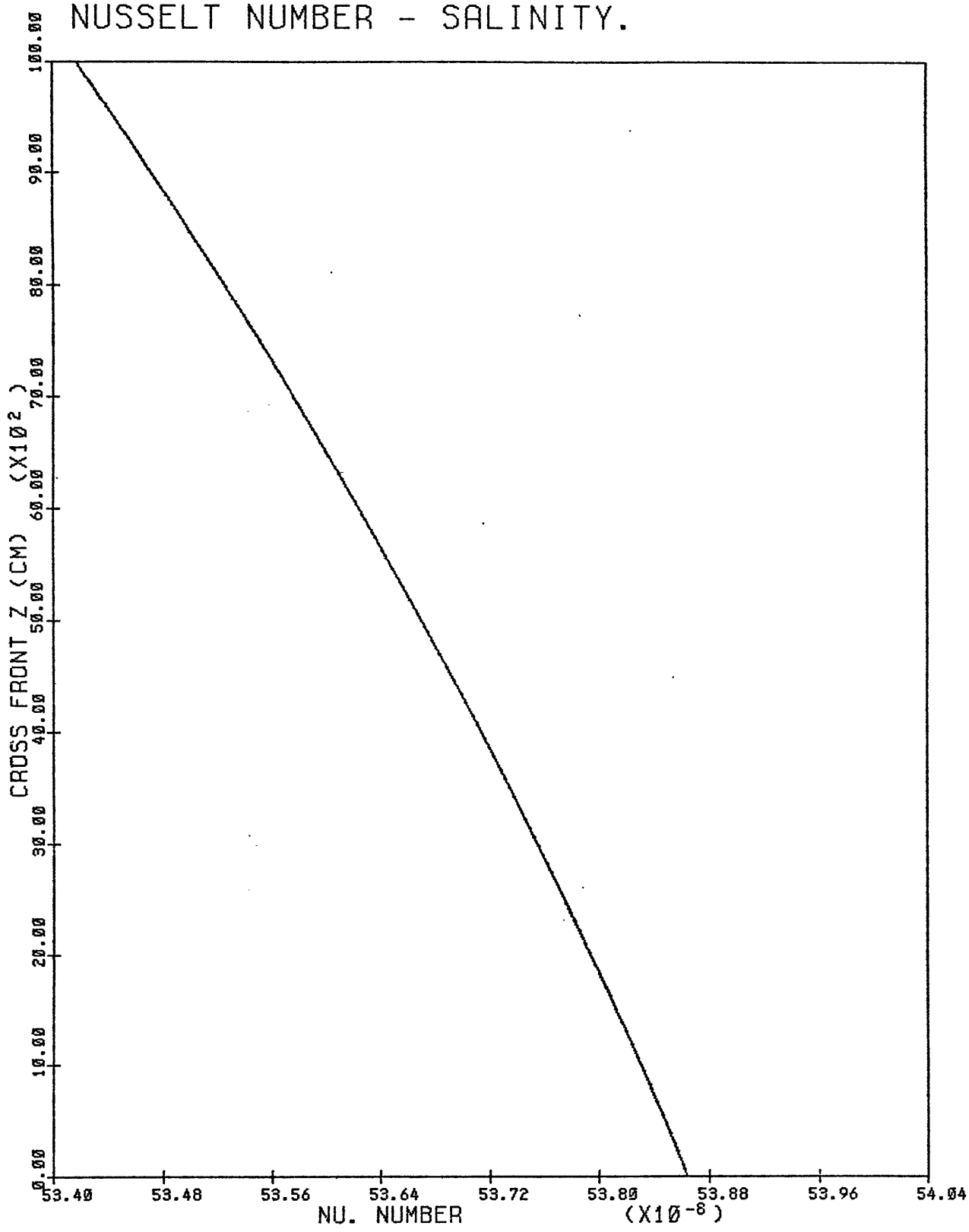


Figure 3.4.7. Nusselt number corresponding to the wave induced salt flux of figure 3.4.3.

3.5 Discussion and results

In this chapter we attempted to show what would be the effect of an internal wave propagating along a front, here visualized as a stratified region of finite thickness having given gradients of temperature and salinity. The results of this chapter can be considered general, since the case of high frequency internal waves is included in the dynamical equations through the inclusion of terms $O(\alpha)$. Although we are assuming a structure like a front, the along front shear was neglected on the basis of scaling arguments. The basic idea of a internal wave field acting on the temperature and salinity gradients through the diffusion of both properties would a priori suggest that the basic dynamics of a front is not being violated. The effect of the shear will be to disperse the layers horizontally.

Even though based on the small perturbation assumption, i.e., that the particle displacements caused by the waves be small compared to the length scale of variability in the mean temperature and salinity field, the non inclusion of nonlinear terms could produce unacceptable errors. The inverse of the wave number along the front suggested as length scale would lead us to the conclusion that the longer the wavelength the less important the nonlinear term in this direction. This was proven from computation of each term of the temperature equation, including the non linear ones, for different frequencies and wave numbers. The computations also have shown that at high frequencies the balance in the temperature equation is between the local and and advective terms, being

the diffusion terms negligible. In this case the wave induced fluxes would expect to be negligible, since the primary physical mechanism is the diffusion.

Another point that deserves comment is the variation of the flux on the thickness of the front which is not shown explicitly. The thickness dependence is included in the dispersion relation (3.3.24c) and its effect on the frequency and wavenumber was tested by calculations. For the same frequency a dispersion relation of a thinner front will yield a larger wave number.

The solution of an internal wave problem, as in Chapter II, for a prescribed distribution of $N(z)$ formally poses an eignevalue problem in which the possible modes and frequencies $\sigma(\ell)$ of small disturbances are to be found. When the $N(z)$ assumed is a stepwise function, like the one we assumed here, it seems that we loose this characteristic of the problem since the mode number is not shown explicitly. But from figures (3.3.2) and (3.3.3) we can identify the wave number as an eigenvalue such that there will be many different wave numbers for a choosen frequency corresponding to higher modes.

The appearance of a temperature and salinity gradient in the expression for the fluxes using the solutions outside the front, where we assumed a constant density, could seem to be odd, but in this case both salinity and temperature gradients are such that $\alpha \bar{T}_s$ balances $\beta \bar{S}_s$.

It was already seen that larger fluxes will occur for low frequency waves and also that if we choose frequencies around the M_2 the

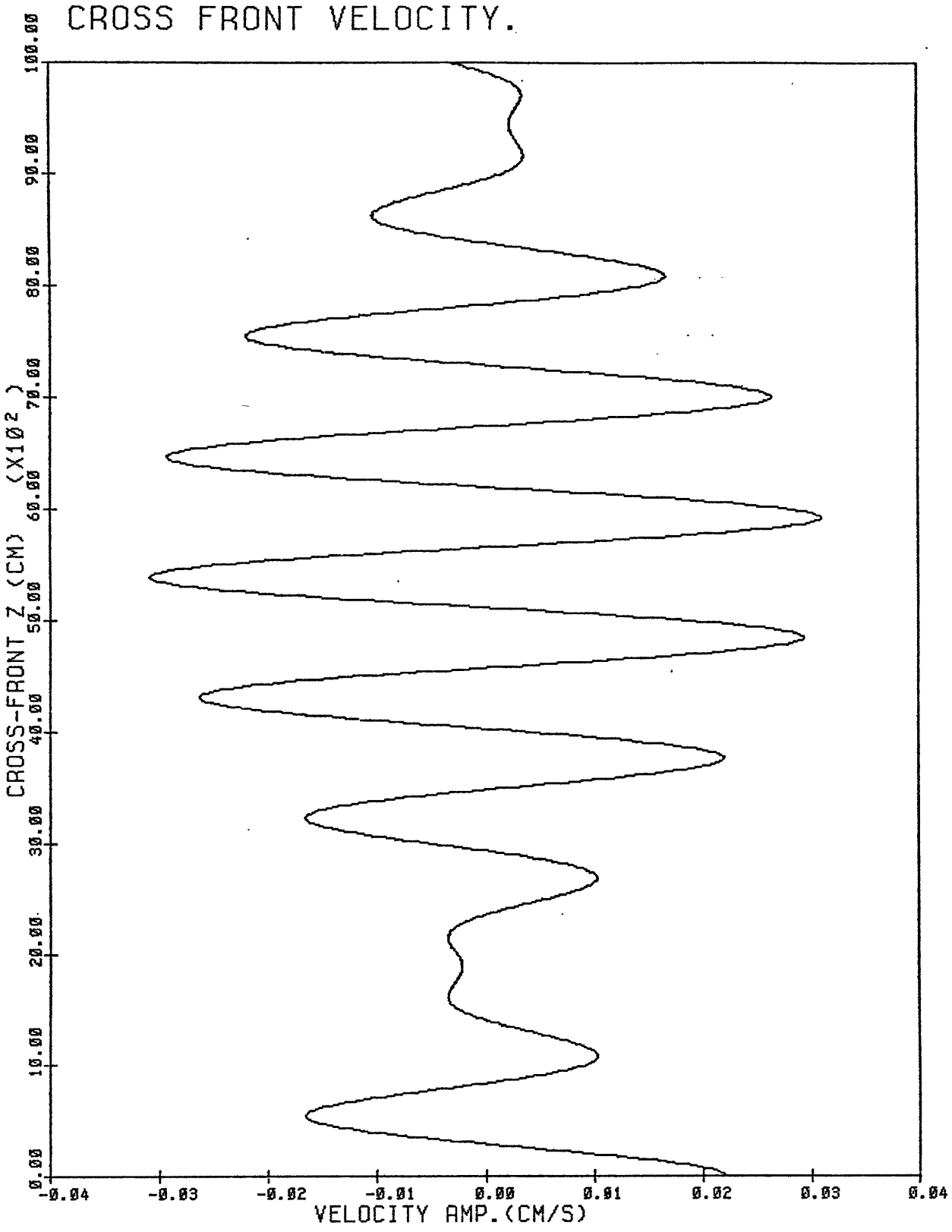


Figure 3.5.1. Cross front velocity amplitude for a wave $\sigma = 10^{-4}\,\mathrm{sec}^{-1}$, $\ell = 10^{-5}$ cm and R=.02 cm/sec in a front 100m thick. The values of f,N,T and S are the same as for NE front.

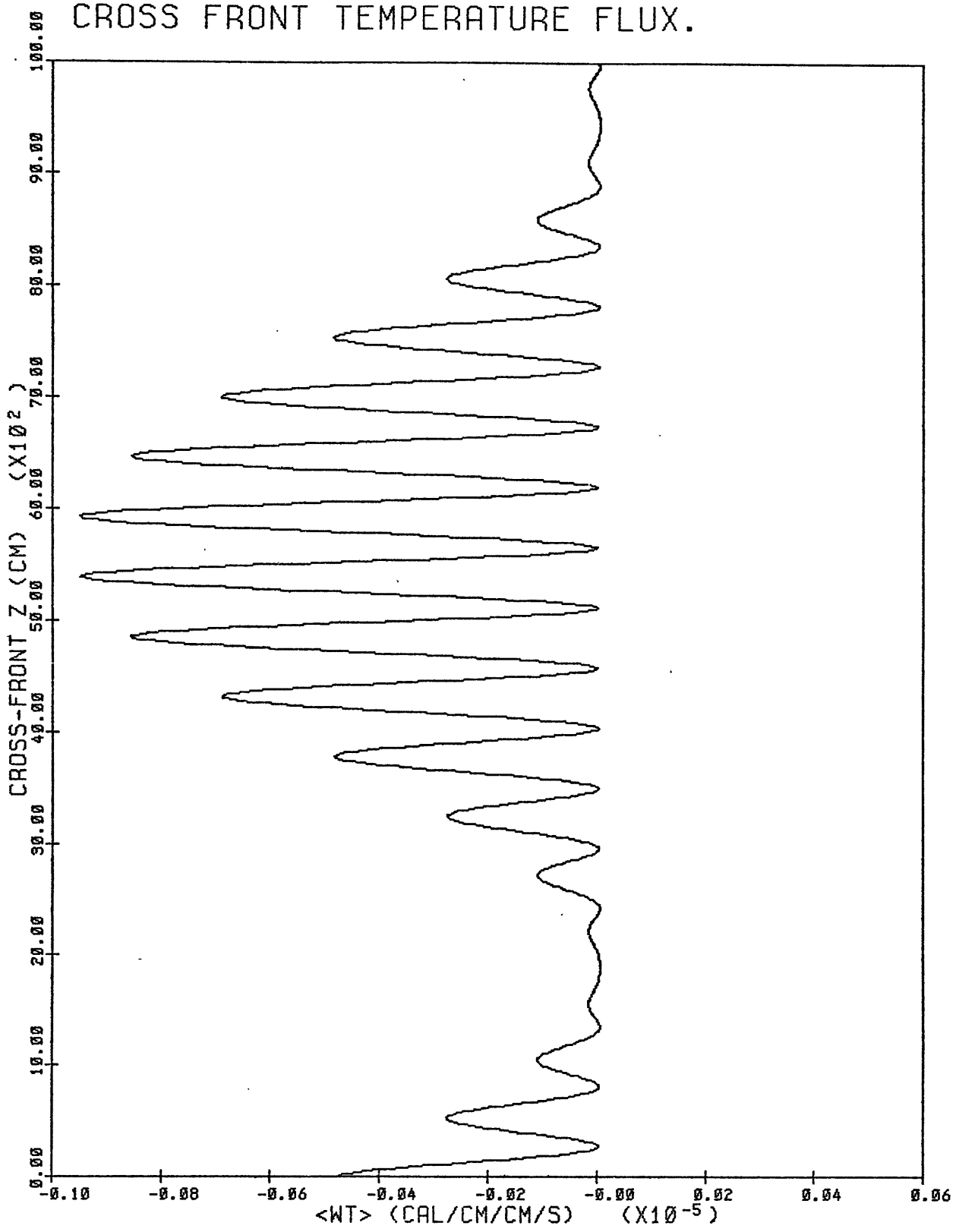


Figure 3.5.2. Cross front wave induced heat flux due to the wave of figure 3.5.1.

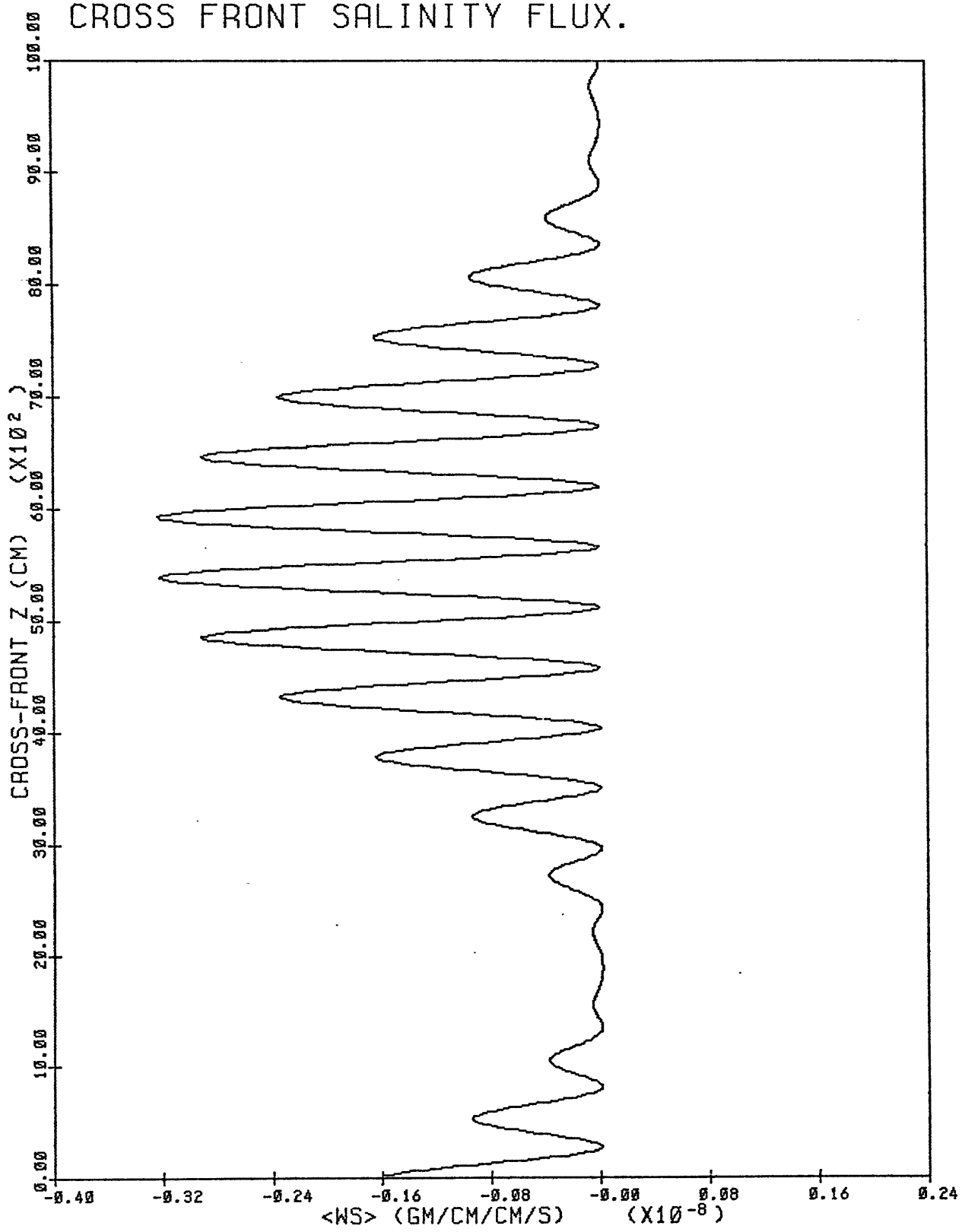


Figure 3.5.3. Cross front wave induced salt flux due to the wave of figure 3.5.1.

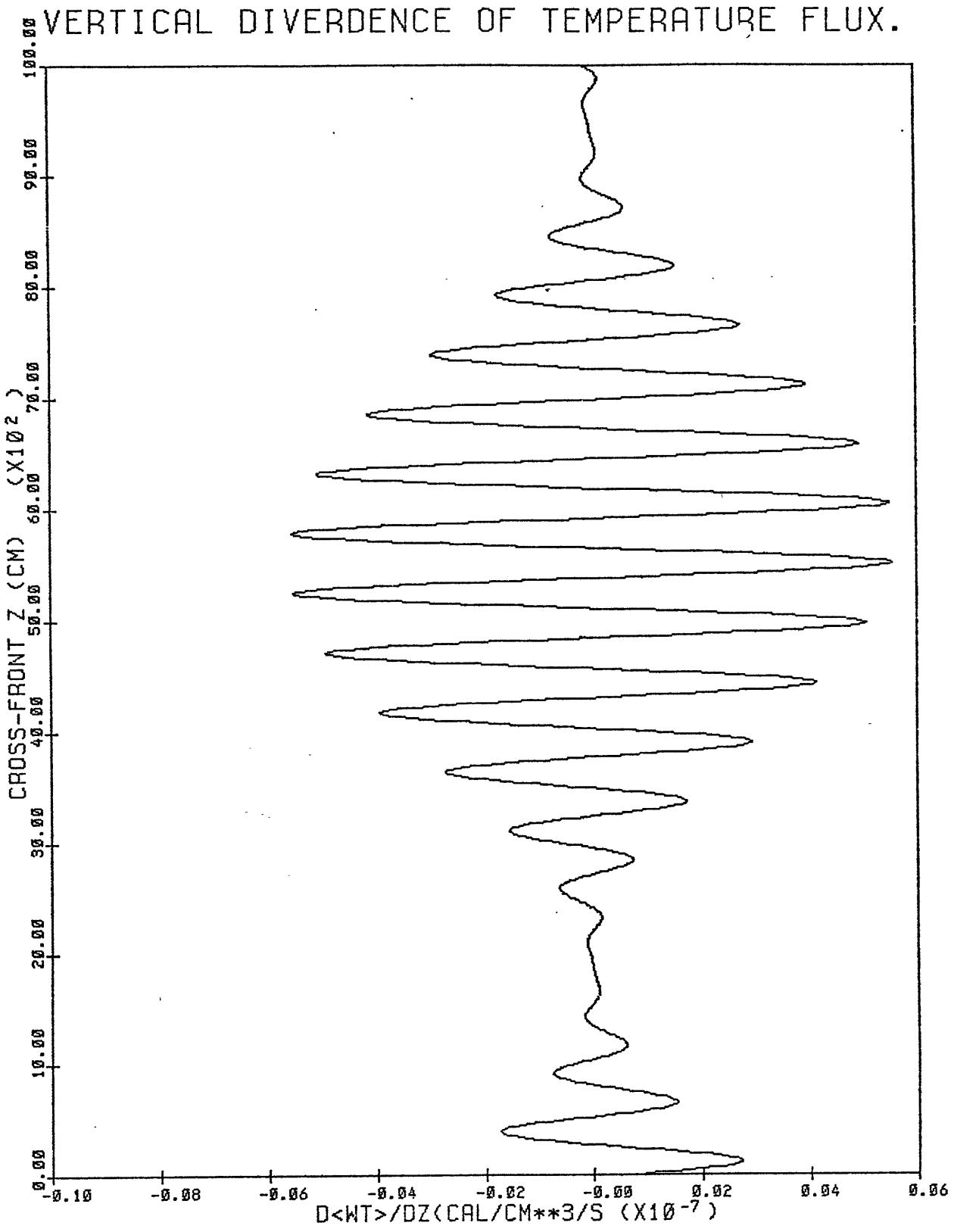


Figure 3.5.4. Vertical divergence of heat flux corresponding to the wave induced flux of figure 3.5.2.

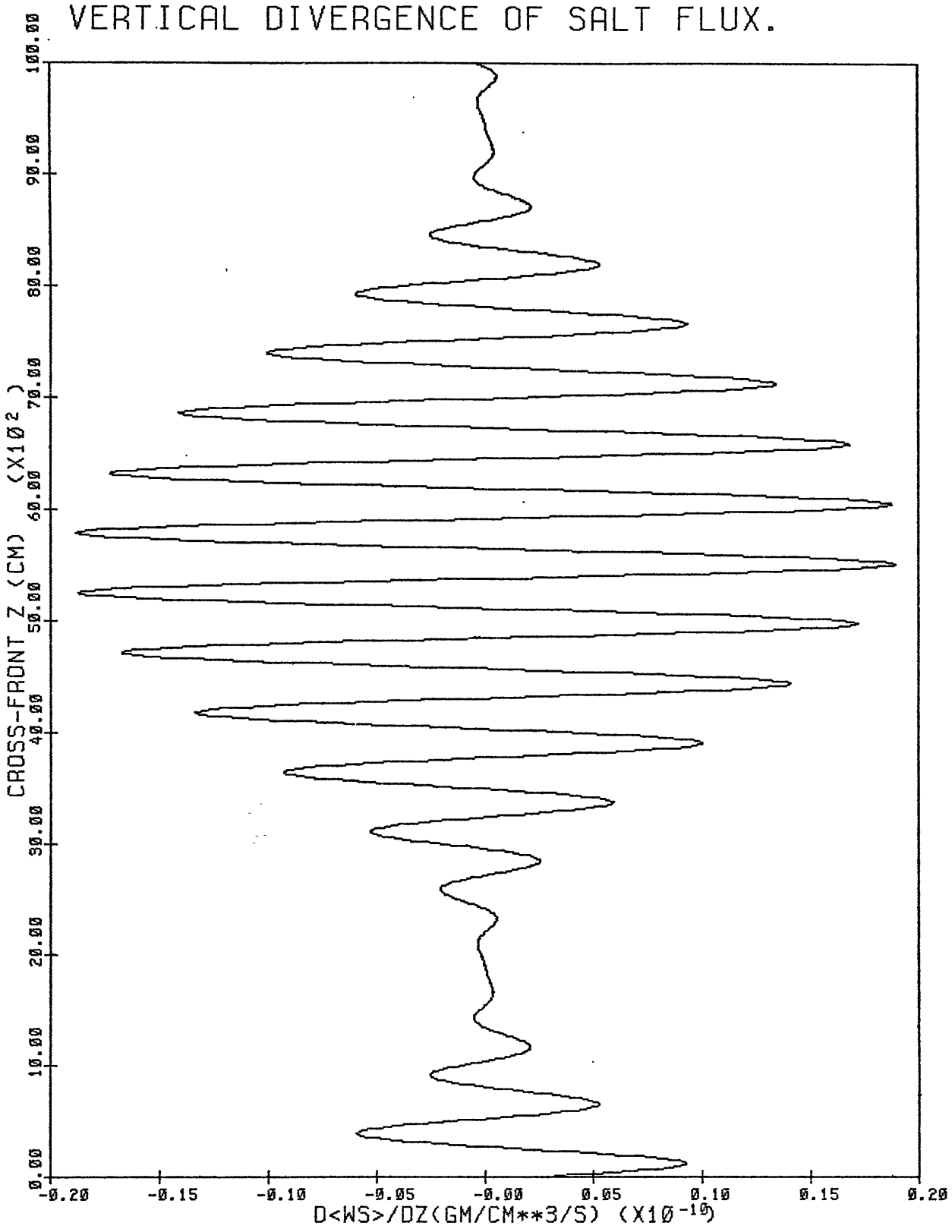


Figure 3.5.5. Vertical divergence of salt flux corresponding to the wave induced flux of figure 3.5.3.

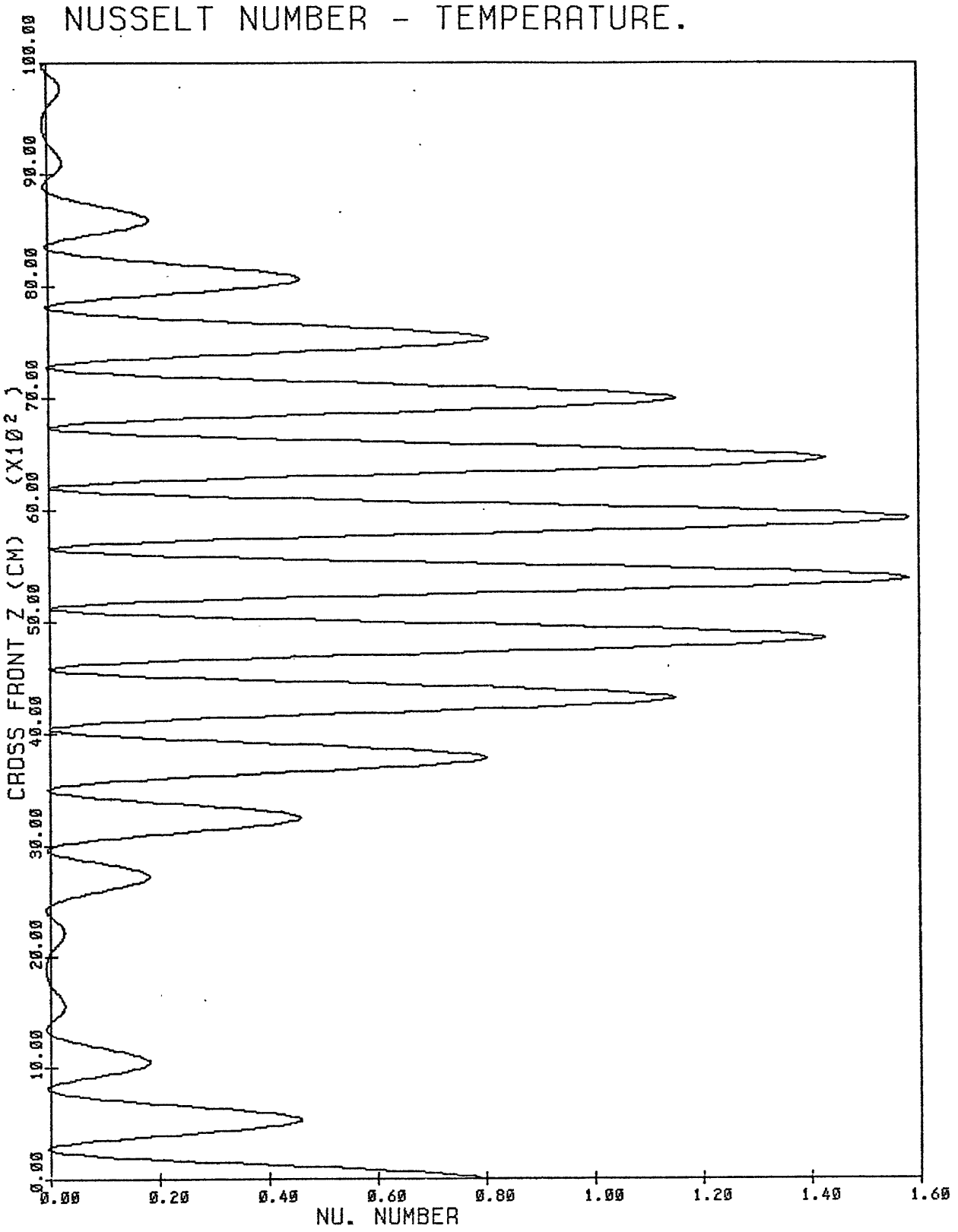


Figure 3.5.6. Nusselt number corresponding to the wave induced heat flux of figure 3.5.2.

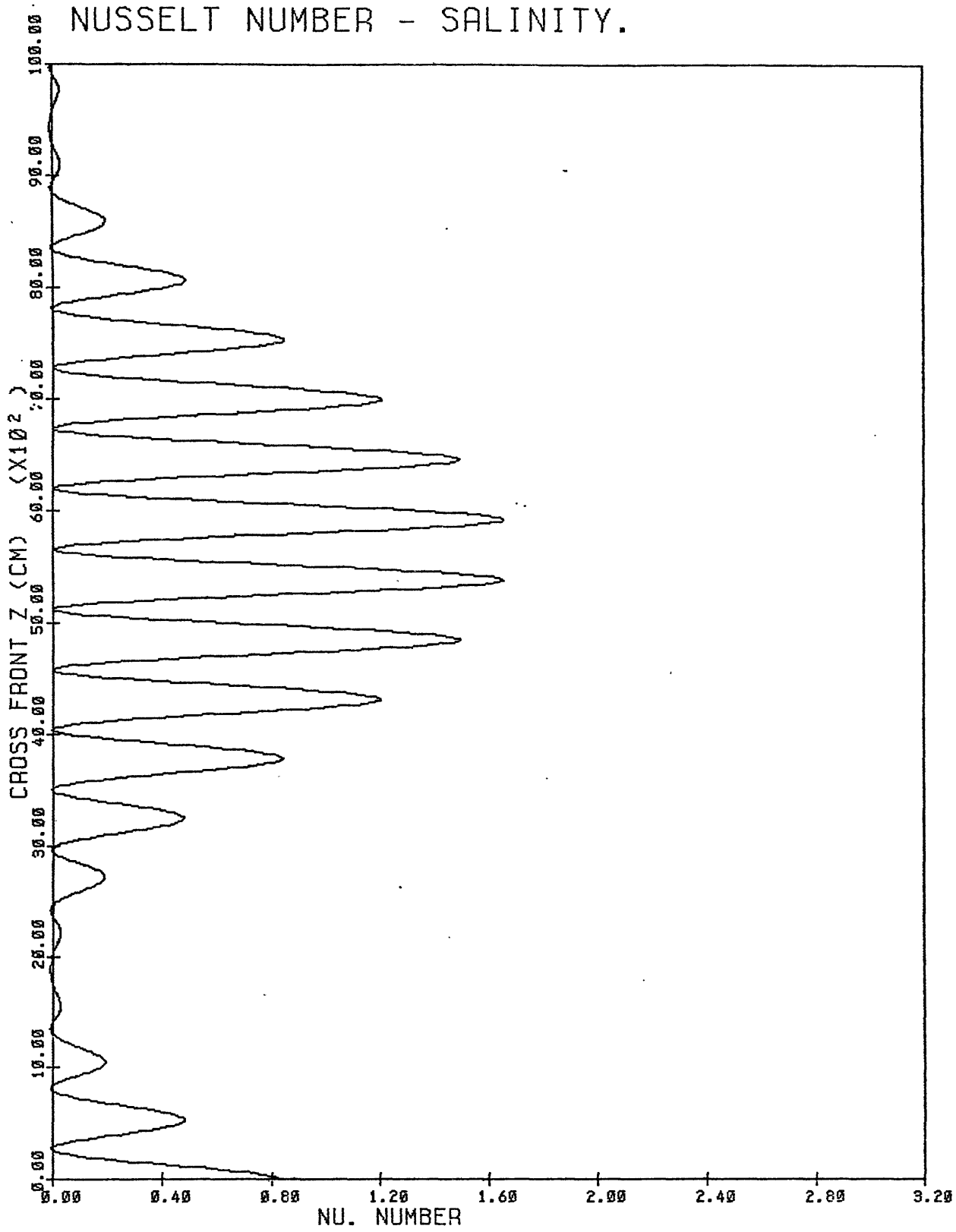


Figure 3.5.7. Nusselt number corresponding to the wave induced salt flux of figure 3.5.3.

corresponding wave number as computed from the dispersion relation will be very small, being necessary to pick high modes. Another result was that small wave numbers will yield negligible fluxes. Since WW_{zz} is a measure of how the temperature (salinity) field is distorted, we expect shorter wavelength waves to yield better results. Based on these facts we choose a frequency $\sigma = 10^{-4}\text{sec}^{-1}$ and ran experiments with different wave numbers and front thickness.

The set of figures 3.5.1 to 3.5.7 show plots of vertical velocity amplitude (w), cross front temperature ($\langle w'T' \rangle$) and salinity ($\langle w's' \rangle$) flux, their divergence $(\langle w'T' \rangle)_z$, $(\langle w's' \rangle)_z$ and Nusselt numbers ($Nu_{_}$, $Nu_{_}$) against cross front coordinate inside a front 100m thick for $\sigma = 10^{-4}\text{sec}^{-1}$ and $\ell = 10^{-5}\text{cm}^{-1}$ and a vertical amplitude corresponding to a 10m vertical diplacement due to semidiurnal internal tide.

The temperature and salinity fluxes are negative in the sense that their direction is opposite to the temperature and salinity gradients, their magnitudes being $10^{-6}\text{cal/cm}^2\text{/sec}$ and 10^{-9}gm of $\text{salt/cm}^2\text{/sec}$ respectively. The rate of heat and salt flow oscillates between positive and negative values of $3\text{x}10^{-9}\text{cal/cm}^3\text{/sec}$ and $10^{-11}\text{gm/cm}^3\text{/sec}$ respectively, while their mean value inside a packet are zero.

If we recall here the results of chapter II, the mean divergence was zero, and the value of the fluxes at the boundary also, because we impose $w=0$ at the surface and at the bottom. Here, due to the fact that we did not impose $w=0$ at the boundaries of the front, but instead, matched with a decaying velocity outside the front, we do not

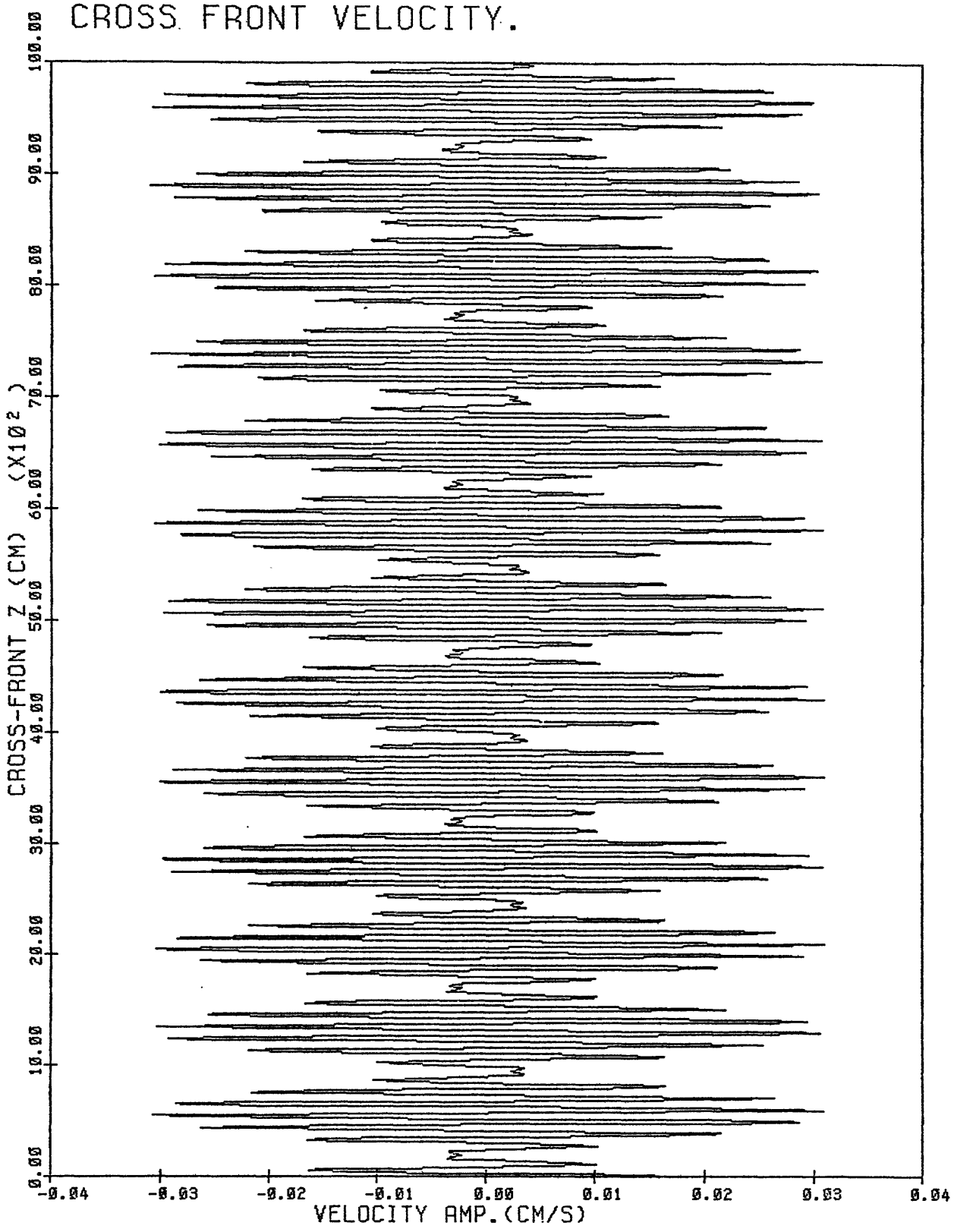


Figure 3.5.8. Cross front velocity amplitude for a wave $\sigma = 10^{-4}\,\mathrm{sec}^{-1}$, $\ell = 10^{-4}$ cm and R =.02 cm/sec in a front 100m thick.

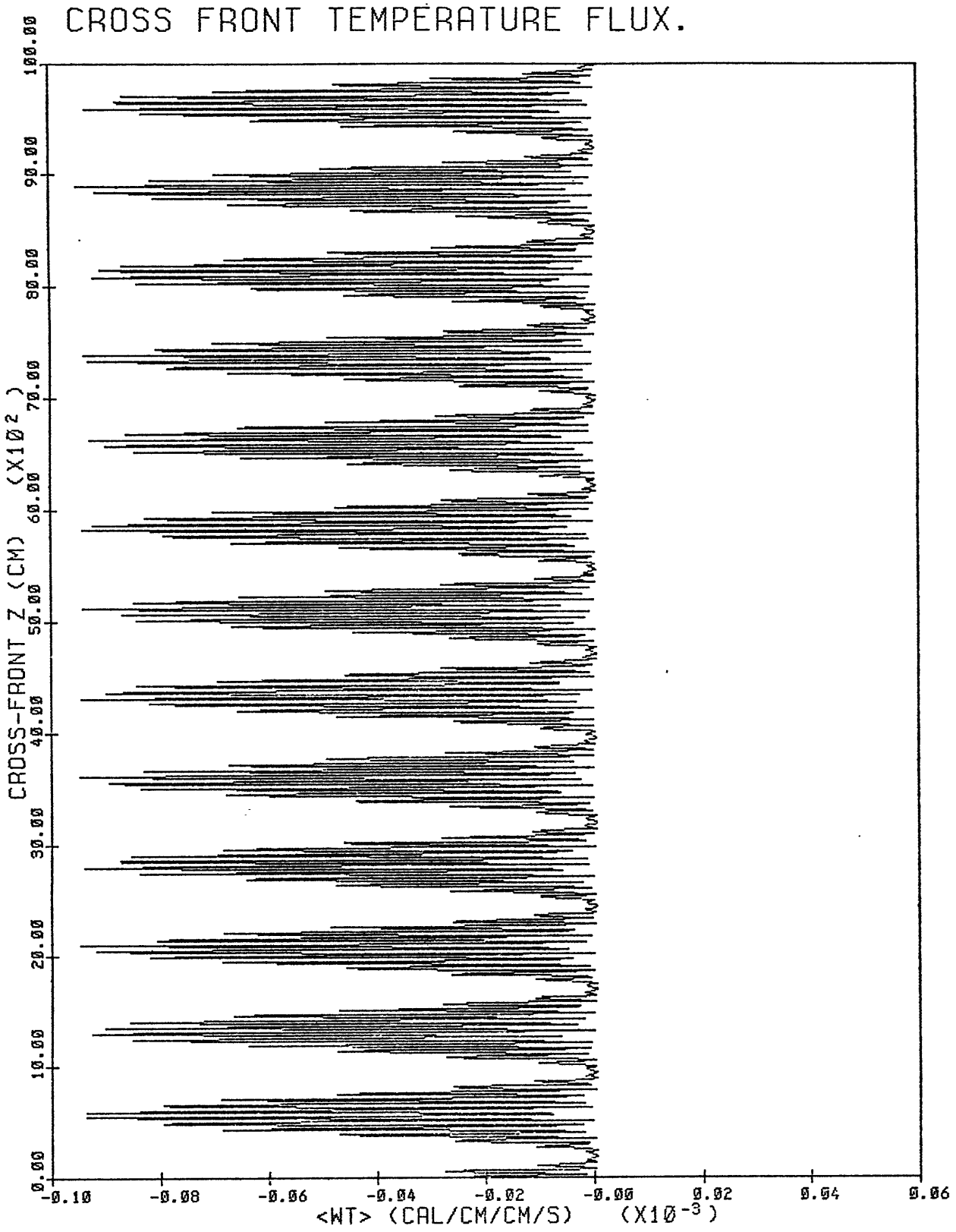


Figure 3.5.9. Cross front wave induced heat flux due to the wave of figure 3.5.8.

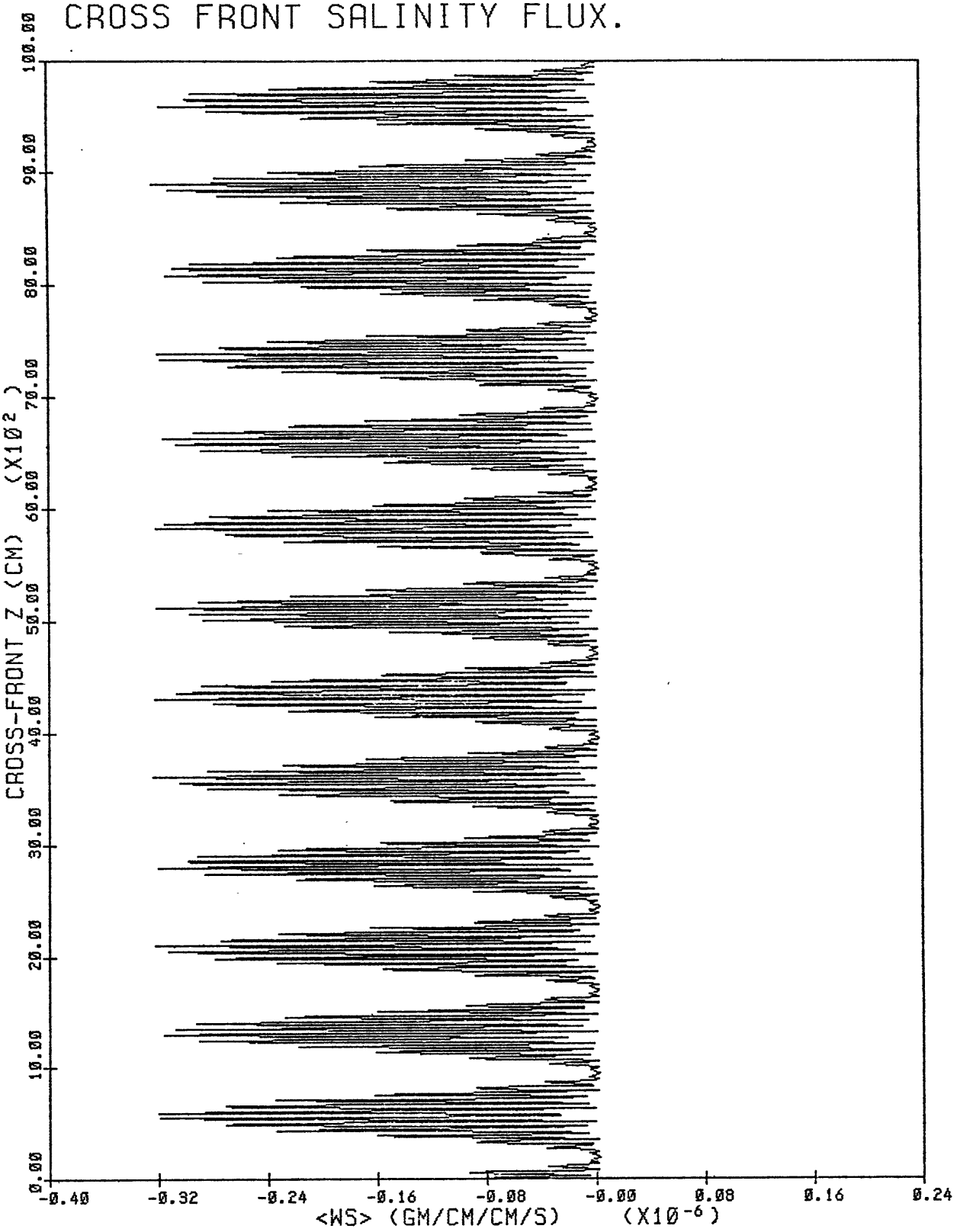


Figure 3.5.10. Cross front wave induced salt flux due to the wave of figure 3.5.8.

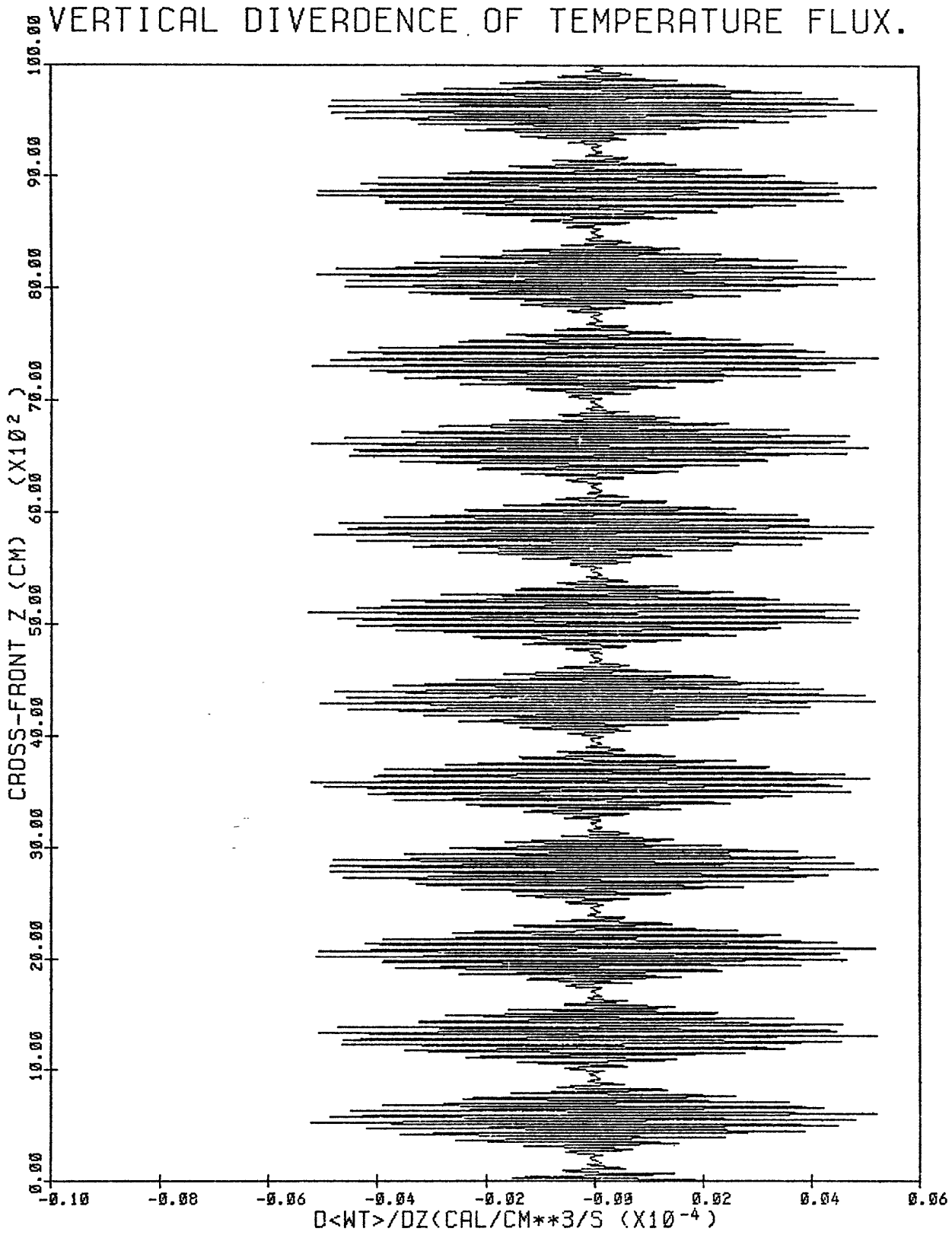


Figure 3.5.11. Vertical divergence of heat flux corresponding to the wave induced flux of figure 3.5.9.

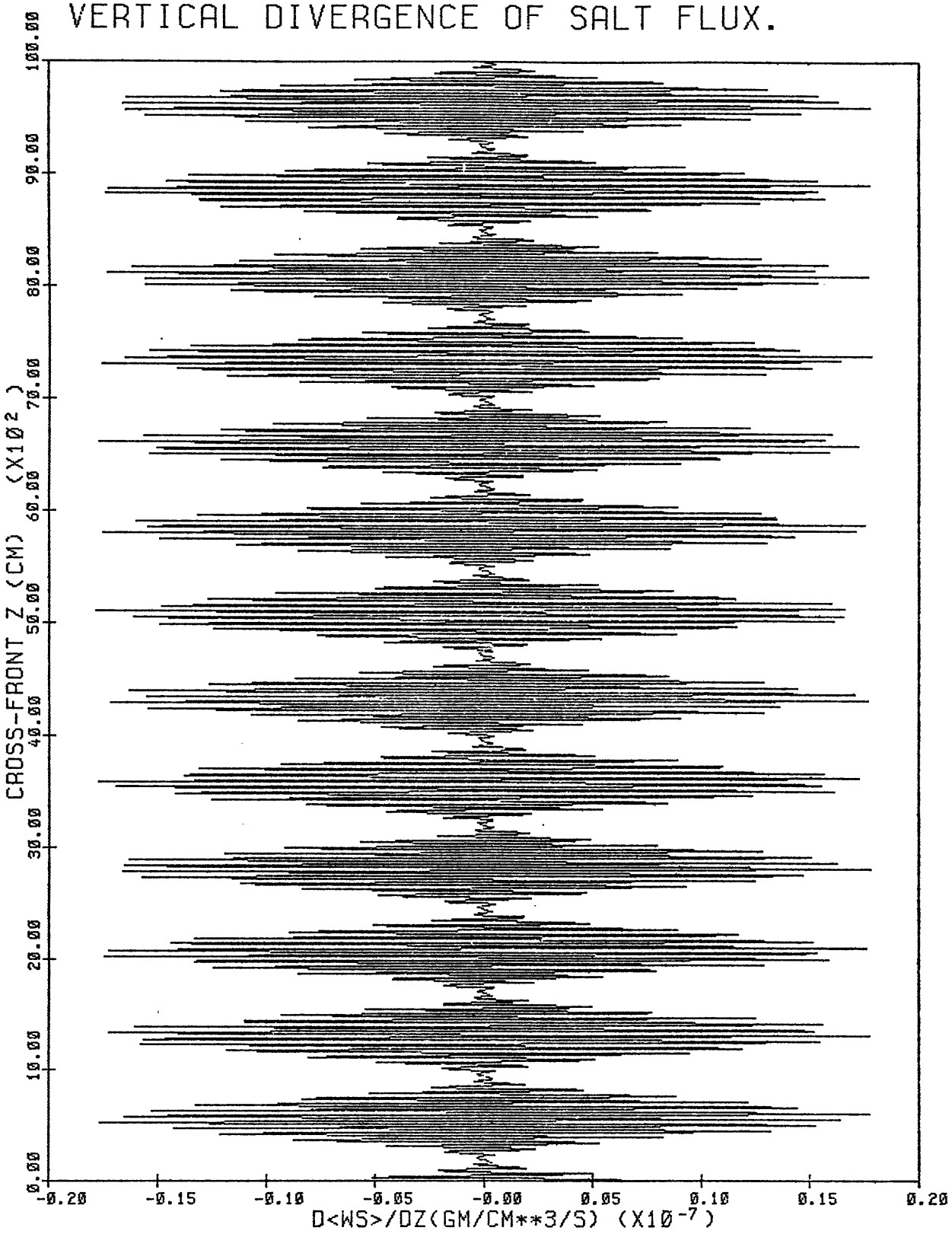


Figure 3.5.12. Vertical divergence of salt flux corresponding to the wave induced flux of figure 3.5.10.

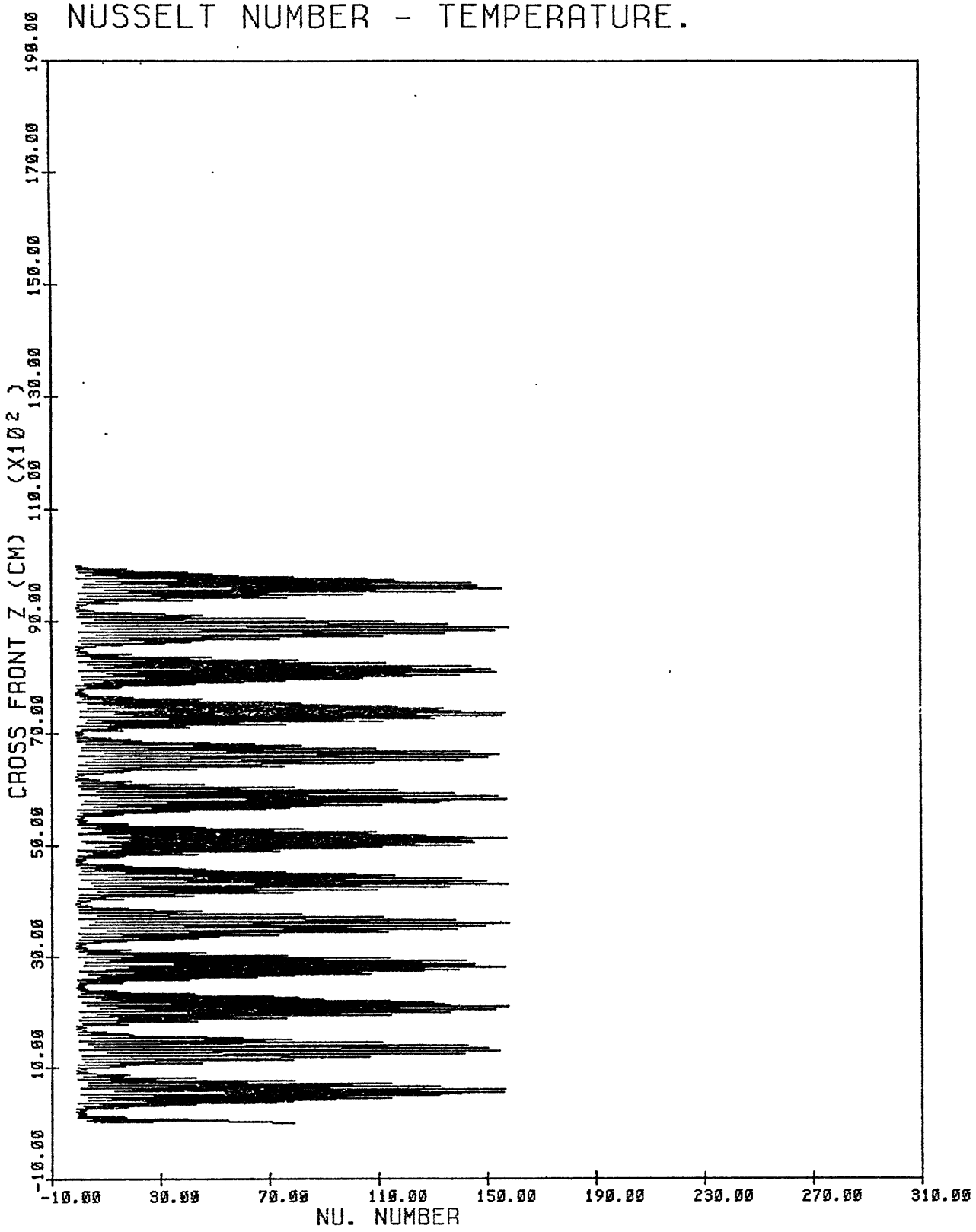


Figure 3.5.13. Nusselt number corresponding to the wave induced heat flux of figure 3.5.9.

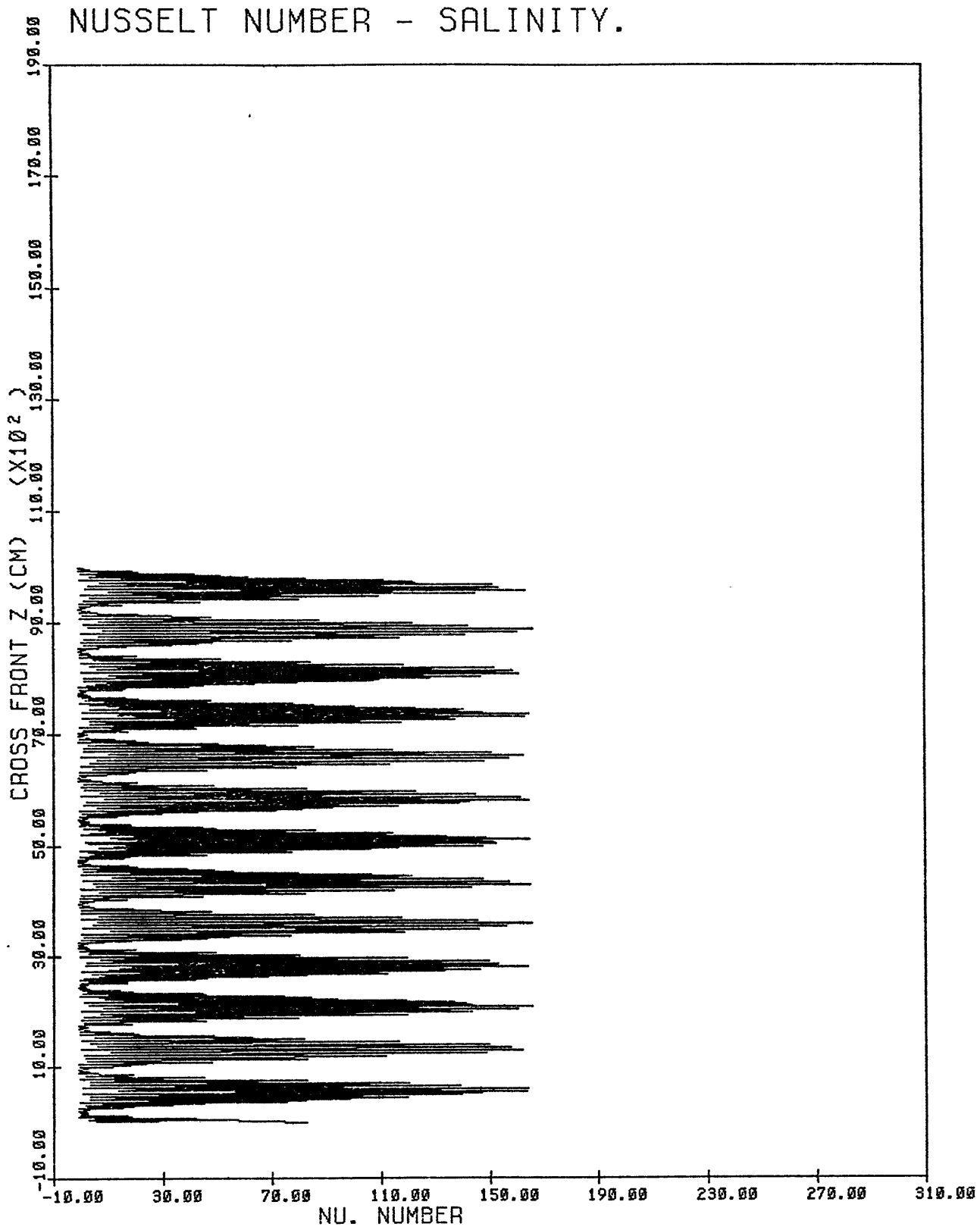


Figure 3.5.14. Nusselt number corresponding to the wave induced salt flux of figure 3.5.10.

have an entire number of wave packets inside the front and also the value of the fluxes are different from zero at the boundaries. But in spite of all this the mean divergence is still zero or negligible, meaning that there is no wave-induced fluxes of either salt or temperature across the front, but only a tendency of form layers.

The Nusselt numbers are approximately equal for temperature and salinity having highest values of 1.6. Remember that they are equal for small wave numbers. If we increase the wave number by one order of magnitude the effect is an increase of two orders of magnitude in all the quantities, the Nusselt number reaching a value of 160 in this case. The plots for $\ell = 10\text{-}4 cm^{-1}$ and same frequency are shown in figures 3.5.8 to 3.5.14. Following a personal communication of Dr. Charles Flagg that suggested as typical thickness of the New England shelf break front 40m, we computed the same quantities for this thickness. The values of $\overline{T}_z$ and $\overline{S}_z$ were changed such that $\alpha\Delta T$ and $\beta\Delta S$ did not change in order to keep N constant. The results of these calculations are shown again for a wave number $\ell = 10^{-4} cm^{-1}$ in figures 3.5.15 to 3.5.21. The values of correspondent quantities are of the same order but a bit smaller due to the decrease of $\overline{T}_z$ and $\overline{S}_z$. From those sets of figures we see that the different thickness does not change, as expected, the character of the wave, but only introduces more or less packets if it is increased or decreased. This happens because we are not computing the wave number through the dispersion relation (3.3.24c). From the plots of the divergence of the fluxes we can have

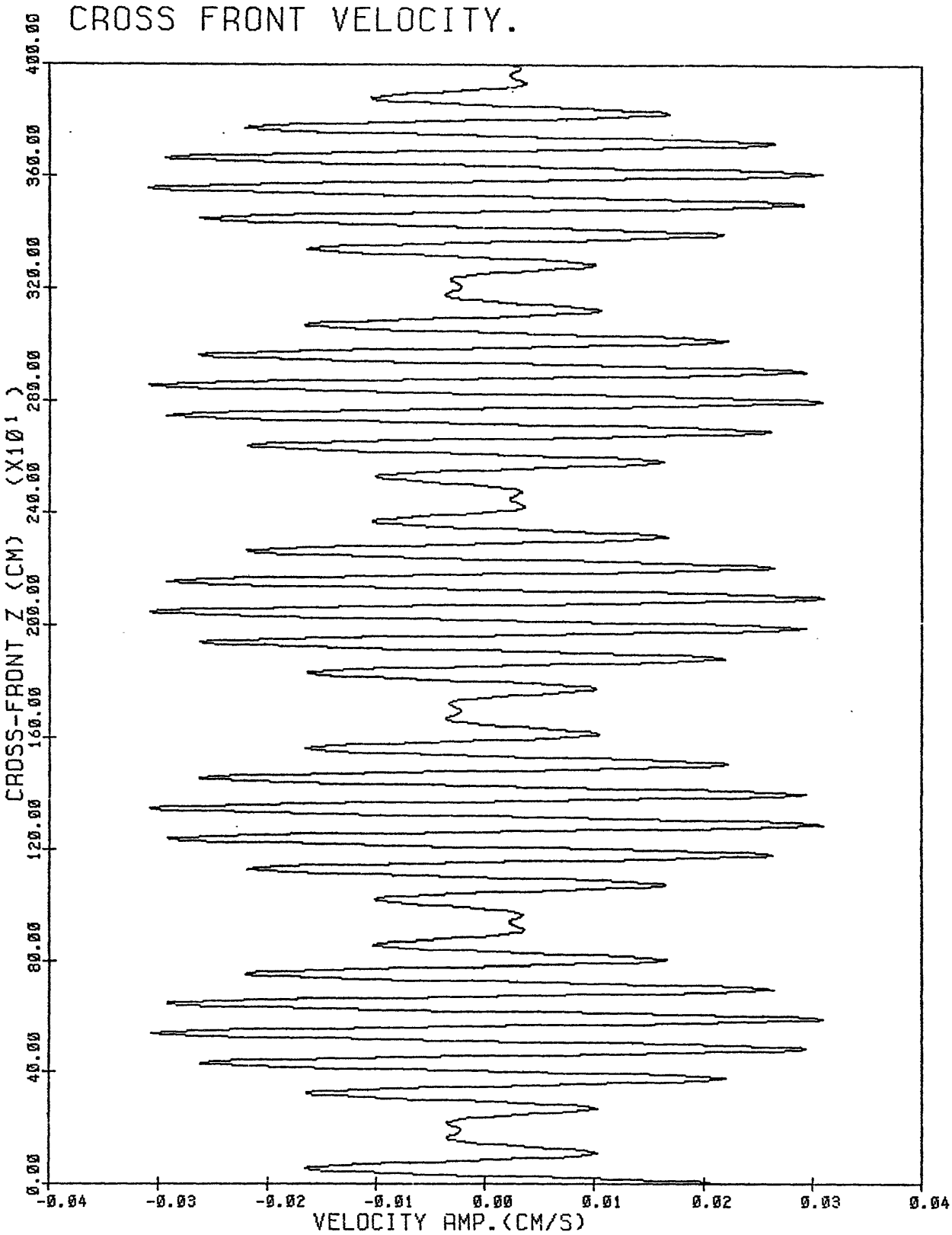


Figure 3.5.15. Cross front velocity amplitude for a wave $\sigma = 10^{-4}\,\mathrm{sec}^{-1}$, $\ell = 10^{-4}$ cm and R =.02 cm/sec in a front 40m thick.

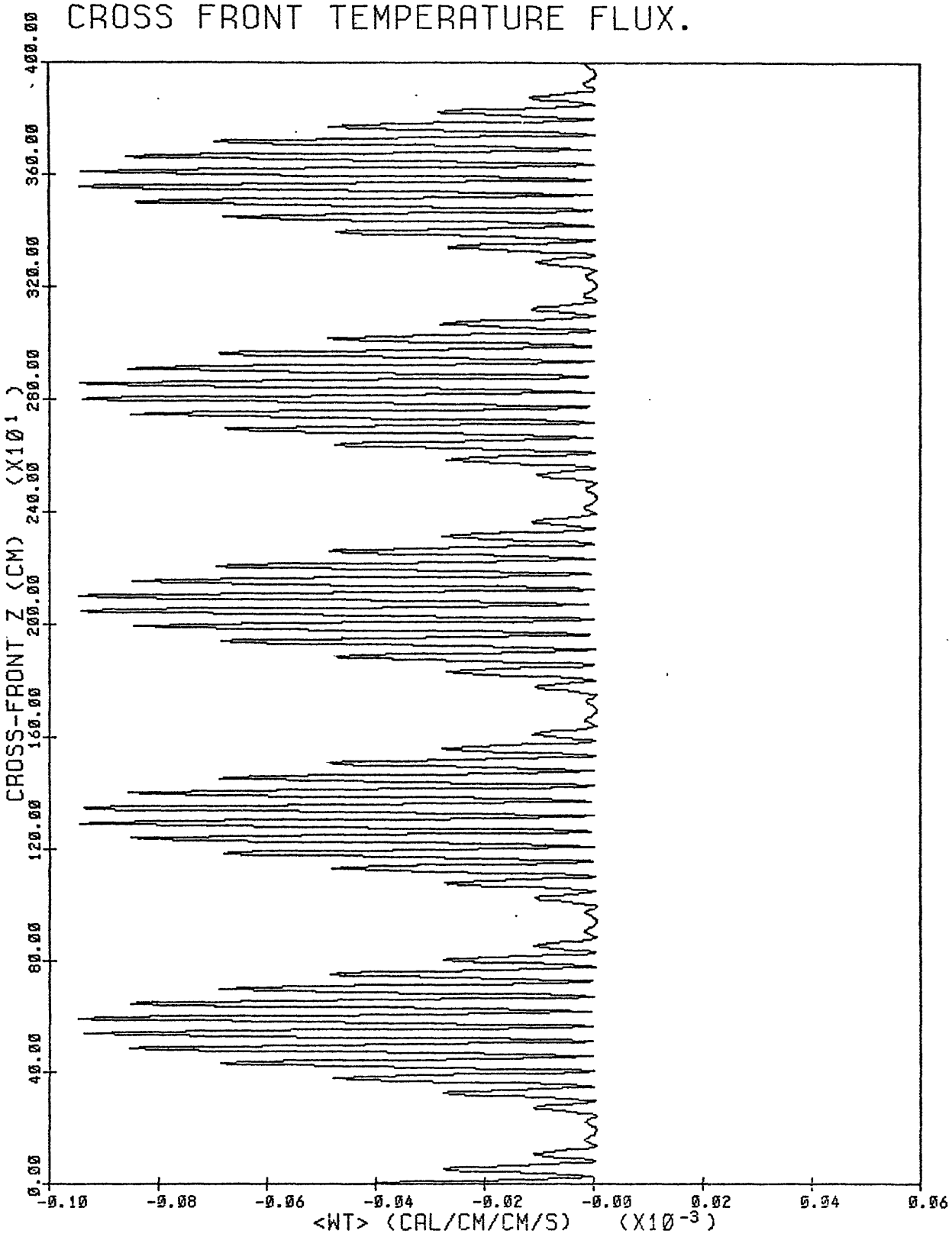


Figure 3.5.16. Cross front wave induced heat flux due to the wave of figure 3.5.15.

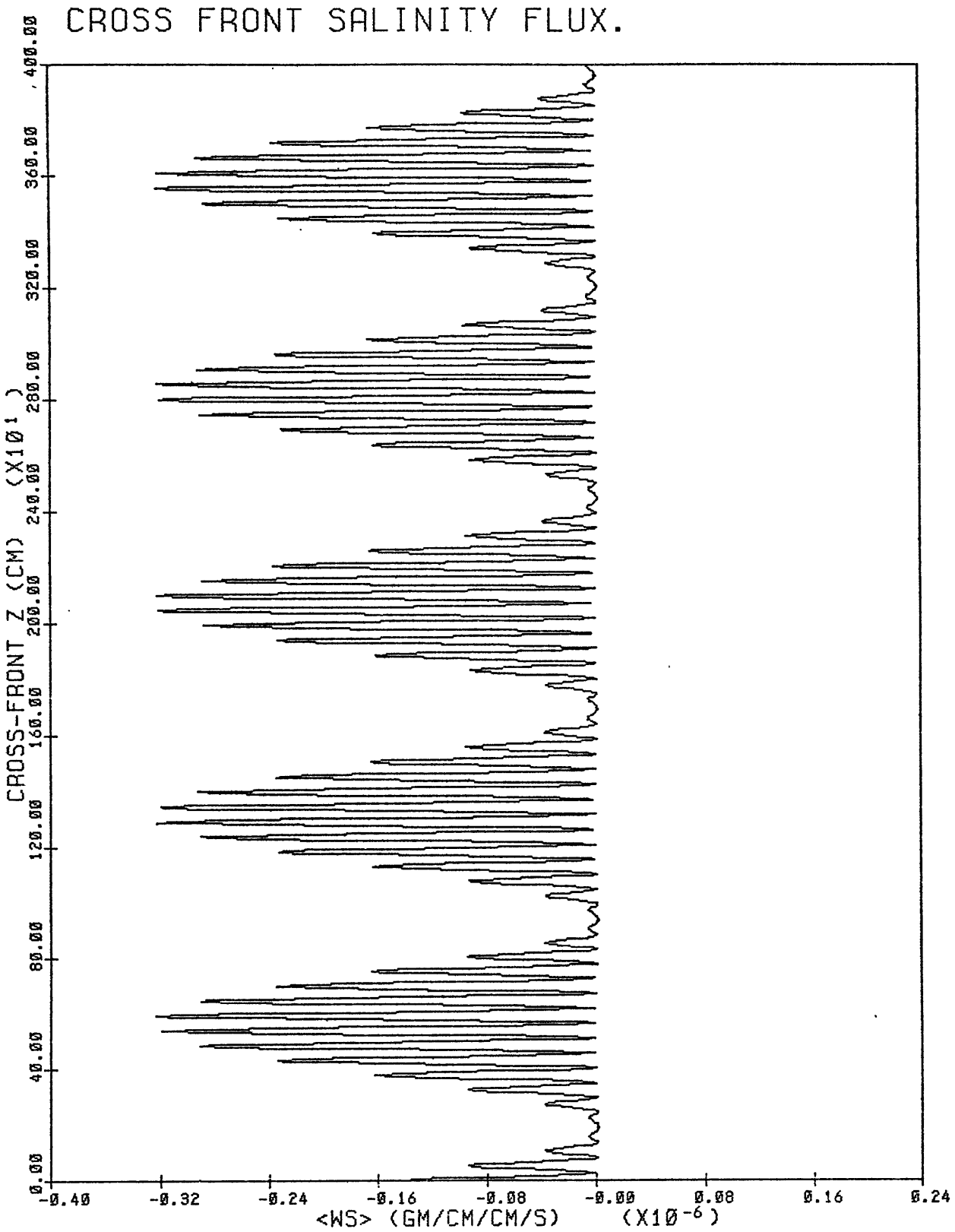


Figure 3.5.17. Cross front wave induced salt flux due to the wave of figure 3.5.15.

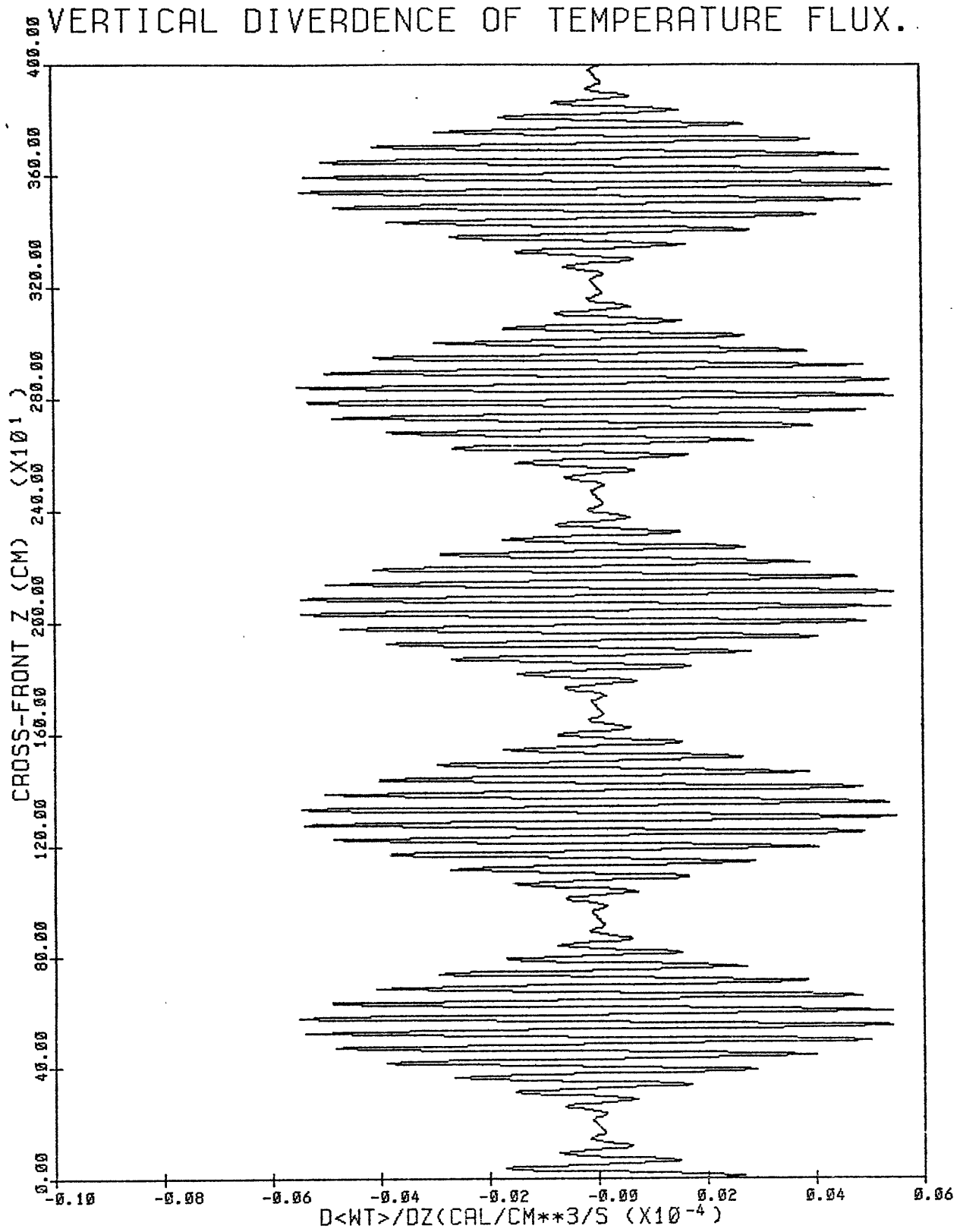


Figure 3.5.18. Vertical divergence of heat flux corresponding to the wave induced flux of figure 3.5.16.

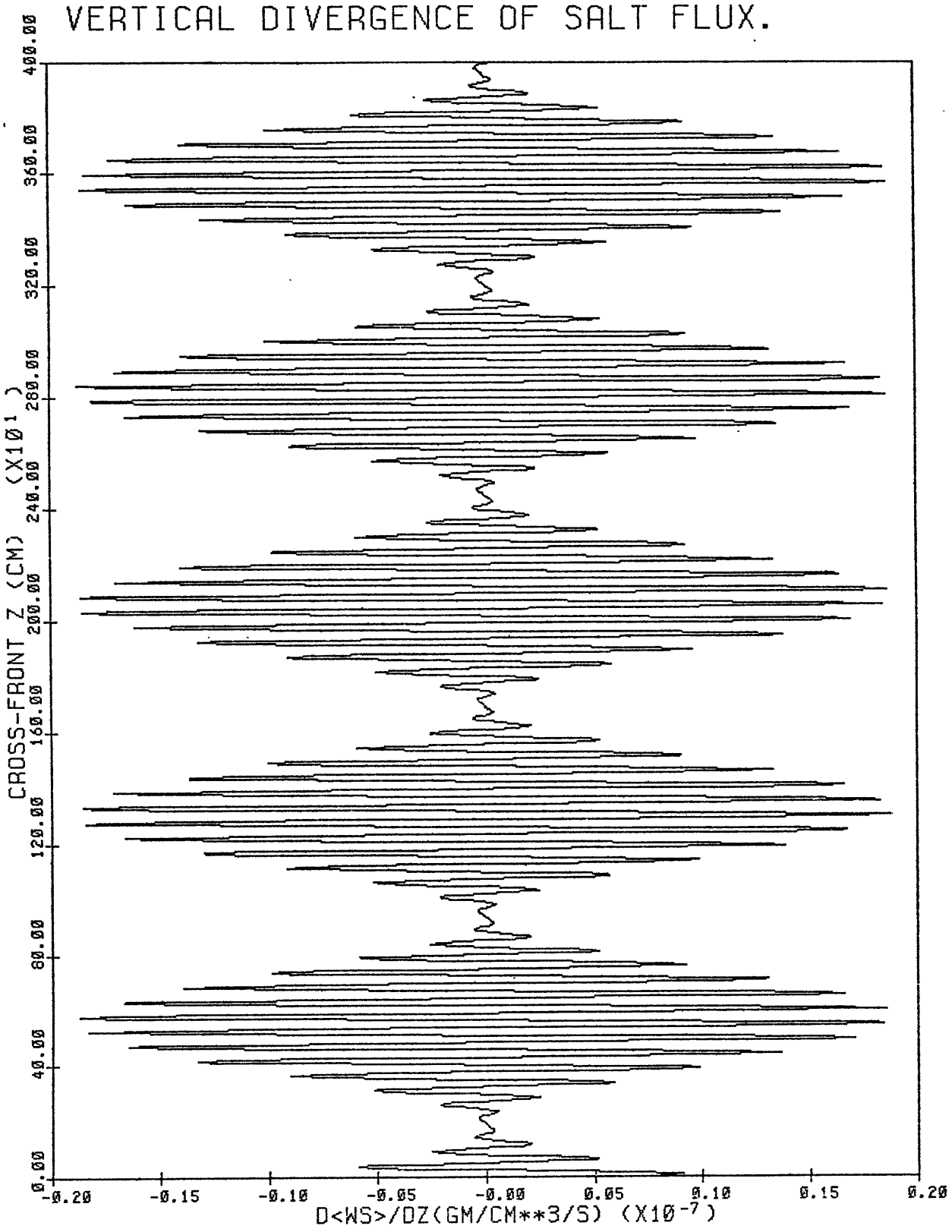


Figure 3.5.19. Vertical divergence of salt flux corresponding to the wave induced flux of figure 3.5.17.

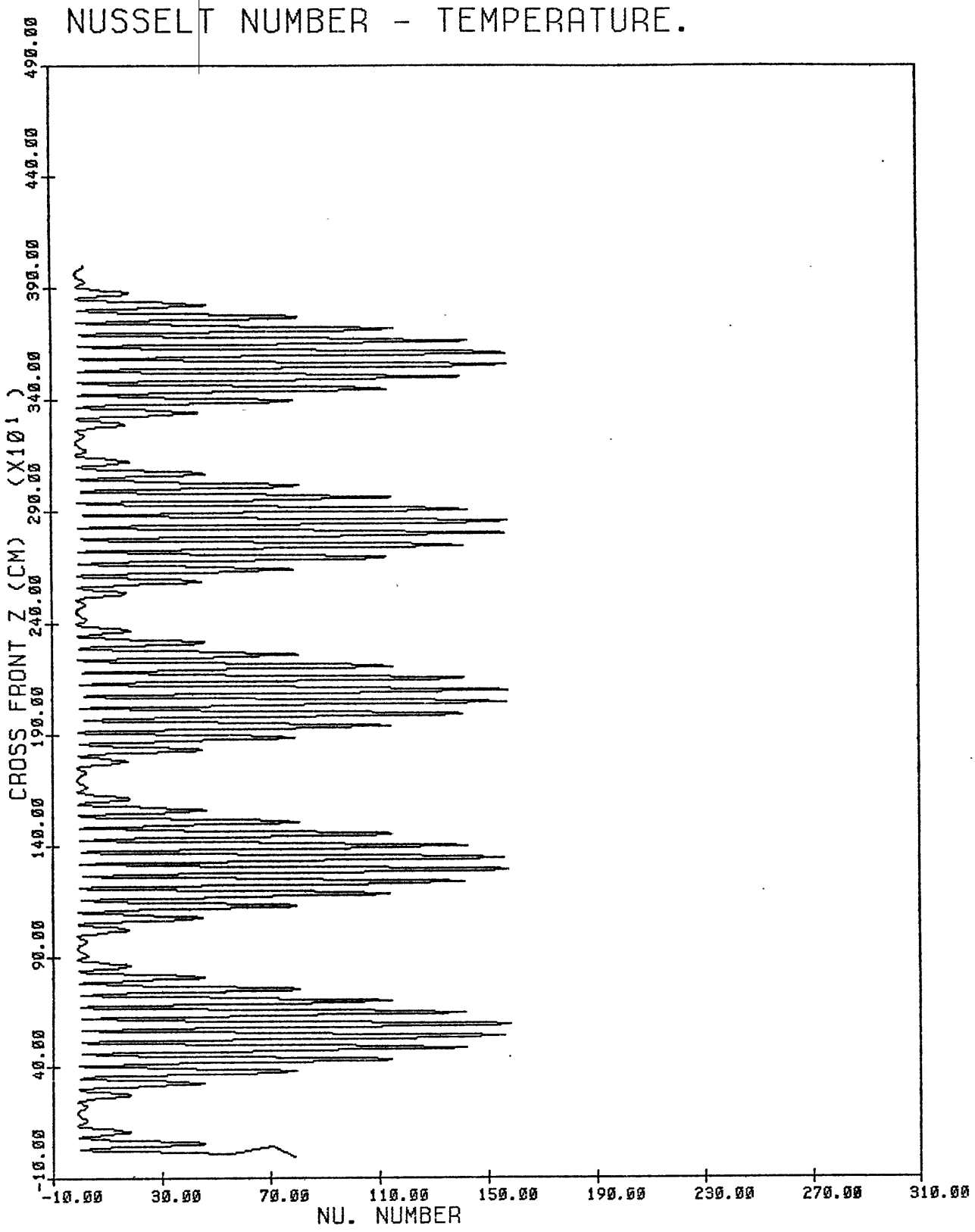


Figure 3.5.20. Nusselt number corresponding to the wave induced heat flux of figure 3.5.16.

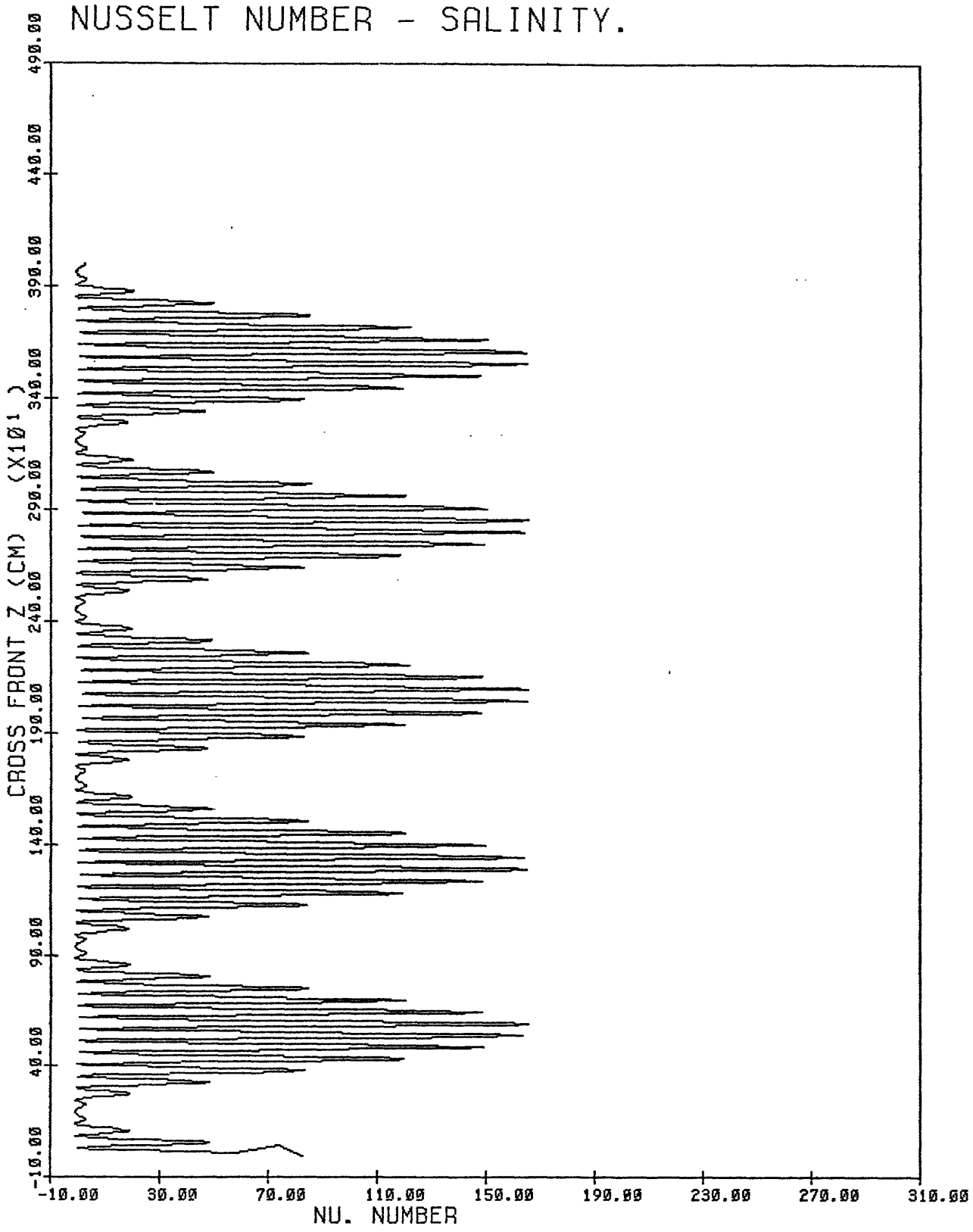


Figure 3.5.21. Nusselt number corresponding to the wave induced salt flux of figure 3.5.17.

an idea of where to expect the layers to be formed. If we assume that a high Nusselt number would indicate mixing a wave with $\sigma = 10^{-4} sec^{-1}$ and $\ell = 10^{-4} cm^{-1}$, propagating in a 100m thick front, according to figure 3.5.11 will induce the largest transports at approximately every 10m. On the other hand the same wave in a 40m thick front will induce largest transports at every 20m approximately (see figure 2.5.20).

Chapter IV

Applications to estimates of fluxes induced by forced internal waves.

4.1 Introduction

In the previous chapters, it was shown that free internal waves will not induce appreciable fluxes and result in negligible Nusselt numbers. The results of the two simple models, the linear stratification and the frontal case showed the flux dependence on amplitude and wave number. From the observed spectra of Siedler (1971, 1974), Webster (1972), Briscoe (1975) and from analytical spectra, Garret and Munk (1972, 1975), Desaubies (1975) we learn that the vertical velocity signal increases with frequency and is expected to decrease with increasing mode numbers, so from the expression for fluxes (2.4.8b) we see that there is a trade-off between σ and n, so that there will be no appreciable change in flux over the wavenumber range. The question to ask is therefore: What kind of wavelike disturbances will be able to induce mixing?

From the results of the previous chapter we learned that a disturbance must have low frequency and, at the same time, a large wavenumber. Besides that, a large amplitude will increase the flux proportionally to the square of amplitude. Only forced internal waves appear to fulfill these requirements. Such waves are mainly results of oscillatory or steady flow over topography, or alternatively, atmospheric forcing, as described by Hunkins and Fliegel (1973) or from unknown cases, Ivanov (1976), Perry and Schimke (1965).

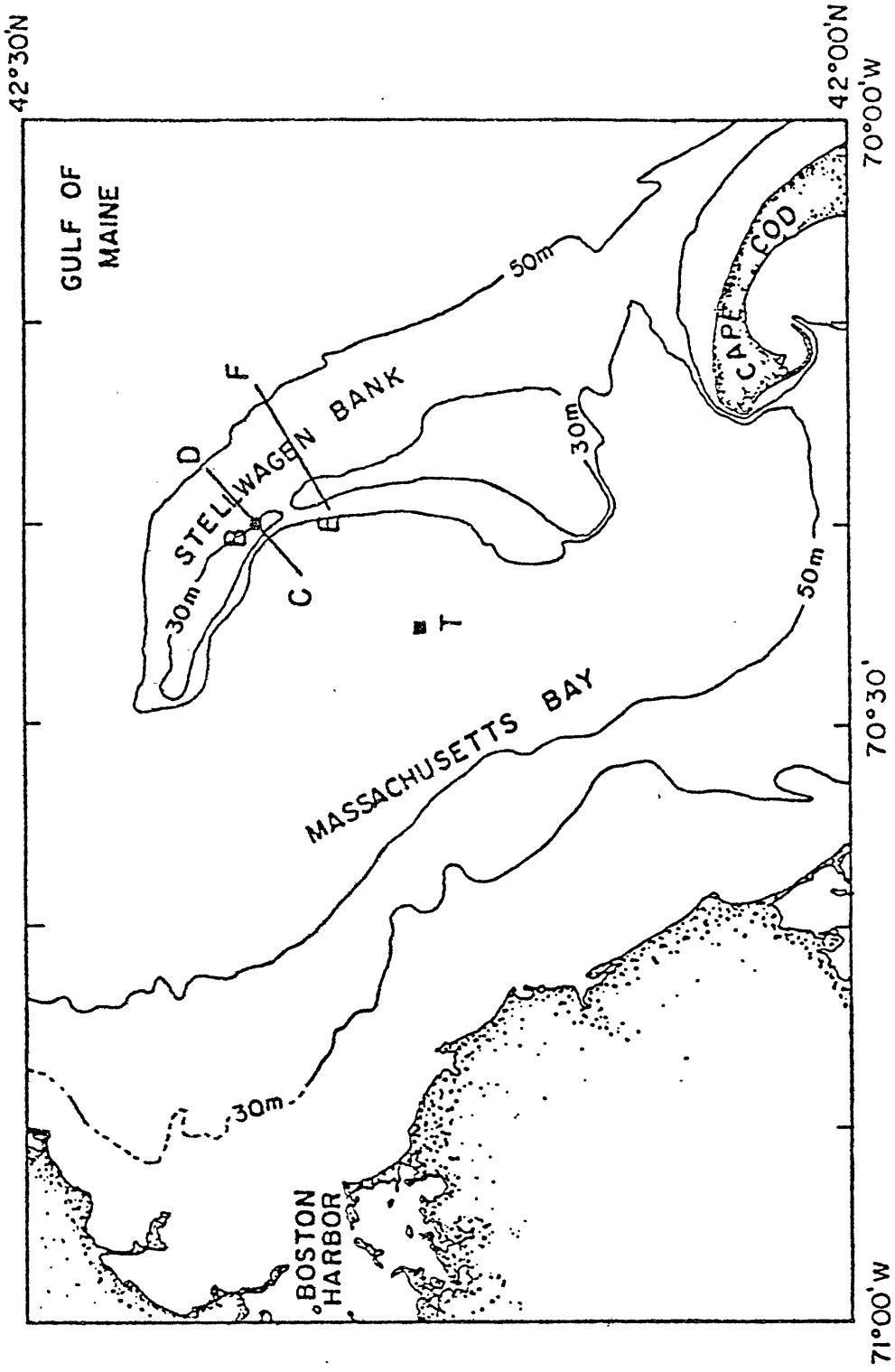


Figure 4.2.1. Chart of Massachusetts Bay showing Stellwagen Bank, the steaming track (CD) performed by Chereskin(1982),the XBT section (ef) by Haury et al,(1979) and also the position of Chereskin (B) and Halpern (T) moorings. (Map after Chereskin,1982).

In Massachusetts Bay, Halpern (1971a) found the following amplitudes for the first five modes of the semi-diurnal internal tide: first mode, 3.68m; second mode, 0.88m; third mode, 1.71m; fourth mode, 2.70m; fifth mode, 2.22m. As is apparent there is no clear relationship for the dependence of amplitude on mode number, at least for forced waves; after all, this is largely determined by the forcing.

In the following sections we are going to use the results from different observations of topographically forced waves, and compute the induced heat fluxes and the corresponding Nusselt numbers.

4.2 Massachusetts Bay observations.

A series of observations concerning the generation and propagation of internal waves at Stellwagen Bank in Massachusetts Bay, shows the evidence of lee waves and waves propagating away from topography, Halpern (1971a, 1971b), Haury et al. (1979), Chereskin (1982). The geographical location of the observation is shown in figure 4.2.1, and details of the measurements can be obtained in the cited papers. According to Haury et al., the ebb tide flow over Stellwagen Bank generates a lee wave on the eastern side. When the tide turns to flood, the lee wave propagates into Massachusertts Bay. From Chereskin's acoustic images and XBT sections we can estimate a wavelength of order 4.6 km, she computed the phase speeds for the first three modes as 23 cm/sec, 10.4 cm/sec and 7.1 cm/sec, respectively. From this we can compute the frequency, and the amplitude of each mode by estimating a

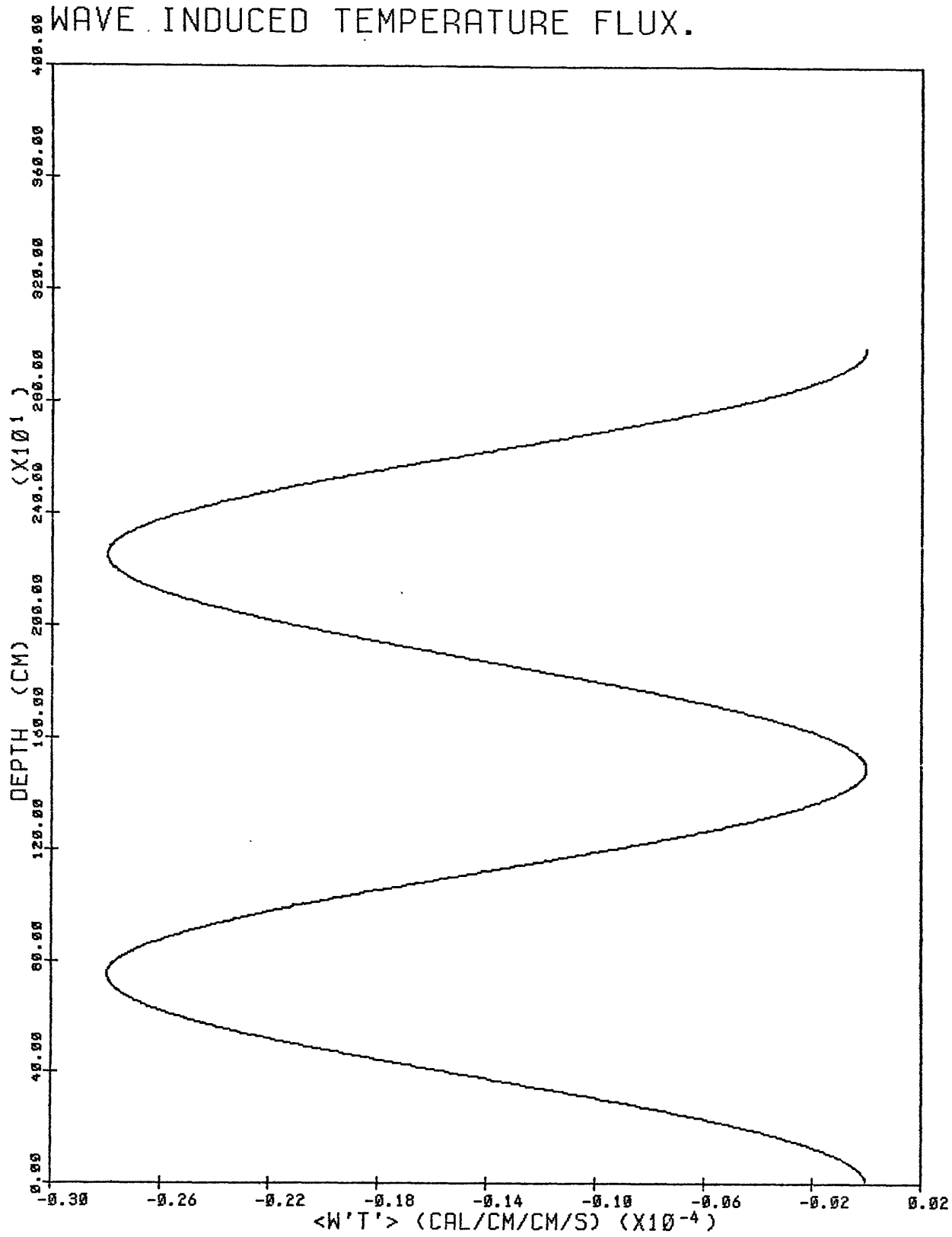


Figure 4.2.2. Wave induced heat flux for a wave with n=2, σ=1.43x10^{-4} sec^{-1}, ℓ=1.38x10^{-5} cm^{-1} and R=.1 cm/sec in a linear stratified ocean 30m deep. The values of f,N,T are the same as for Stellwagen bank region.

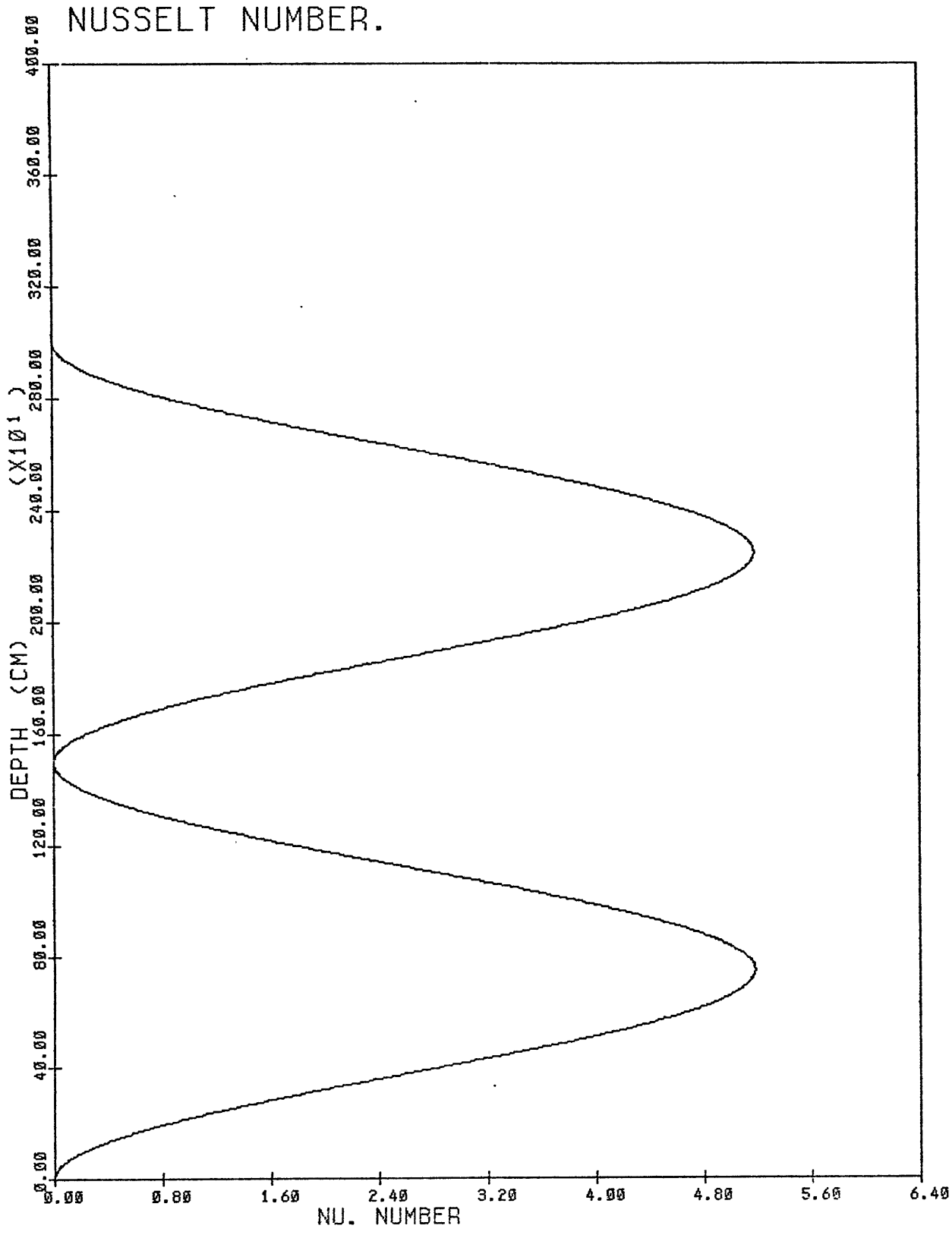


Figure 4.2.3. Nusselt number corresponding to the wave induced heat flux of figure 4.2.2.

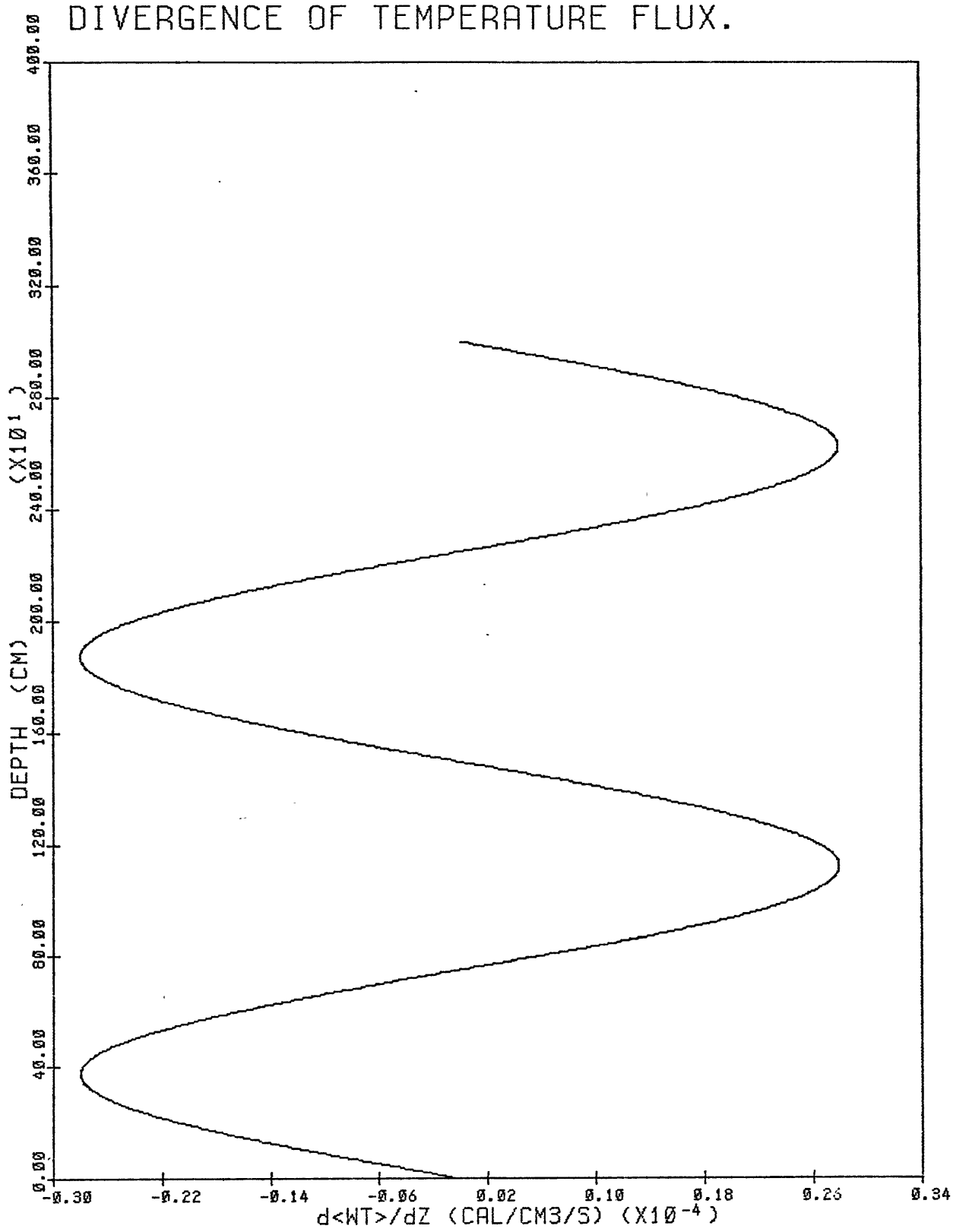


Figure 4.2.4. Vertical divergence of heat flux corresponding to the wave induced flux of figure 4.2.2.

vertical displacement of the 10°C isotherm by 7 meters. A constant Brunt-Vaisala profile was assumed with N equal to 0.25 rad/sec. Figures 4.2.2 to 4.2.4 show the wave induced heat flux calculated from Eq. (2.4.8b), the Nusselt number and the vertical divergence of the heat flux for the wave mode number 2, with ℓ = 1.38×10^{-5} cm^{-1}. σ = $9.79 \times 10^{-5} sec^{-1}$ and R = .1 cm/sec. The Nusselt numbers are of order 5, indicating that the fluxes for this wave will not induce significant additional flux. Figures 4.2.5 to 4.2.7 show the same quantities computed for a wave mode 3, and ℓ = $1.38 \times 10^{-5} cm^{-1}$, σ = $9.79 \times 10^{-5} sec^{-1}$ and R = .068 cm/sec. In this case the Nusselt number is of order 500, indicating significant wave induced fluxes. Figure 4.2.7, of the vertical divergent of heat flux, would suggest mixing at depths 8m, 16m and 26m. The local depth of the experiment was 28m. For the sake of easier calculations we assumed 30m, so the 26m depth would be in the bottom boundary layer. Figure 4.2.8 shows the vertical profile of Brunt-Vaisala frequency that, even when being measured discretely, shows bumps typical of the stair case layered distribution. The bumps of the profile coincide with the depths of the wave induced mixing. This example of a topographic wave in tidal flow indicates that wave induced mixing can be appreciable, and that the wave induced fluxes may well be the cause of the stepwise structure seen in the temperature profiles shown in Figure 4.2.8. The measurements of Halpern (1971b) also indicated the presence of fine structure due to mixing.

Halpern (1971) observed discrete traces of high frequency internal waves in Massachusetts Bay to the incoming semidiurnal tidal flow over

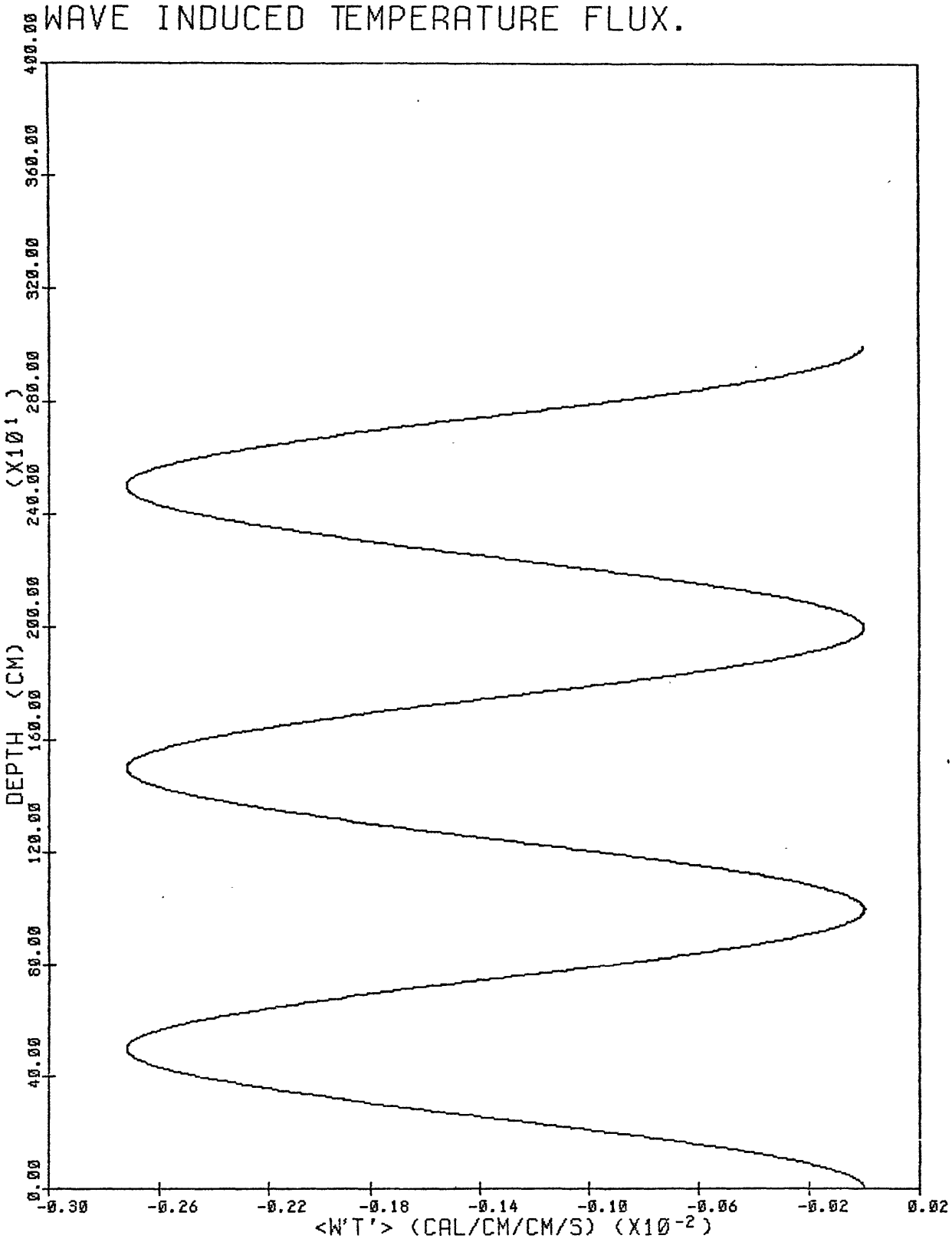


Figure 4.2.5. Wave induced heat flux for a wave with n =3, σ=9.79x10^{-5} sec^{-1}, ℓ =1.379x10^{-5} cm^{-1} and R =.0685 cm/sec.

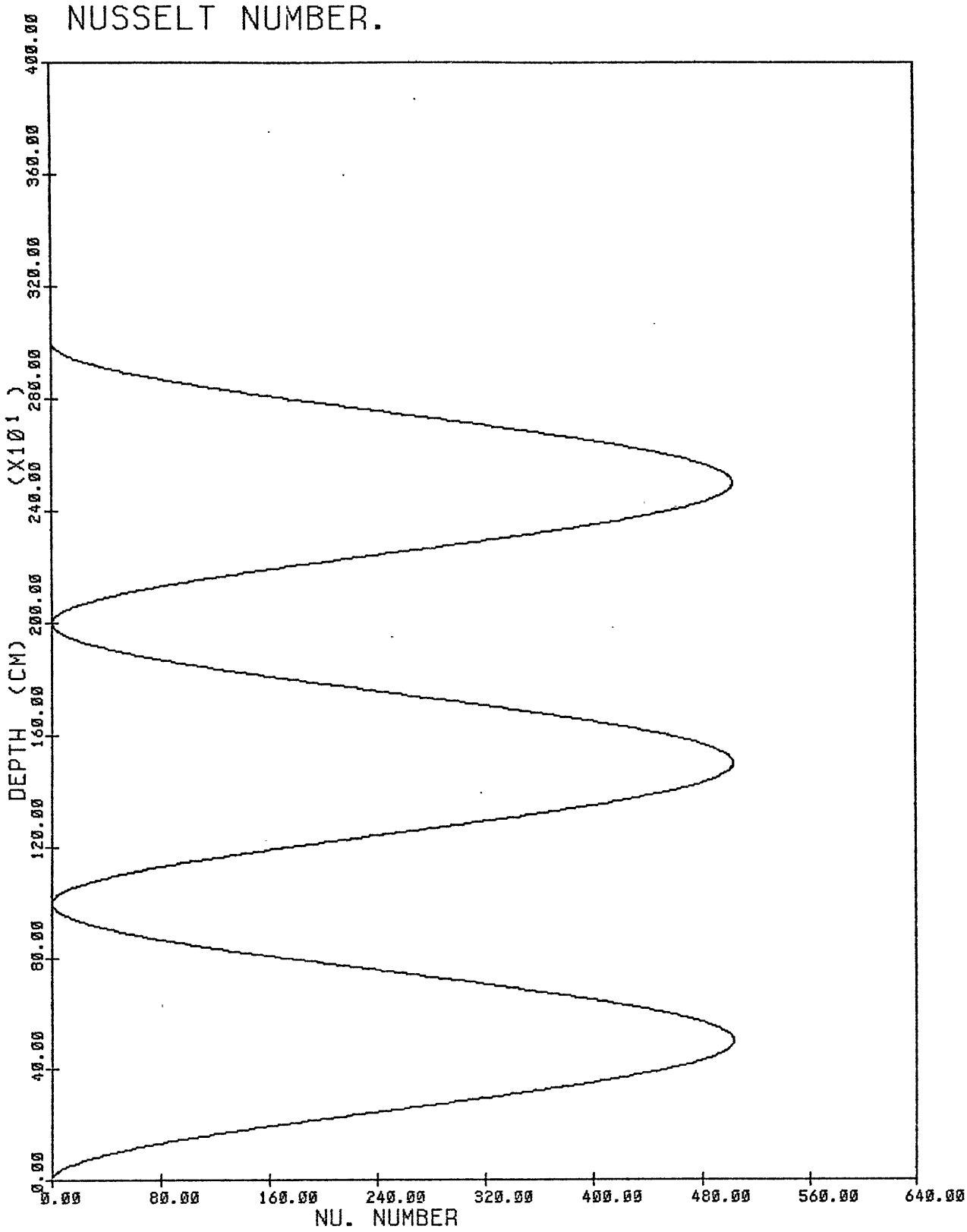


Figure 4.2.6. Nusselt number corresponding to the wave induced heat flux of figure 4.2.5.

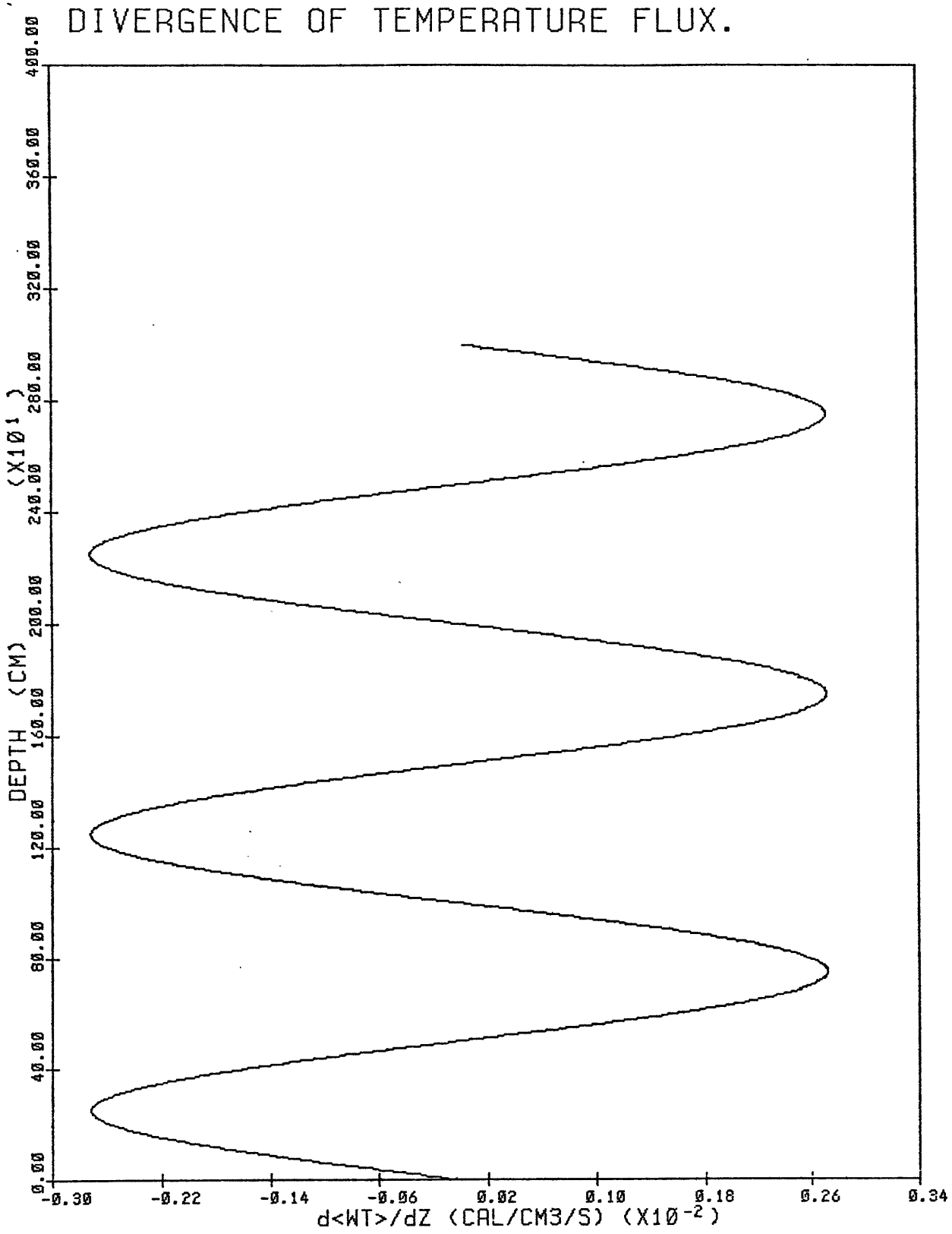


Figure 4.2.7. Vertical divergence of heat flux corresponding to the wave induced flux of figure 4.2.5.

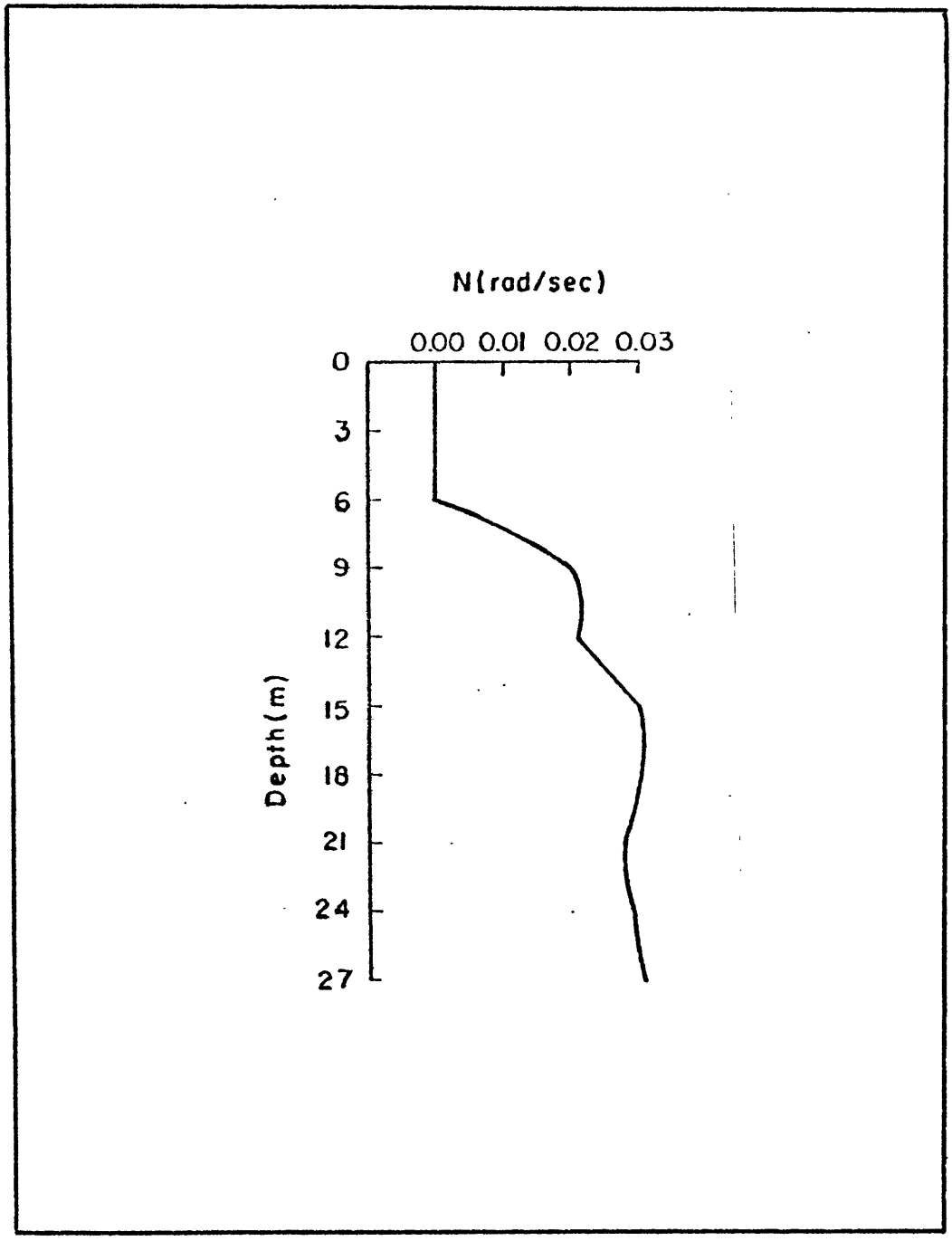


Figure 4.2.8. Vertical profile of Brunt-Vaisala frequency calculated from density inferred from an average of 6 hand-lowered CTD casts made in the vicinity of the mooring B. (After Chereskin,1982).

Stellwagen Bank. These observations were made during midsummer by using moored vertical thermistor chains.

Computations using values of the observed waves like, σ = $1.4\text{x}10^{-2}\text{sec}^{-1}$, ℓ = $1.8\text{x}10^{-4}\text{cm}^{-1}$, n=1 and R = 2.7 cm/sec yielded heat fluxes of order $10^{-6}\text{cal/cm}^2\text{/sec}$ and Nusselt numbers of order 10^{-1} as expected since high frequency waves will not induce fluxes as shown in chapter II. On the other hand, a semi-diurnal internal wave mode 5, with a wavenumber $1.96\text{x}10^{-5}\text{cm}^{-1}$ (wavelength of 3.2 km) will yield fluxes of order $10^{-5}\text{cal/cm}^2\text{/sec}$ and Nusselt number of order 1. In this case the wave number despite being of the same order of the lee waves, observed by Chereskin, but the amplitude is small, so not fulfilling the conditions to induce mixing.

4.3. Knight Inlet observations.

A pilot study in Knight Inlet,British Columbia,by Farmer and Smith (1977) yielded measurements of large amplitude internal waves. They found the same kind of internal wave packets observed by halpern and Chereskin in Massachusets bay. They were observed as a train of several waves with amplitudes exceding 10 meters and periods of a few minutes that passed the vessel on each flood tide.

A map of Knight Inlet,indicating the position of the stations is shown in figure 4.3.1. We notice the bank near station 5 resemble Stellwagen Bank in that it has the same kind of assymetry in the flow

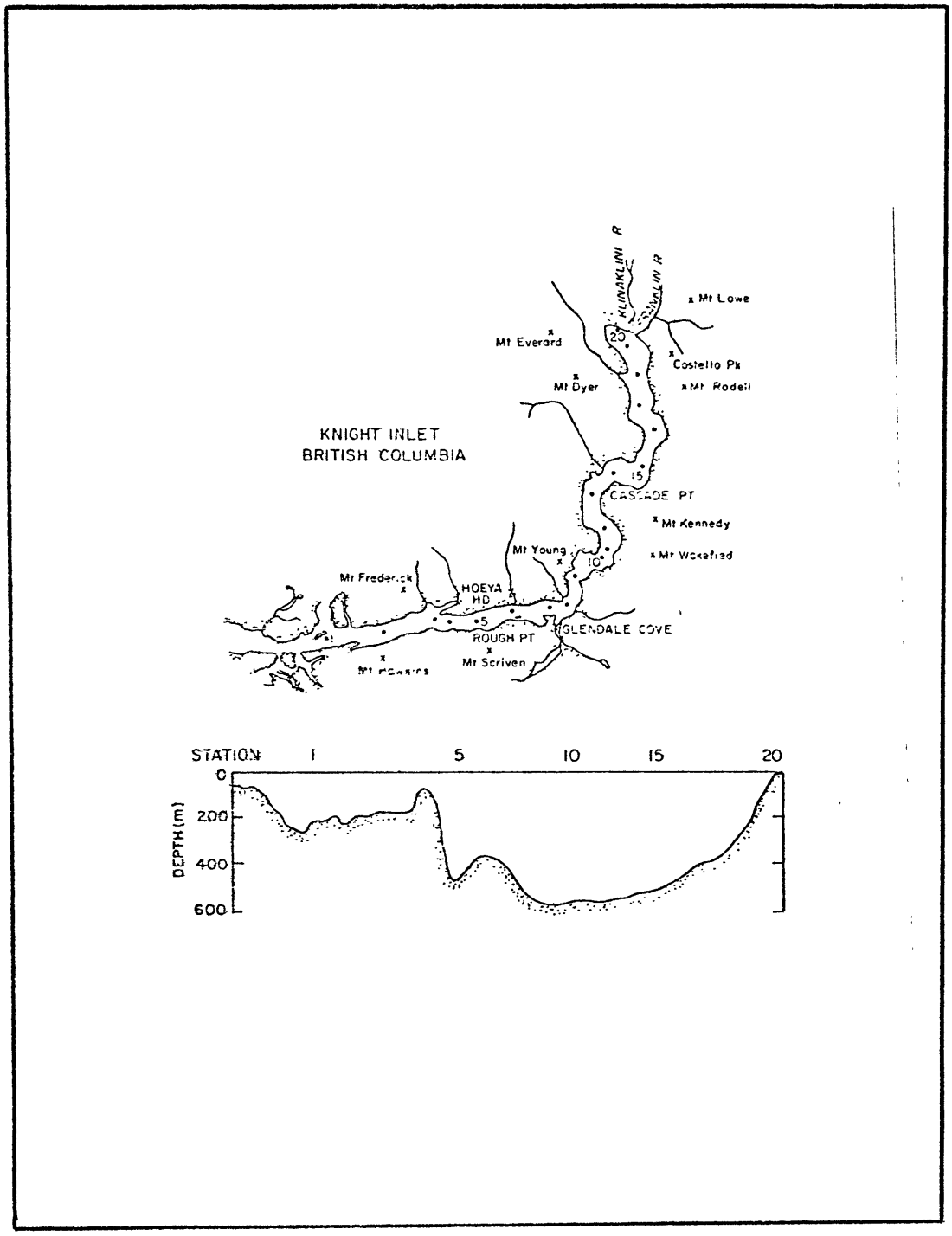


Figure 4.3.1. Map of Knight Inlet indicating CTD station locations, numbered from 1 to 20 and a longitudinal section showing the approximate depth and bottom topography. (After Farmer and Smith,1977).

direction. But in this case the density is mostly determined by salinity.

Computation of wave induced salinity fluxes and the corresponding Nusselt numbers, using the conditions of Farmer and Smith observations were carried out. A wave mode 4 with σ =.00698 sec^{-1}, ℓ =.000139 cm^{-1} and R =17.2 cm/s will induce salinity fluxes of order 10^{-7} gm of salt/cm /sec and Nusselt numbers of order 2. Those numbers are comparable to those found for Halpern's high frequency waves. On the other hand Farmer and Smith does not mention the lee wave that would be formed in a previous stage of the high frequency waves formation.

Figure 4.3.2, that is figure 7 in Farmer and Smith, shows clearly formation of layers indicating mixing during the ebb tide, which is exactly when the lee wave is formed (assuming an analogy with Stellwagen Bank). This layered structure is repeated approximately 12 hours latter again in the next ebb tide, when another lee wave should be expected to form.

From the three observations discussed here, only Chereskin was able to get data on the lee wave, since she steamed back and forth across the bank during a tidal period. With sufficient information for the Farmer and Smith experiment, we should probably find high Nusselt numbers and evidence for mixing.

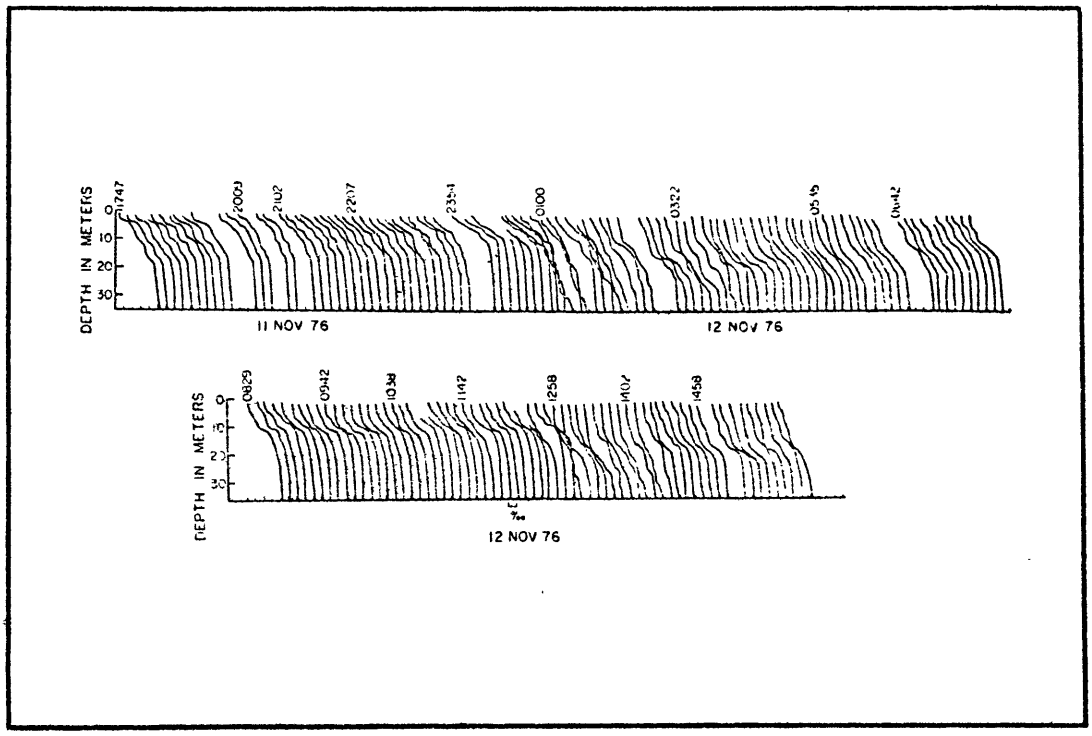


Figure 4.3.2. Salinity profiles obtained at station 5 in figure 4.3.1. Note the effects of internal waves arond 01:00 and again around 13:00 on November 12. The step like structure is formed at the ebb tide and them smoothed out during the flood tide period. (After Farmer and Smith,1977).

Chapter V.

Remote Sensing of Frontal Structures

5.1 Introduction

Remote sensing is a powerful source of data on medium and large structure of oceanographic phenomena. The sensing devices used for this purpose are mostly radiometers that measure electromagnetic radiation ranging from the visible to the microwave region of the spectrum. The two important properties that characterize a sensing device are its spectral and spatial resolutions. These two properties are important when analyzing images of medium scale, such as the structure of an oceanic front.

Fronts like that at the New England shelf break are often visible in satellite infrared imagery during winter and early spring, where the temperature contrast between coastal and offshore water can exceed 5°C. The layered structure is much more difficult to detect because of the limited spatial resolution of the sensor. On the other hand, fronts like the Gulf Stream are always visible under cloud-free conditions since the horizontal temperature contrast are large enough. Better images of the structure of the fronts have been obtained by the Multi Spectral Scanner(MSS) of LANDSAT and by the Synthetic-Aperture Radar (SAR) of the SEASAT. Both have a better spatial and spectral resolution; 80m x 80m for LANDSAT MSS and 25m x 25m for SEASAT SAR. An udated review of environmental satellites and sensors is given in Cornillon (1982).

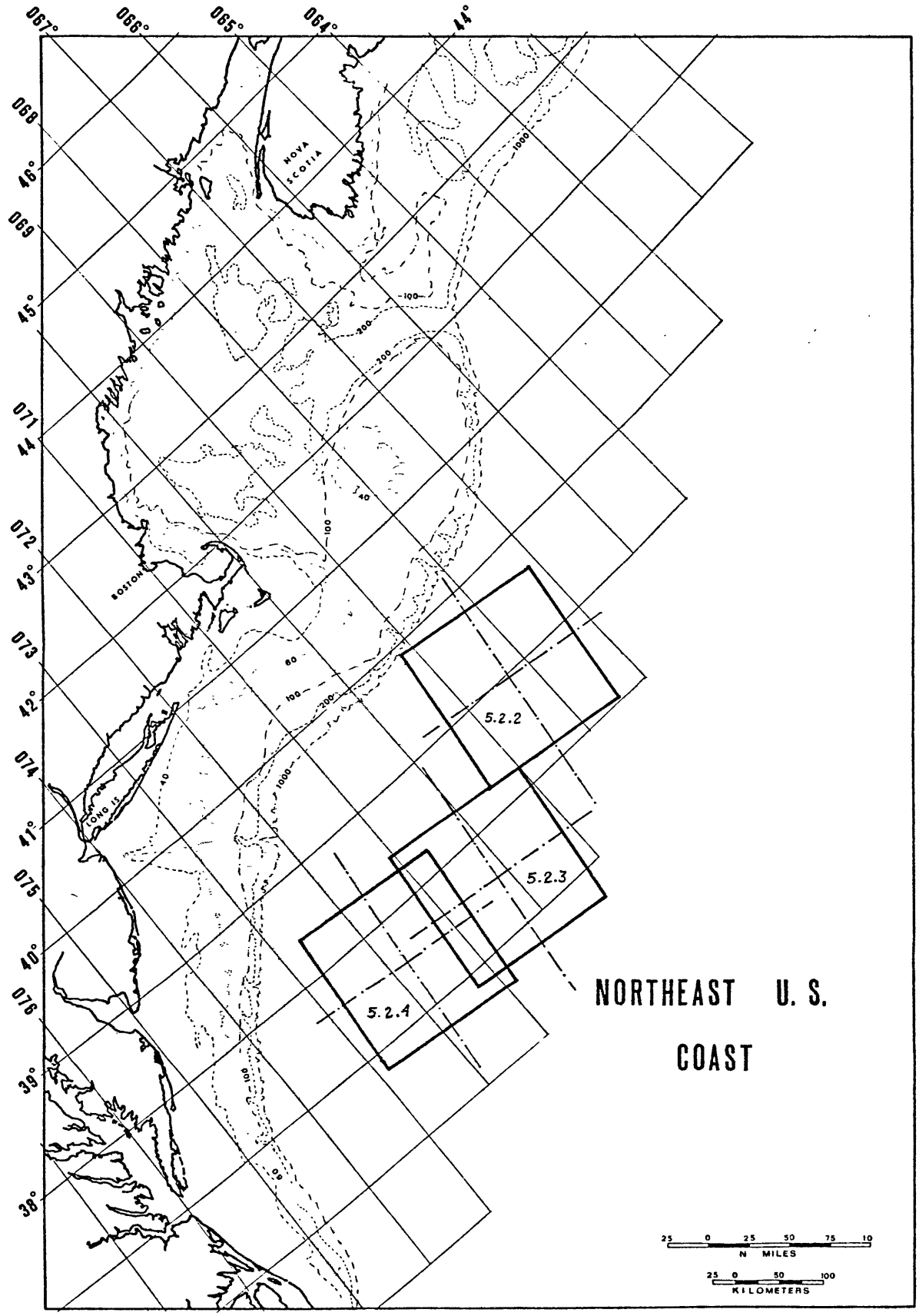


Figure 5.2.1. Geografical position of the LANDSAT images shown in figures 5.2.2.5.2.3 and 5.2.4.

5.2 LANDSAT-2 Images

Satellite images of the front formed between the waters of the Gulf Stream and slope waters are shown in figure 5.2.2, 5.2.3 and 5.2.4. Their geographical position is shown in figure 5.2.1. They are images obtained in the visible region of the spectrum in the window (.5-.6) . The first one was taken in May 15, 1977. The geographical coordinates of the center of the image are 38°59'N and 068°18'W. The boundary of the front is visible due to the differences in the optical properties of each water mass (e.g. extention coefficient, scattering volume function, etc.). The sea surface cloud-like structure in the image identifies the Gulf Stream region, that can also be identified at the convective clouds, associated with warmer sea surface temperatures. In this particular picture the layers are not as well defined as in the next ones.

The Multispectral Scanner Channel 5 images of the sea surface show the horizontal distribution of the green-yellow light diffused from the upper layer of the ocean. Ocean surface features can also be seen by changes in the reflectivity of the sea surface, since the reflectivity is a bi-directional property as well as a spectral one, and will exhibit different features in the different channels, but almost no difference along the line of sight, since the satellite is programmed to take the images at approximately the same conditions of illumination and altitude of the satellite. The patchy structure of the Gulf Stream in the three images can be associated with turbulence associated with shear.

Figure 5.2.3 shows a second image of the Gulf Stream front where one can see the layer structure at the front. This was taken one day later (May 16, 1977), further south (37 35'N, 070 12'W). It is a cloud-free image, excepting a few patches of cirrus clouds. The layering can be seen in the warm side of the front, and seems to involve different length scales, the thickest layers being approximately 28 km apart and the small scale layers about 500 m apart. A more careful analysis of the images show striations spaced probably by the size of the spatial reso ution of the image. The measurement indicates that they are less than 500m apart. In images like LANDSAT MSS, the nominal resolution of 80 m. is only achieved when one has c ose targets with very different spectral responses. This does not usually happen in sea surface features, so for sea surface targets the best spatial resolution would be 150 meters approximately. The last LANDSAT image (5.2.4) shows the same feature of the Gulf Stream front further west (37°31N,071°39W), and again the layered structure is shown.

5.3 Synthetic-aperture radar images.

5.3.1 Orbital level.

Frontal regions exhibit many features that make them appealing for remote sensing detection, namely their sharp temperature and salinity gradients and strong shear. According to Fu and Holt (1982) the mechanisms that make these features visible to a spacebourne SAR are the following:

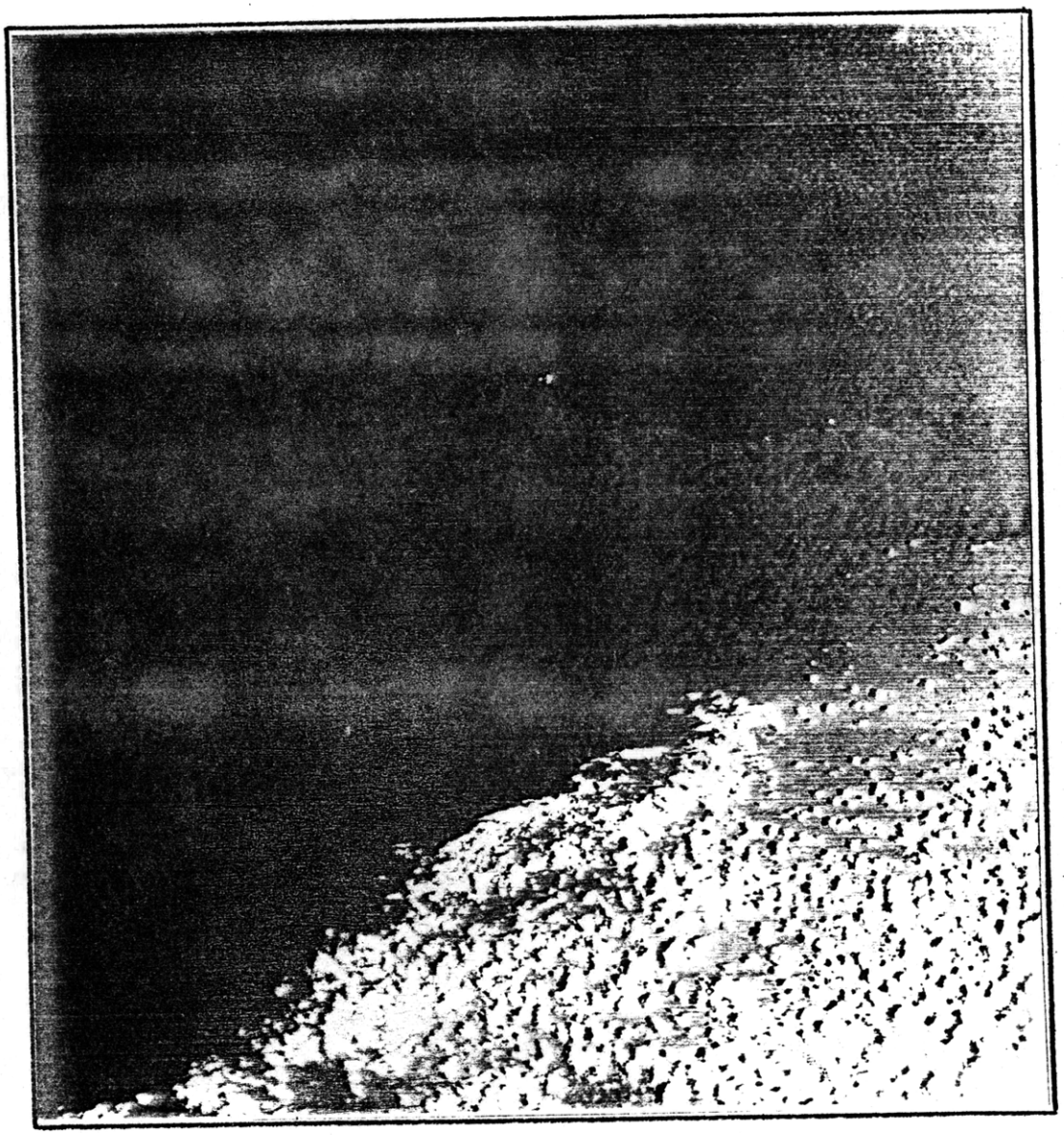


Figure 5.2.2. LANDSAT MultiSpectral Scanner image E-2 844-14142-5 chanel 5, taken on May 15 1977, showing the inshore side of the Gulf Stream front.

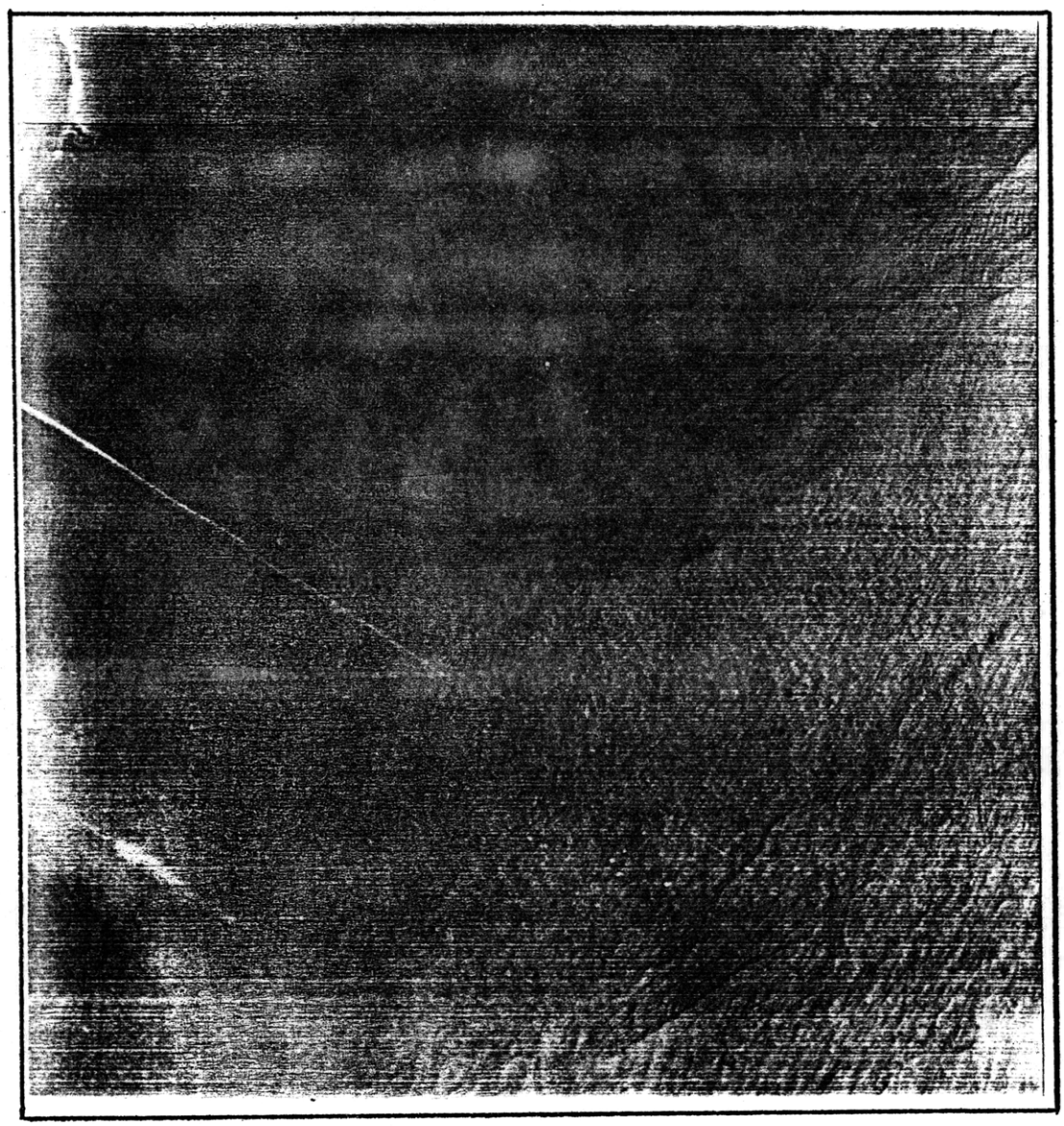


Figure 5.2.3. LANDSAT MultiSpectral Scanner image E-2 845 14203-5, chanel 5, taken on May 16 1977.showing the inshore side of the Gulf Stream front.

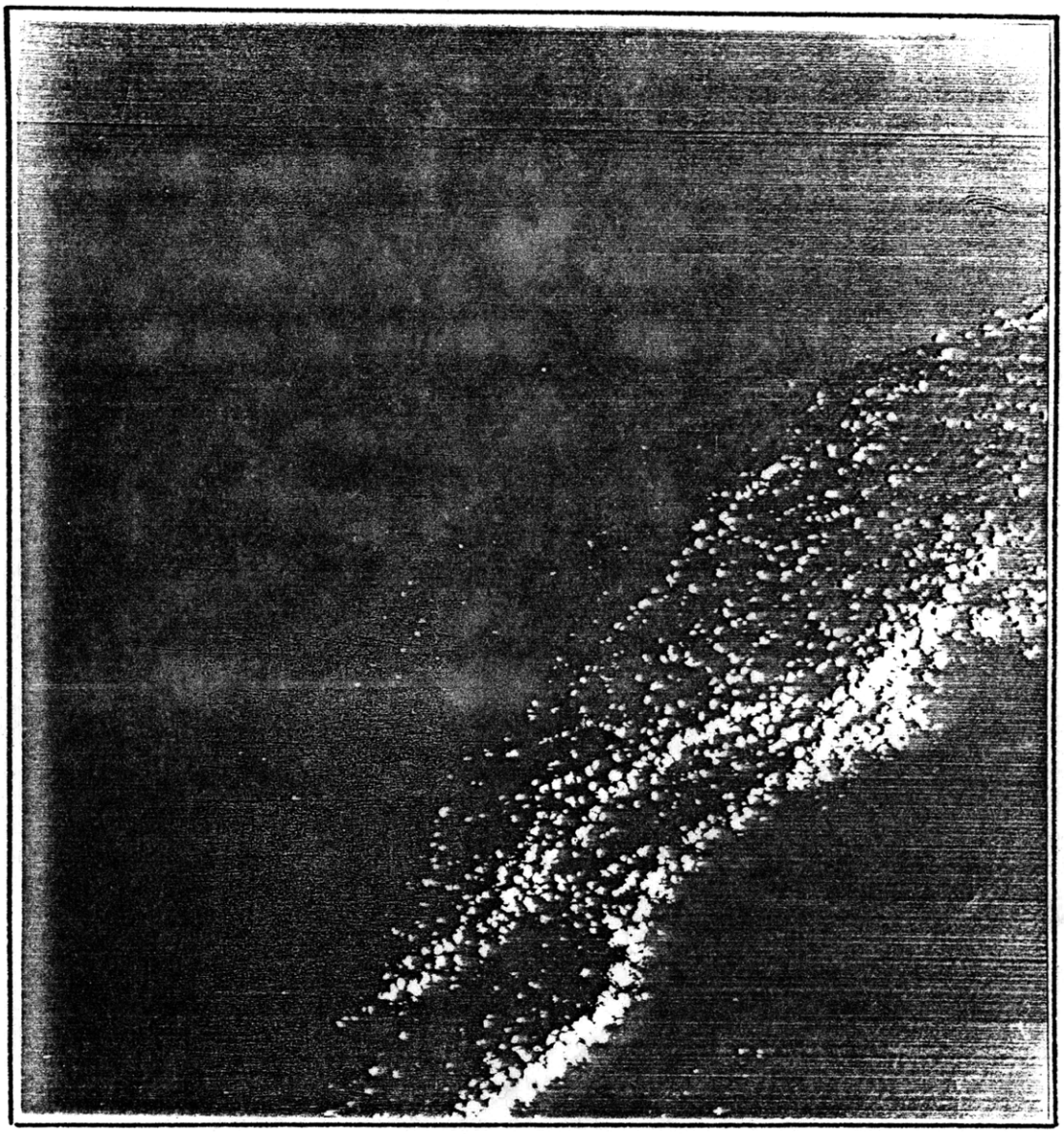


Figure 5.2.4. LANDSAT MultiSpectral Scanner image E-2 846 14261-5, chanel 5, taken on May 17 1977, showing the inshore side of the Gulf Stream front.

i) a change in the surface wind stress that generates Bragg resonant waves usually occurs across a current boundary as a result of the difference in water temperature on the two sides of the current, with smaller wind stress occurring on the colder side where the boundary layer above the sea surface is more stable.

ii) due to wave-current interactions, the Bragg resonant waves are modulated when they cross a current boundary, resulting in either increased or decreased back scatter, depending on the orientation of the wave field relative to the current.

iii) under a uniform wind field, the velocity of the air relative to the water surface is different within a current than outside a current, thus resulting in a variable durface wind stress.

iv) the line-of-sight component of a current produces an azimuthal displacement of its image, thus making the current detectable on SAR imagery as processed using Doppler shift as a location parameter. In the case of coastal fronts several processes as coastal upwelling and river discharge will result in a formation of a relatively cold and fresh water on the continental shelf. The exchange and mixing of this shelf water with the warmer and saltier offshore water often produces pronounced variations in sea-surface roughness detectable on SAR images. The tremendous advantage of SAR images over any other kind of remote sensing data is that it can be obtained even with completely overcast conditions. It is an all weather sensor.

Figure 5.3.1 shows the geographical locations of the next three SAR images. The Gulf Stream boundary is again shown in the figure 5.3.2,

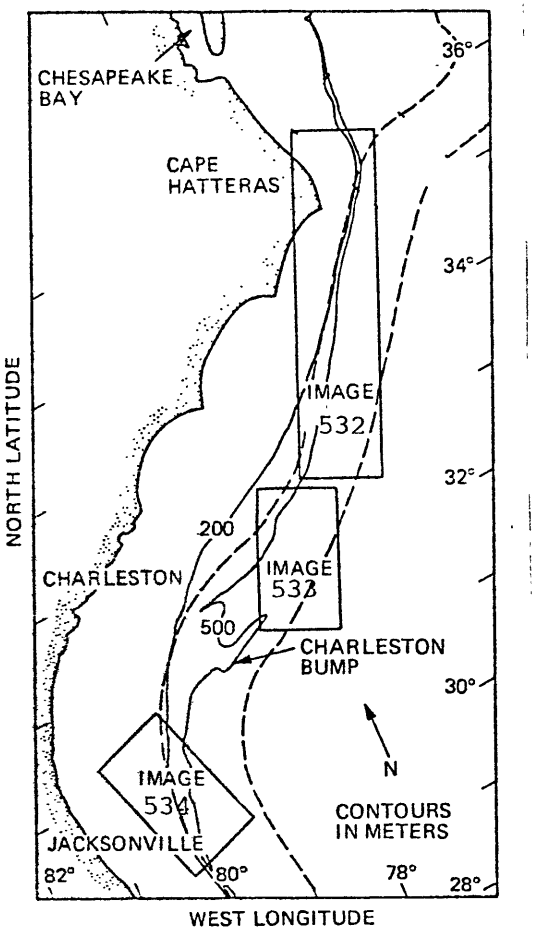


Figure 5.3.1. Geographical position of the Synthetic-Aperture Radar images shown in figures 5.3.2, 5.3.3 and 5.3.4. Also the path of the Gulf Stream (dashed lines) between Florida and Cape Hatteras is shown. (After Fu and Holt, 1982).

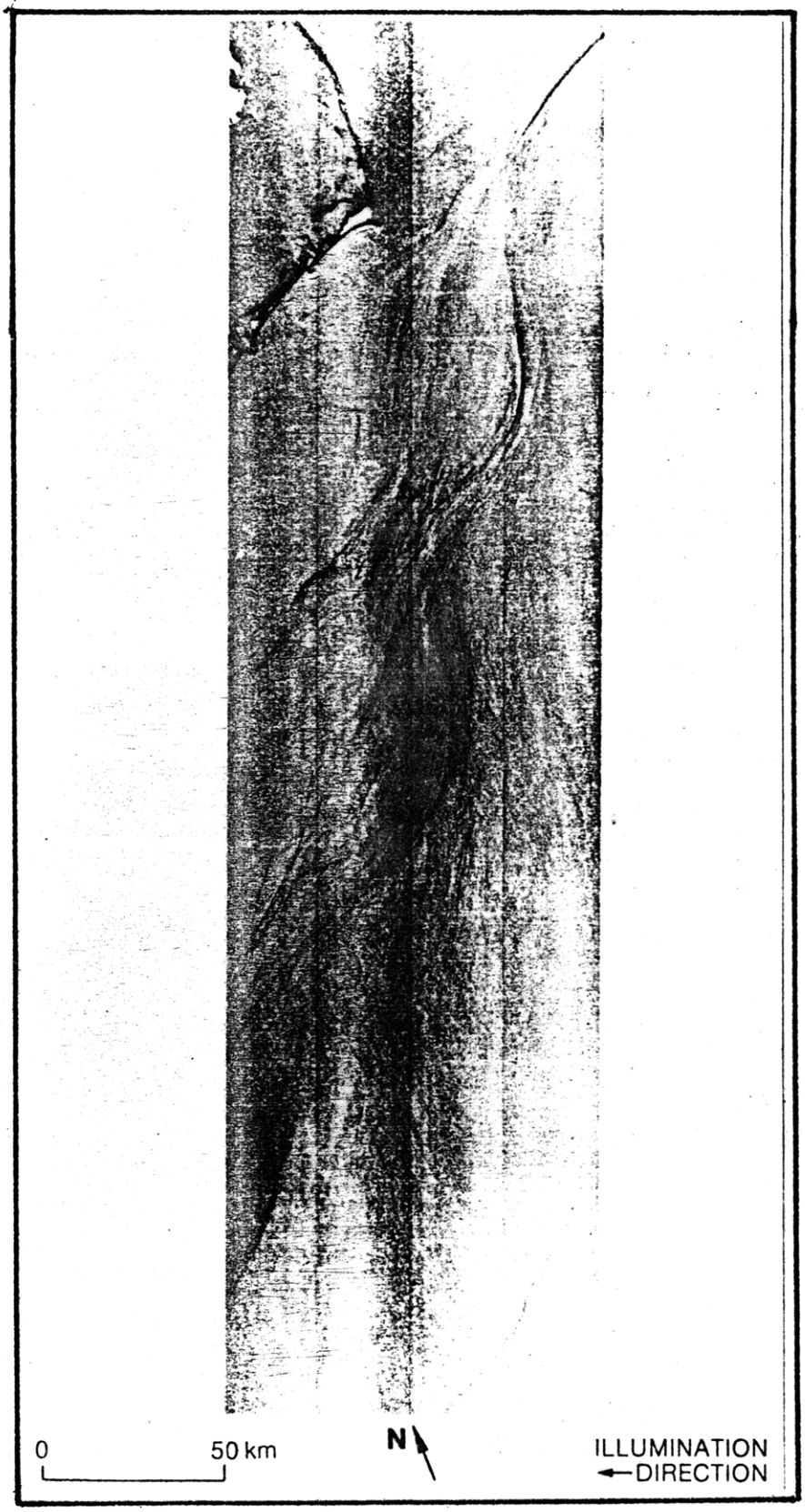


Figure 3.5.2. S.A.R. image of the Gulf Stream off Cape Hatteras,Rev. 931; 02:40 GMT,August 31,1978. (After Fu and Holt,1982)

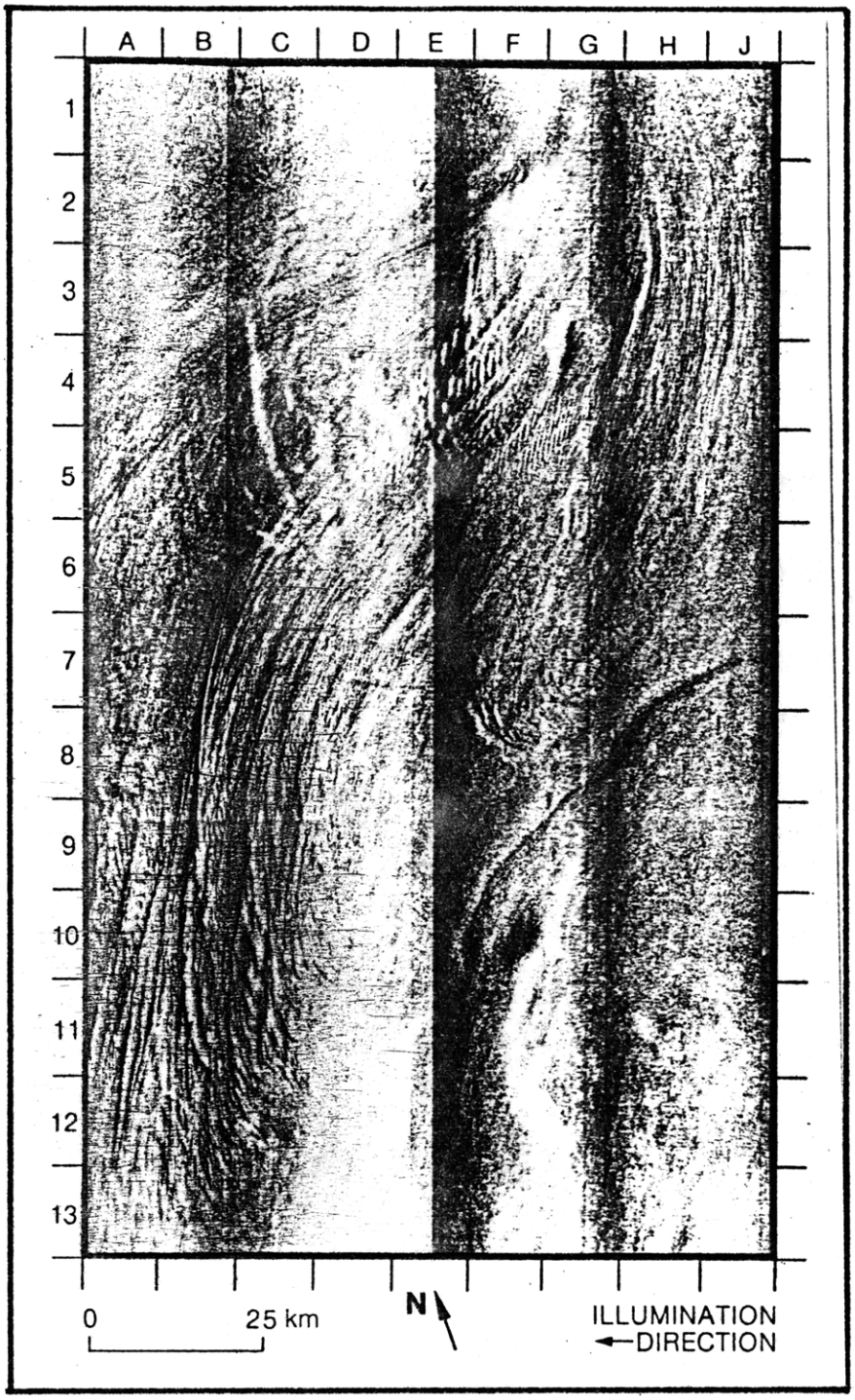


Figure 5.3.3. S.A.R. image of the Gulf Stream northeast of Charleston Bump,Rev. 400; 00:06 GMT, July 25,1978. (After Fu and Holt,1982).

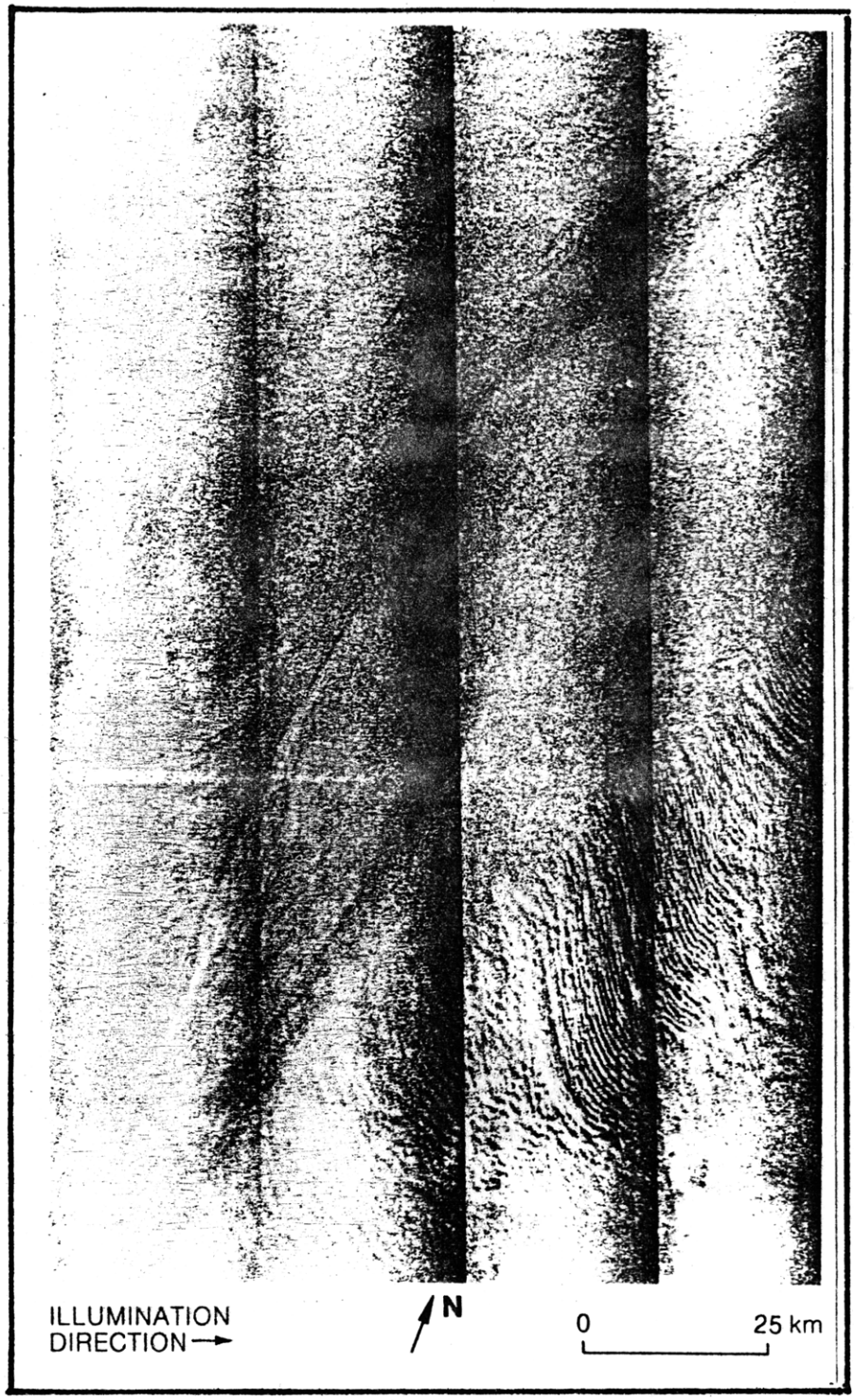


Figure 5.3.4. S.A.R. image of the Gulf Stream about 100 km east of Jacksonville,Florida, Rev. 1110, 14:44 GMT, September 12 1978. (After Fu and Holt,1982).

exhibiting the weavy-like behavior that can be used to calculate its velocity as in Mollo-Christensen et al. (1980), as well as the layered structure. Again a rough estimate of the distance between the layers ranges from 1 km to 20 km; meanwhile the smaller scale striations a few hundred meters apart. Another view of the Gulf Stream front is shown in a SAR image in figure 5.3.3. This and the next are some of the best examples of small-scale linear striations believed to be typical of layer formation in fronts. The features of figure 5.3.3 were found just northeast of the Charleston Bump in the continental shelf edge. As written by Fu and Holt (1982):

> "Note the small-scale linear situations trapped between the two boundaries. Their wavelengths range from 300 to 1200 meters, and their long crests aremore or less parallel to the current boundaries. Because these features have never been observed by surface measurements, the physics of their generation and interaction with the Gulf tream is essentially unknown. However, a plausible account was given by Mollo-Christensen (1981), who proposed that these striations were the surface effects of the adjustment of the bottom boundary layer to changes in the interior flow."

One of the reasons why the striations were not seen before from spaceborne sensors is the poor spatial resolution, mainly on the previous infrared scanners. As will be seen next, low flight altitude infrared images will show the layered structure.

In the case of the image 5.3.3, there is a topographic feature (Charleston Bump) that might well generate internal waves of the kind examined in Chapter Four.

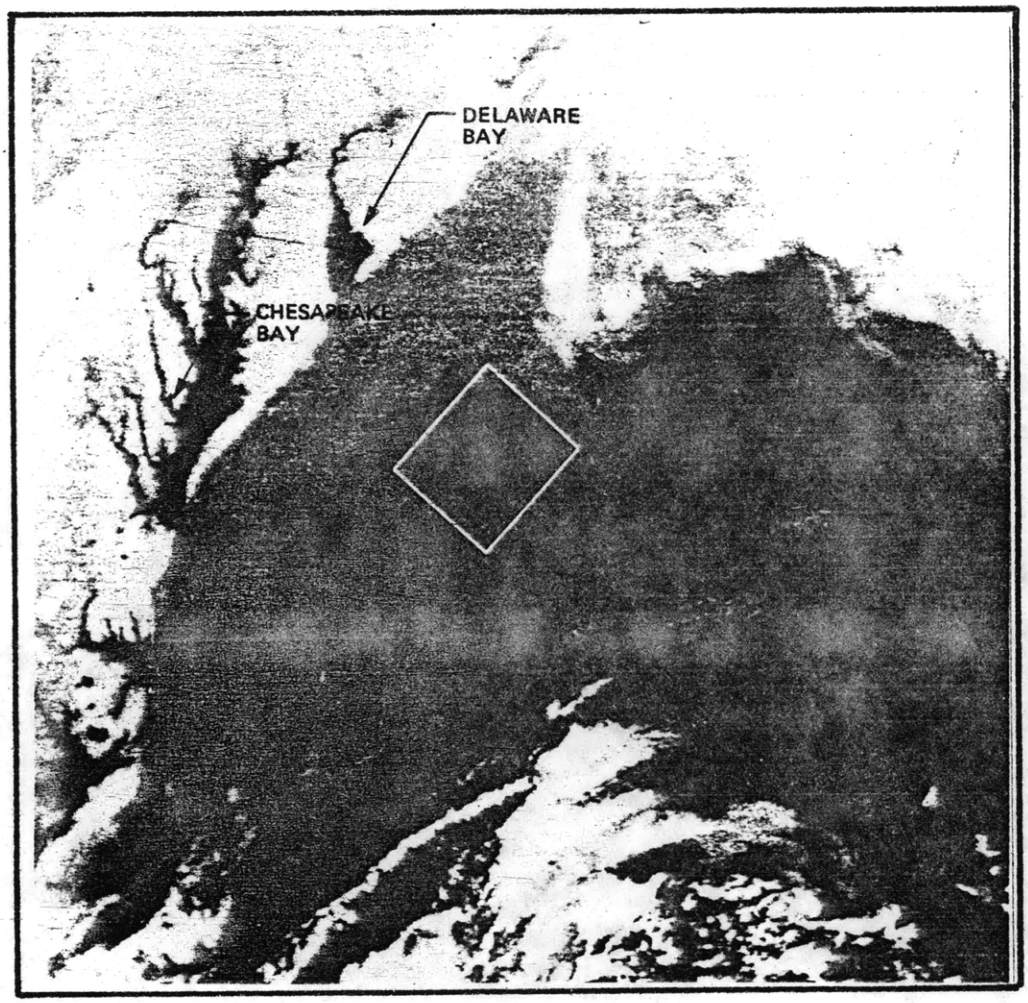


Figure 5.3.5. NOAA-5 infrared image of a warm-core ring taken at 00:21 GMT, September 21,1978, about 100 km southeast of Delaware Bay. (After Fu and Holt,1982).

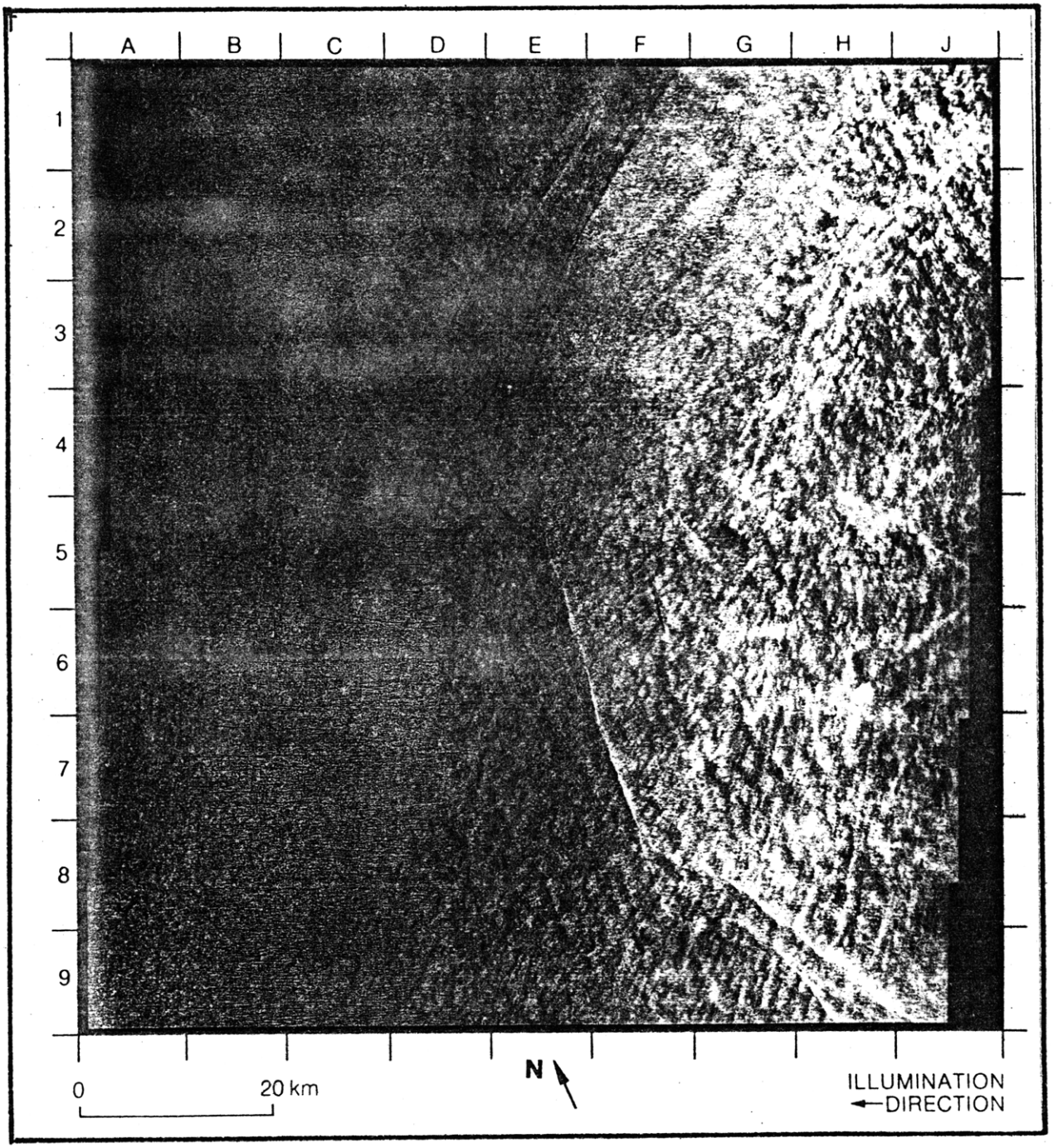


Figure 5.3.6. S.A.R. image of the western portion of the warm core ring shown in figure 5.3.5. (After Fu and Holt,1982).

The figure 5.3.4 is again the Gulf Stream front, just off Jacksonville. Here the richness of detail in the layer structure show the many scales present. To the east of the current boundary are small-scale linear striations similar to those found in the previous images. Again bathymetric features are present, propiatiating formation of high amplitude internal waved needed to induce mixing.

The next image, figure 5.3.6, is of the western portion of a warm-core ring about 100 km southeast of Delaware Bay, being the geographic location shown in figure 5.3.5. which is a NOAA-5 infrared image of the same ring taken at 0021 GMT, September 21, 1978, about 4 hours before the SEASAT pass. A boundary delineated by concentric curvilinear lines and small scale patches can be seen, but the striations characterizing layers of many scales cannot be observed. Although a ring will delineate a front, it seems that there are no topographic internal waves present.

The next figure, 5.3.8, is an image of a coastal front in the Gulf of Mexico, just off Galvaston, which geographical position is shown in figure 5.3.7. As pointed out by Fu and Holt (1982), the eddy-like feature on the images may be manifestations of cross-shelf mixing. In this image, the layered structure cannot be well identified because it is masqueraded by wave-like intabilities and other phenomena.

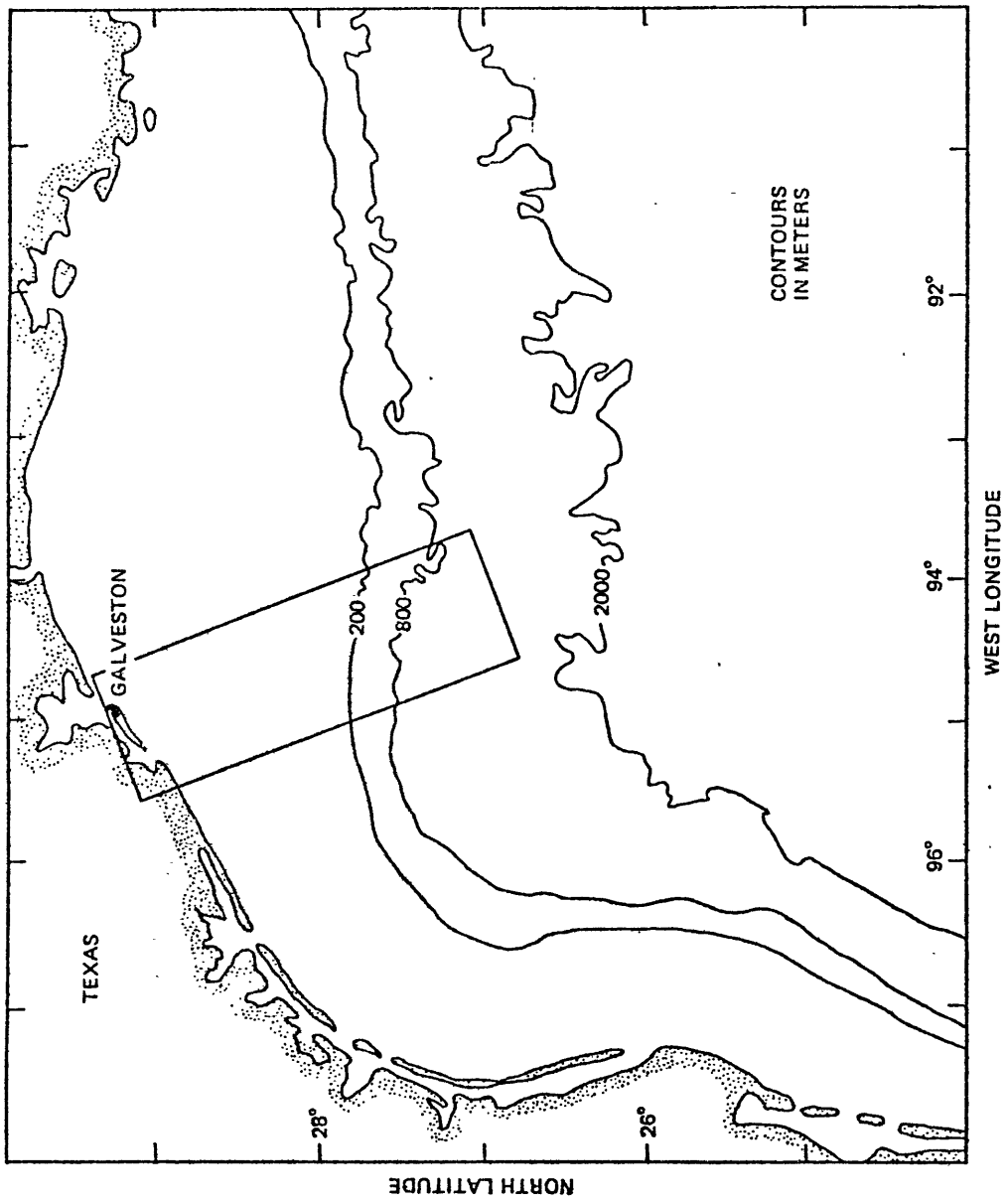


Figure 5.3.7. Geographic position of the S.A.R. image of the figure 5.3.8. (After Fu and Holt,1982).

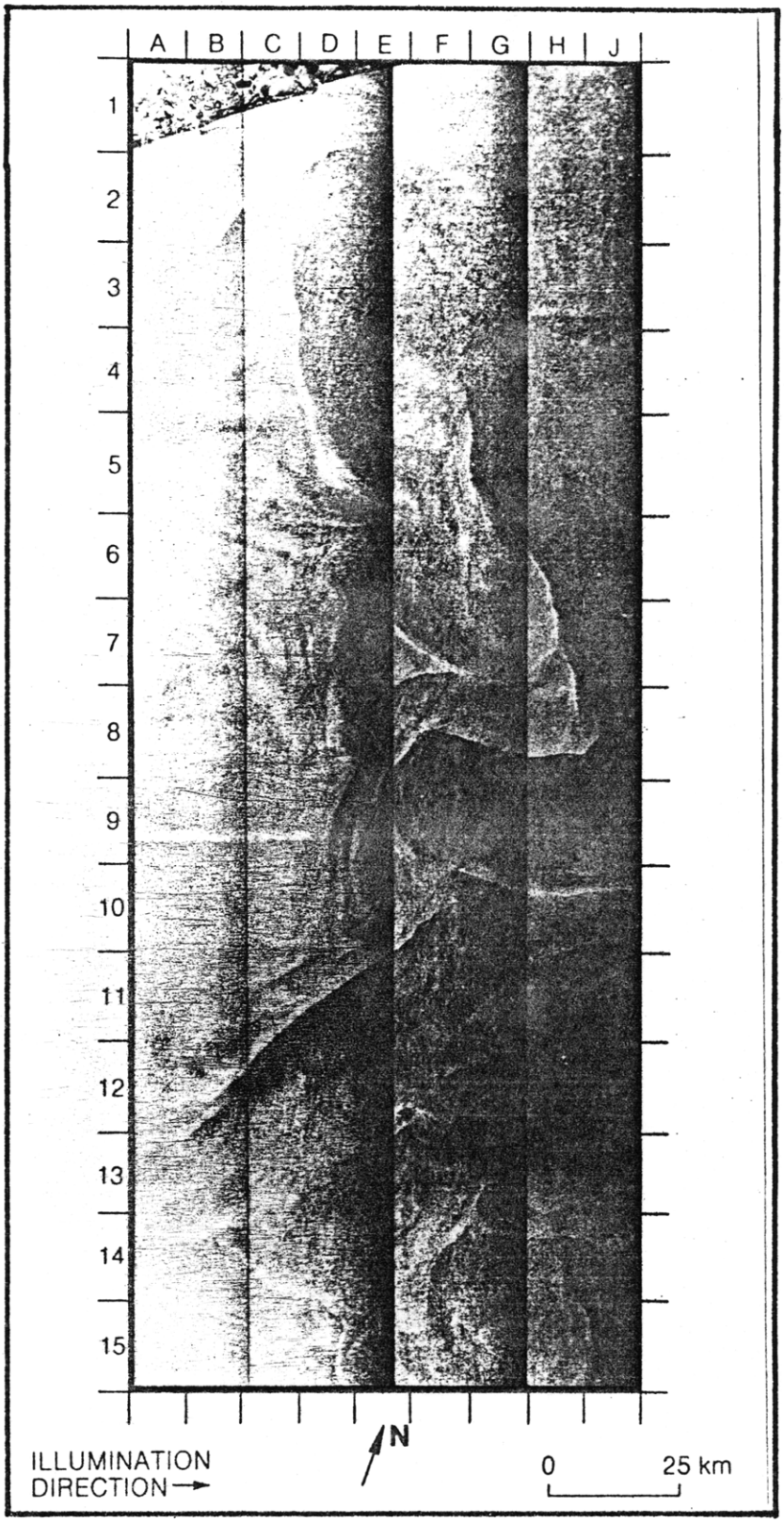


Figure 5.3.8. S.A.R. image of the Gulf of Mexico south of Galveston. (After Fu and Holt,1982).

5.3.2 Aircraft level.

The next set of data that exhibit layering structure was kindly provided by Dr. Duncan Ross. It is from a low level flight crossing the Gulf Stream, starting at 35°23.1 N, 074°20.5 W and ending at 35°48.5 W. The figure 5.3.9 is a radar image of the front, where we can see clearly the layer structure. Those can be better appreciated from figure 5.3.10 where the sea surface temperature is recorded along the flight path. We can see a jump of almost 7°C and small scale layers ranging from 150 meters to 4.2 kilometers. We can see from these data that the small scale structure is much more comples than we thought.

5.4 Infrared Radiometer

5.4.1 Satellite Level

Since most of spaceborne infrared radiometers have a spatial resolution beyond 1 km, they are not fitted to show the phenomena studied here. An example of the spatial resolution is shown in image 5.3.6.

5.4.2 Aircraft Level

The last image, figure 5.4.1, is an infrared scanner image showing striations along the front. The image shows a portion of the Gulf

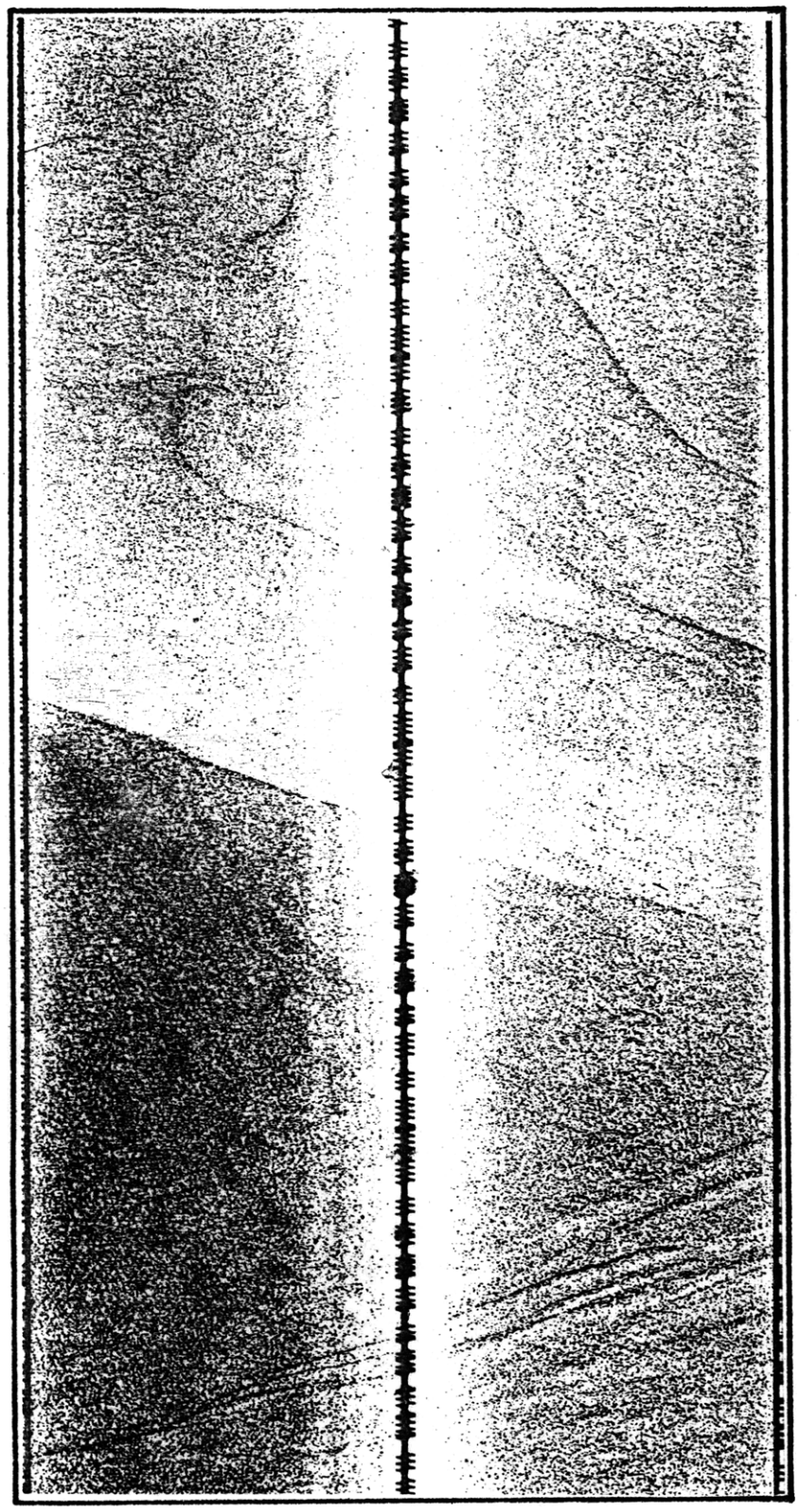


Figure 5.3.9. Aircraft level S.A.R. image crossing the Gulf Stream front at approximately 35°30 N and 074°20 W. (Image provided by Dr. Duncan Ross).

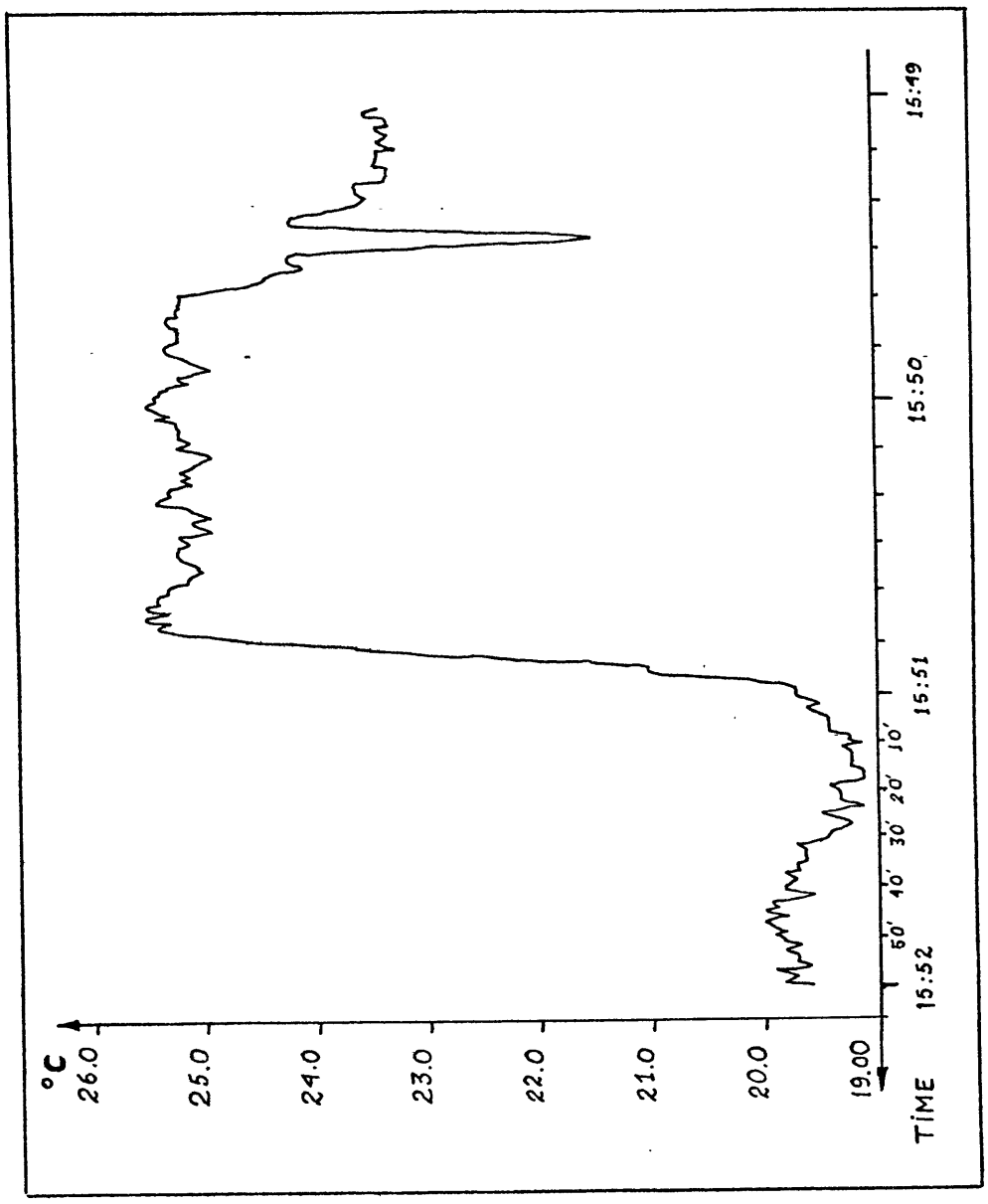


Figure 5.3.10. Infrared sea surface temperature along the flight path corresponding to same image as the S.A.R. image of figure 5.3.9. The right end of both images match.

Stream. We can assert that the layering structure could be a ubiquitous phenomena in all kinds of fronts, much more because it is associated with another ubiquitous phenomenon, namely, internal waves. The fact that free internal waves will not induce flux places a constraint in layering formation. Most of the satellite images presented here have shown the layer structure of fronts. We notice their presence more frquently in the warmer side of the front where the stratification is stronger.

5.5 Possible correlation between results of previous chapters and remote sensed frontal features.

In the frontal case discussed in chapter III, the imposed boundary conditions (3.3.17) excluded the region near the intersection of the front and the surface. In this section we are going to try to extrapolate some of the results of chapter III and speculate about the effects of the wave induced heat and salt fluxes at the intersection between the front and the sea surface.

The results of Olbers (1982) suggest that the amplitude of scattered internal wave field is amplified in a front, and also that one should expect the wave spectrum in the vicinity of a front to show anisotropy with more energy along the frontal axis than normal to it.

The divergence of the cross-front wave induced flux will generate a stratification across the front as was shown previously. In the

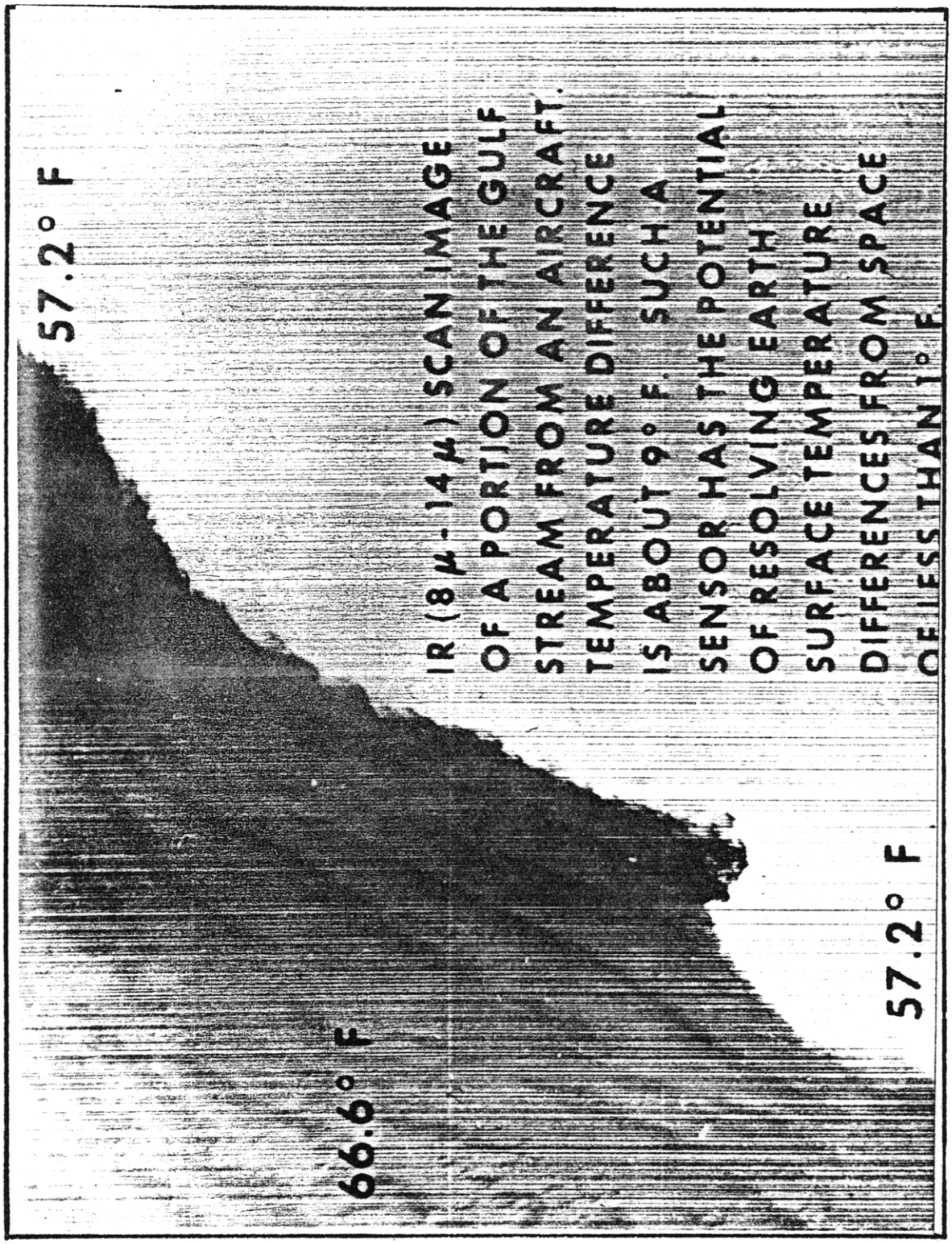


Figure 5.4.1. Aircraft level infrared scanner image of the Gulf Stream front.

neighborhood of the surface, there will be a surface layer formed by diurnal effects and wind. Waves, travelling along the front, will be partially reflected at the surface. But also, because of the narrowing distance between the front and the surface, the wave amplitude should increase as the wave approaches the surface, since the wave energy will be confined.

In addition to the reflected wave, which will also tend to increase the magnitude of the disturbance near the surface, there will, generally, be a near field evanescent disturbance at the surface. This is needed to satisfy the complicated boundary conditions in the intersection region.

The near field disturbance, the increased amplitude and the inhomogeneous propagation conditions in the intersection area combine to cause the disturbances there to have large amplitude and to have wave numbers and frequencies different from the homogeneous linear dispersion case.

There will therefore in all likelihood be large wave induced fluxes across the front near the surface, with a divergence field that generates a steplike distribution of heat and salt.

At the same time, since there is a stratification along the front because of the surface layer, there will also be mixing parallel to the front, and the fluxes due to this mixing will also tend to make the surface layers horizontally non-uniform. The shear flow associated with the front will also tend to stretch any variation along the front into bands parallel to the front.

In the specific case of the inshore side of the Gulf Stream front off Cape Hatteras it can be estimated as 400 m thick front (Richardson, et al., 1969).

Chapter VI

Conclusions and Suggestions for Future Work

It is an accepted hypothesis that much observed fine structure in the ocean is due to internal waves distorting a smooth profile rather than due to persistent layers arising from other mechanisms. The mechanism which account for mixing require turbulence or overturning. The overall Richardson number for internal waves is usually above unity meaning the flux is stable.

Here we propose a mechanism that does not require turbulence of overturning to mix. Internal waves, propagating in a stratified region will induce fluxes of heat and salt that have a non zero mean. It was found that to induce mixing the waves must have low frequency, high wave number and high amplitude. In other words, freely propagating internal waves on a thermocline or on a front have a relatively small effect.

The wave-like disturbances with the required characteristics are forced internal waves, like waves forced by flow over topography. They will induce large fluxes and large Nusselt numbers. Disturbances forced by air-sea interaction can also cause enhanced diffusion but the magnitude is unknown.

High frequency waves will not induce mixing since there is not enough time for diffusion. On the other hand the high wavenumber waves will induce mixing due to the shear diffusion advection effect in the temperature and salinity gradient.

The wave induced fluxes are always negative, meaning that they are in the down gradient direction. The depth average divergence of heat flux is zero indicating that there is no vertical exchange of heat but only a tendency to form layers in the stratification.

For a front, which will act like a wave guide, there is a tendency of high wave numbers we then should expect mixing along the front. The striations along the Gulf Stream front seen in the Synthetic Aperture Radar images could well be a surface manifestation of wave-induced mixing process.

Here we have focused our attention much more on vertical mixing than on lateral mixing. The wave induced horizontal up and along the front fluxes are expected to be larger than the vertical one, since they are divided by wave number.

The examples of topographic mixing show that this may be an important mechanism in many localities, and one should look for evidence elsewhere in the ocean. One should start looking at 30° latitude where tides can exite inertial resonance.

Concerning future work, we suggest a program of measurements across fronts by towing a thermistor chain. The towing should be performed through a boom in the bow of the vessel or laterally to avoid the mixing of the vessel's wake.

A program of CTD casts during various tidal periods in the vicinity of a topographic feature, and simultaneous vertical sections of temperature and salinity parallel to the flow will yield enough information in order to compute the induced fluxes. We also suggest future work in wave-induced momentum in fronts.

REFERENCES

Chereskin, T.K., 1982. The development of nonlinear surface and internal wave groups. Ph.D. thesis. Massachusetts Institute of Technology and Woods Hole Oceanografic Institution,325 pp.

Bender, C.M., and S.A. Orszag, 1978. Advanced Mathematical Methods for Scientists and Engineers. McGraw-Hill Book Co., New York, 593 pp.

Bowman, M.J. and W.E. Esaias, 1978. Oceanic Fronts in Coastal Processes, Proceedings of a workshop held at the Marine Sciences Research Center, May 25-27, 1977. Springer-Verlag, 114 pp.

Briscoe, M.G., 1975. Preliminary results from the trimoored Internal Wave Experiment (IWEX). J. Geophys. Res., 80, 3872-3884.

Cornillon, P., 1982. A guide to environmental satellite data. NOAA/Sea Grant, University of Rhode Island Marine Technical Report 79, 469 pp.

Desaubies, Y.J.F., 1975. A linear theory of internal wave spectral and coherences near the Vaisala Frequency. J. Geophys. Res., 80, 895-899.

Elliott, J.A. and N.S. Oakey, 1979. Average microstructure levels and vertical diffusion for phase III, GATE, in GATE-1, oceanography and surface layer meteorology in the B/C scale, Eds. A. Siedler and J.D. Woods, Supplement 1 to Deep Sea Research, part A, Vol. 26, Pergammon Press, New York.

Farmer, D. and J.D. Smith, 1977. Nonlinear internal waves in a Fjord. In Hydrodynamics of Estuaries and Fjords ed. by Jacques C.J. Nihoul,Elsevier Scientific Pub. Co., N.Y.,546 pp.

Fofonoff, N.P., 1969. Spectral characteristics of internal waves in the ocean. Deep-Sea Res., Supplement to Vol. 16, 58-71.

Fofonoff, N.P. and F. Webster, 1971. Current measurements in the Western Atlantic. Phil. Trans. Roy. Soc. A, 270, 423-436.

Flagg, C.N., 1977. The kinematics and dynamics of the New England continental shelf and shelf/slope front. Ph.D. thesis, MIT-WHOI, 207 pp.

Fu, L.L. and B. Holt, 1982. Seasat Views Oceans and Sea Ice with Synethic-Aperture Radar. Jet Propulsion Lab. publication 81-120.

Garrett, C.J.R. and W.H. Munk, 1972. Space-time scales of internal waves. Geophys. Fluid Dyn., 2, 225-264.

Garrett, C.J.R. and W.H. Munk, 1972. Space-time scales of internal waves: A progress report. J. Geophys. Res., 80, 291-297.

Garret, C.J.R., 1979. Mixing in the ocean interior. Dyn. of Atmospheres and Oceans, 3, 239-265.

Gould, W.J., W.J. Schmitz, and C. Wunsch, 1974. Preliminary field results for a Mid-Ocean Dynamics Experiment (MODE-0). Deep-Sea Res., 21, 911-923.

Halpern, D., 1971a. Observations on short-period internal waves in Massachusetts Bay. J. of Marine Res.,29, 116-132.

_____, 1971b. Semidiurnal internal tides in Massachusetts Bay. J. Geophys. Res.,76, 6573-6583.

Haury, L.R.; M.G. Briscoe; M.H. Orr, 1979. Tidally generated internal wave packets in Massachusetts Bay. Nature, 278, 312-316.

Horne, E.P.W., M.S. Bowman and A. Okubo, 1978. Cros frontal mixing and cabbeling, in Oceanic Fronts in Coastal Processes, M.J. Bowman and W.E. Esias eds., Springer-Verlag, Berlin, New York.

Hunkins, K. and M. Fliegel, 1973. Internal ondular surges in Seneca Lake : A natural occurence of solitons. J. Geophys. Res.,78, 539-548.

Huppert, H.E. and J.S. Turner, 1981. Double-diffusive convection. J. Fluid Mech., 106, 299-329.

Ivanov, V.A. and K.V. Konyayev, 1976. A bore on the Thermocline. Izv. Atmosp. and Ocean. Phys., 12, 416-423.

Mascarenhas, A.S.,Jr., 1979. Characteristics of upper heated oceanic layer from satellite observations. SM thesis, MIT, 83 pp.

Mollo-Christensen, E.L., 1981. Surface signs of internal ocean dynamics in Spaceborne Synthetic Aperture Radar for Oceanography, R.C. Beal, P.S. DeLeonibus and I. Katz, The Johns Hopkins University Press, Baltimore, London.

Mollo-Christensen, E.L., P. Cornillon, A.S. Mascarenhas, Jr., 1981. Method for estimation of ocean current velocity from atellite images. Science, 212, pp. 661-662.

Munk, W., 1981. Internal waves and small-scale processes, in Evolution of Physical Oceanography: Scientific Surveys in Honor of Henry Stommel, B.A. Warren and C.I. Wunsch eds., MIT Press, Cambridge, Massachusetts.

Olbers, D.J., 1981. A formal theory of internal wave scattering with applications to ocean fronts. J. Phys. Oceanogr., 11, 1078-1099.

Osborn, T.R. and C.S. Cox, 1972. Oceanic fine structure. Geophys. Fluid Dyn., 3, 321-345.

Pedlosky, J., 1979. Geophysical Fluid Dynamics. Springer-Verlag, 624 pp.

Perry, R.B. and G.R. Schimke, 1965. Large-amplitude internal waves observed off the Northwest coast of Sumatra. J. Geophys. Res., 70, 2319-2324.

Phillips, O.M., 1977. The dynamics of the upper ocean. Cambridge University Press, Cambridge, New York, 336 pp.

Ruddick, B.R., and T.M. Joyce, 1979. Observations of interaction between the internal wave field and low-frequency flows in the North Atlantic. J. Phys. Oceanogr., 9, 498-517.

Schmitt, R.W. Jr. and D.L. Evans, 1978. An estimate of the vertical mixing due to salt fingers based on observations in the North Atlantic Central Water. J. Geophys. Res., 83, 2913-2919.

Turner, J.S., 1973. Buoyancy effects in fluids. Cambridge University Press, Cambridge, New York, 368 pp.

_____, 1981. Small-scale mixing processes, in Evolution of Physical Oceanography: Scientific Surveys in Honor of Henry Stommel, B.A. Warren and C.I. Wunsch eds., MIT Press, Cambridge, Massachusetts.

Voorhis, A.D., D.C. Webb, and R.C. Millard, 1976. Current structure and mixing in the shelf/slope water front south of New England. J. Geophys. Res., 81, 3695-3708.

Voorhis, A.D., 1968. Measurements of vertical motion and the partition of energy in the New England slope water. Deep Sea Res., 15, 599-608.

Webb, D.C. and L.V. Worthington, 1968. Measurements of vertical water movements in the Cayman Basin. Deep Sea Res., 15, 609-612.

Webster, F., 1972. Estimates of the coherence of ocean currents over vertical distances. Deep Sea Res., 19, 35-44.

Worthem, S, E.L. Mollo-Christensen, F. Ostapoff, 1983. Effects of rotation and shear on double diffusive instability. (manuscript in preparation.)